The Dissertation Committee for Joseph Michael McCrate Certifies that this is the approved version of the following dissertation:

CHARACTERIZATION OF LOW DENSITY OXIDE SURFACE SITES USING FLUORESCENT PROBES

Committee:

John G. Ekerdt, Supervisor

Brian A. Korgel

Charles B. Mullins

George S. Hwang

Alex A. Demkov

CHARACTERIZATION OF LOW DENSITY OXIDE SURFACE SITES USING FLUORESCENT PROBES

by

Joseph Michael McCrate, B.S.Ch.E.; M.S.E.

Dissertation

Presented to the Faculty of the Graduate School of

The University of Texas at Austin

in Partial Fulfillment

of the Requirements

for the Degree of

Doctor of Philosophy

The University of Texas at Austin

December 2013

Dedication

To Melissa and my parents, for their unending love and support.

Acknowledgements

Any accomplishments I have made during my time as a graduate student would not have been possible without the support of numerous people. First, I would like to thank my advisor, Dr. John Ekerdt, for his guidance, wisdom, and, most importantly, patience. He always provided me great freedom in exploring particular aspects of my research project and then supported me when I encountered problems. I truly consider myself fortunate to have had the opportunity to work with and learn from him. I would also like to than the members of my committee, Dr. Korgel, Dr. Mullins, Dr. Hwang, and Dr. Demkov, for providing their valuable time and insights. I wish to express my gratitude to my fellow group members, both past and present, including Navneet Salivati, Blair Cox, Tyler Elko-Hansen, Martin McDaniel, Brad Leonhardt, Thong Ngo, Wen Liao, Sonali Chopra, Dan Bost, Daniel Groom, Luke Henderson, Ryan Fitzpatrick, Kelly Thom, Tuo Wang, Wes Ahearn, Ben Spivey, Hyun-Woo Kim, and Songyan Jia for their invaluable knowledge, advice, assistance, and support. Additionally, the staff in the Chemical Engineering department, especially Kevin Haynes, Randy Rife, Eddie Ibarra, T Stockman, Patrick Danielewski, Carrie Brown, and Jessica Kramm, has always been helpful. In particular, Jim Smitherman and Butch Cunningham have helped me with numerous tasks and always provided me with valuable knowledge and advice. I would also like to thank Dr. Hugo Celio, Dr. Karin Keller, and Dr. Joshua Bolinger for assistance with instruments.

Financial support for my research project was provided by the Robert Welch Foundation and the National Science Foundation. Additionally, I wish to thank the Uniden Corporation for sponsoring a THRUST Fellowship, which I received.

I was fortunate to have had the opportunity to work with several excellent mentors prior to coming to UT. Dr. Kurt Gaskill at the Naval Research Laboratory and Dr. Charles Smith and Dr. Hao Li at the University of Missouri-Columbia all provided me the opportunity to work on various research projects in their labs and develop as a researcher. Also, I would like to thank Dr. Tom Marrero at the University of Missouri-Columbia for serving as a mentor throughout my undergraduate studies and encouraging me to pursue a graduate degree.

I also wish to express my gratitude to my friends and family for their continued support and encouragement during my time at UT. Most importantly, I wish to thank my fiancée Melissa. In addition to making countless personal sacrifices, she always brightens my day and reminds me of what is truly important in life.

Characterization of Low Density Oxide Surface Sites using Fluorescent Probes

Joseph Michael McCrate, Ph. D.

The University of Texas at Austin, 2013

Supervisor: John G. Ekerdt

Low density surface sites are believed to play an important role in processes occurring on oxide surfaces, including catalysis and particle and film nucleation. However, our understanding of the role and chemical nature of such sites play in these processes is limited by the inability to experimentally detect minority surface sites in many oxide systems. The research performed for this dissertation is focused on developing a surface science technique utilizing fluorescent molecules to titrate specific surface sites on planar fused silica surfaces in an ultra-high vacuum (UHV) environment. High sensitivity (low detection limit) is achieved by using derivatives of perylene, a high quantum yield fluorophore. High specificity is attained by employing perylene derivatives with functional groups designed to react chemically with and titrate various sites. In addition to titrating the well-studied hydroxyl sites with perylene-3-methanol (density ~ 10^{14} cm^{-2}), which is used to establish the technique, the detection of strained siloxane sites (~10^{12} cm^{-2}) with perylene-3-methanamine and oxygen vacancy sites (~10^{11} cm^{-2}) with 3-vinyl perylene is demonstrated. Particle nucleation on oxides is suspected to involve defects that trap adatoms and form critical nuclei. Using this technique, the possible role strained siloxane and oxygen vacancy sites play in trapping adatoms during the nucleation of Ge nanoparticles on silica surfaces is examined.

Table of Contents

List of Tables xi

List of Figures xii

Chapter 1: Introduction 1

1.1 Overview 1

1.2 Background 2

1.3 Objective and Overview of Chapters 6

1.4 References 9

Chapter 2: Hot-wire CVD of Ge nanoparticles on Si-etched Silicon Dioxide 13

2.1 Introduction 13

2.2 Experimental Procedure 16

2.3 Results and Discussion 18

2.4 Conclusion 25

Chapter 3. Titration of Free Hydroxyl and Strained Siloxane Sites on Silicon Dioxide with Fluorescent Probes 30

3.1 Introduction 30

3.2 Experimental 35

3.3 Results and Discussion 38

3.2.1 Titration of silanol sites with P3M: 40

3.3.2 Titration of strained siloxane sites with P3A 48

3.4 Conclusions 54

3.5 References 55

Chapter 4: Coverage Dependent Luminescence from Two-Dimensional Systems of Covalently Attached Perylene Fluorophores on Silica 60

4.1 Introduction 60

4.2 Experimental Methods 64

4.3 Results 67

4.3.1 Emission Spectra 68

4.3.2 Absorption and Excitation Spectra 75
4.3.3 Time-Resolved Emission Spectra 78
4.3.4 Fluorescence Decays 81
4.3.5 Decay Analysis 85
4.4 Discussion 89
4.4.1 Intensity of Emission Features 89
4.4.2 Identification of Emission Features 92
4.4.3 Analysis of γ Term in Decay Model 98
4.4.4 Influence of Coverage on Luminescence 100
4.5 Conclusions 101
4.6 References 103

Chapter 5: Detection of Oxygen-Vacancy Defect Sites on the Silica Surface using Fluorescent Probes 107
5.1 Introduction 107
5.2 Experimental 109
5.3 Results and Discussion 112
5.3.1 Titration of sites using 3-vinyl perylene 112
5.3.2 Influence of atomic deuterium on surface sites 117
5.3.3 Influence of Si exposure on surface sites 122
5.3.4 Nature of Si exposure process 127
5.3.5 Proposed mechanism for atomic deuterium and SiH_x interaction with strained siloxane sites 129
5.4 Conclusions 131
5.5 References 132

Chapter 6: Research Summary 135
6.1 Conclusions 135
6.2 Recommendations for Future Work 136
6.3 References 137

Appendix A: Supporting Information for Chapter 3 139
A.1 Synthesis of Compounds 139

A.1.1 Synthesis of Perylene-3-Carbaldehyde 139
A.1.2 Synthesis of Perylene-3-Methanol (P3M).....140
A.1.3 Synthesis of Perylene-3-Carbaldehyde Oxime 141
A.1.4 Synthesis of Perylene-3-methanamine (P3A) 141
A.2 Experimental 142
A.2.1 Preparation of Wafers 142
A.2.2 Preparation of Standards 142
A.2.3 Solution Fluorescence Measurements.....142
A.3 Results.....144
A.4 References.....151
Appendix B: Supporting Information for Chapter 4.....152
B.1 Results 152
Appendix C: Supporting Information for Chapter 5.....162
C.1 Results 162
References.....164
Vita….....180

List of Tables

Table 4.1: Results of global analysis of Equation 1 using decays from specified wavelengths. 87

List of Figures

Figure 1.1: Schematic of defect mediated nucleation processes. 1

Figure 1.2: Schematic showing influence of particle density on the minimum thickness, t_{min}, of a continuous film for materials that grow in a three-dimensional growth mode. 3

Figure 2.1: Schematic describing process used to deposit Ge NPs on fused silica surface. 15

Figure 2: Ge $2p_{3/2}$ XP spectrum taken after HW and thermal CVD using GeH_4 for various samples. The higher binding energy peak (~1223 eV) is from the silica surface while the lower binding energy peak is from the Mo foil holding the sample in place. 19

Figure 2.3: Ge $2p_{3/2}$ XP spectrum taken after exposing samples to thermal CVD with germane precursor without any HWCVD.....20

Figure 2.4: SEM images showing (a) control experiment and Ge particles on samples given (b) 0 ML, (c) 0.2 ML, (d) 0.4 ML, (e) 0.6 ML, and (f) 1.0 ML Si doses. The right half of each image has been enhanced to make particle density more obvious. The lack of contrast in (a) indicates the absence of particles. 22

Figure 2.5: Ge particle densities for samples dosed with various amounts of Si. Particles were counted manually for one SEM image from each sample and a computer routine was used to estimate the number of particles in four images from each sample. 23

Figure 2.6: Mean particle diameter for samples given various Si doses. The error bars are two standard deviations in diameter. 24

Figure 3.1: (a) Structures of perylene-3-methanol (P3M) and perylene-3-methanamine (P3A). (b) Reaction between P3M molecule and a free hydroxyl site. (c) Reaction between P3A molecule and a strained siloxane site.....35

Figure 3.2: Absorption (A) and fluorescence emission (B) spectra from 1×10^{-6} M perylene (———), P3M (– – – –), and P3A (------) compounds in cyclohexane. The excitation wavelength for the emission spectra was 405 nm, the same wavelength as the laser use in *in situ* measurement. 39

Figure 3.3: *In situ* PL spectra from fused silica wafers pretreated to 700 °C and then titrated with either perylene (------), P3M (— . —), or P3A (———).40

Figure 3.4: *In situ* PL spectra after P3M exposure (— . —) and after a subsequent anneal at 300 °C (———) from fused silica samples pretreated at 700 °C. 43

Figure 3.5. *In situ* emission spectra from fused silica samples pretreated to various temperatures after P3M exposure and annealing at 300 °C. The control sample is described in the text. 44

Figure 3.6: Plot of P3M density (+) versus sample pretreatment temperature and total (□) and free (○) hydroxyl densities from Zhuravlev [7]. The P3M density on the control sample (×) is slightly lower than the density on the 700 °C pretreated sample. 46

Figure 3.7: *In situ* PL spectra from fused silica samples with various densities of chemically bound P3M, showing the transition from monomer to high density emission.....48

Figure 3.8: *In situ* emission spectra from fused silica samples pretreated to various temperatures after P3A titration. 50

Figure 3.9: Comparison of *in situ* PL spectra from 700 °C pretreated fused silica samples either titrated with P3A (——) or exposed to a low quantity of P3M (— . —). 52

Figure 3.10: Estimated densities of chemisorbed P3A on samples pretreated to various temperatures. 53

Figure 4.1: Schematic of reaction between perylene-3-methanol (P3M) molecule and hydroxyl sites on silica surface leading to covalently attached perylene fluorophores. 68

Figure 4.2: Emission spectra from 700 °C pretreated samples with various bound P3M densities. **(A)** *In situ* spectra showing the change in both intensity and position of the spectra as a function of fluorophore density. **(B)** Plot of normalized intensities of *ex situ* spectra showing clear changes in peak positions as a function of bound P3M density. The excitation wavelength was 405 nm. 70

Figure 4.3: *In situ* emission spectra from samples pretreated at either 300 or 700 °C with low densities of bound P3M or P3A molecules. 73

Figure 4.4: *In situ* emission spectra from samples pretreated to various temperatures and then given high P3M exposures. Densities of 1.58, 1.53, and 0.86 P3M / nm^2 were found for the 300, 500, and 700 °C pretreated samples, respectively. 74

Figure 4.5: **(A)** Absorption spectra from samples with various densities of P3M. **(B)** Excitation spectra from the same samples as in (A). The emission wavelength was 520 nm. 77

Figure 4.6: Excitation spectra at various emission wavelengths from sample with P3M density of 0.86 nm^{-2}.....78

Figure 4.7: Normalized time-resolved emission spectra from samples pretreated at 700 °C with various P3M densities.....79

Figure 4.8. Normalized time-resolved emission spectra from samples pretreated to various temperatures and given high P3M exposures. The densities of the 300, 500, and 700 °C pretreated samples were found to be 1.58, 1.53, and 0.86 P3M / nm^2, respectively. 80

Figure 4.9: Fluorescence decay profiles collected at various emission wavelengths from 700 °C pretreated samples with P3M densities of 0.03 nm^{-2} (A) and 0.86 nm^{-2} (B). The decay labeled solution in (A) is from a 1×10^{-6} M P3M solution in cylcohexane collected at an emission wavelength of 475 nm. IRF is the instrument response.....82

Figure 4.10: Decay profiles from samples with various P3M densities collected at emission wavelengths of (A) 475 nm, (B) 520 nm, and (C) 600 nm. The curve in (C) labeled "particles" is the decay from P3M particles deposited on fused silica. 84

Figure 4.11: Schematic of molecular organization of fluorophores bound to the silica surface as a function of density leading to various observed emission features. 90

Figure 4.12: *Ex situ* emission spectra from samples with various P3M densities resolved into partially relaxed (centered at 535 nm) and fully relaxed (centered at 600 nm) excimer-like features. 96

Figure 5.1: *In situ* emission spectra from samples pretreated to various temperatures and titrated with 3VP. 112

Figure 5.2: **(Left)**: *In situ* emission spectra collected from 700 °C pretreated samples titrated with either P3A or 3VP. **(Right):** Normalized spectra from the top figure showing the differences between emission features. 114

Figure 3: Proposed reactions between 3VP and possible surface sites.....115

Figure 5.4: *In situ* emission spectra collected from 700 °C pretreated samples exposed to various quantities of atomic deuterium and then titrated with P3M. The bound P3M densities measured by hydrolytic cleavage of the molecules into solution are shown in brackets. 118

Figure 5.5: *In situ* emission spectra from 700 °C pretreated samples exposed to various amounts of atomic deuterium and subsequently titrated with P3A. 119

Figure 5.6: *In situ* emission spectra from 700 °C pretreated samples exposed to various amounts of atomic deuterium and subsequently titrated with 3VP. 120

Figure 5.7: *In situ* emission spectra collected from 700 °C samples given an atomic deuterium exposure and titrated with 3VP with and without a heating step between the atomic deuterium exposure and titration process.121

Figure 5.8: *In situ* emission spectra from 700 °C pretreated sample given various Si exposures and then titrated with P3M. Densities measured by hydrolytic cleavage of bound P3M into solution are given in brackets. 123

Figure 5.9: *In situ* emission spectra from 700 °C pretreated samples given various amounts of Si exposure and then titrated with P3A.....124

Figure 5.10: *In situ* emission spectra from 700 °C pretreated samples given various Si exposures and subsequently titrated with 3VP. 125

Figure 5.11: *In situ* emission spectra showing influence of n-propylamine exposure prior to Si exposure. 126

Figure 5.12: *In situ* emission spectra collected after various exposure steps showing relationship between sites. 127

Figure 5.13: Plot of Si^0 2p peak area versus Si exposure. 128

Figure 5.14: Proposed reaction between atomic deuterium and strained siloxane sites. 129

Figure 5.15: Proposed mechanism for the interaction of SiH_x fragments with strained siloxane sites, leading to the formation of OVD-like sites capable of trapping adatoms. 131

Figure A.1: Schematic of synthetic route taken to create compounds used in this work. 139

Figure A.2: *In situ* photoluminescence (PL) spectra collected after anneal step from 700 °C fused silica samples exposed to P3M using P3A (———), n-propylamine (– – – –), or nothing (— . . —) to catalyze the reaction between P3M and the silanol sites. n-Propylamine was introduced into the exposure chamber through a leak valve such that the uncorrected ion gauge pressure was maintained at 2×10^{-6} torr for the duration of the P3M exposure step. 144

Figure A.3: *Ex situ* high resolution X-ray photoelectron (XP) spectra of the carbon 1s (left) and nitrogen 1s (right) regions from a 700 °C pretreated sample titrated with P3M (——) and a 300 °C pretreated sample exposed to 500 mTorr n-propylamine vapor for 5 min (– – – –). The spectra were collected with a takeoff angle of 60 ° to enhance surface sensitivity. A readily detectable peak is present in the C 1s spectrum for the P3M titrated sample, while only a weak peak attributed to adventitious carbon is present on the n-propylamine exposed sample. No features are observed in the energy range where N 1s peaks occur for either sample. 145

Figure A.4: Atomic force microscopy (AFM) image of 400 °C preteated sample after P3M titration, demonstrating no particles are present on the surface after the titration process. 146

Figure A.5: *In situ* PL spectra from fused silica samples preheated to various temperatures after P3M exposure. 147

Figure A.6: Fluorescence emission measurements of 0.01 M n-propylamine solutions containing various concentrations of P3M, using an excitation wavelength of 405 nm.....147

Figure A.7: Fluorescence standard curve prepared using the 443 nm emission peak from the standards in the previous figure. This peak was used to avoid overlap with the water Raman peak at ~470 nm. A linear relationship was observed between emission intensity and concentration over the range of concentrations used in this work.....148

Figure A.8: Fluorescence emission measurements from solutions created by cleaving bound P3M into solution. The spectrum labeled "Backside" corresponds to a solution prepared by removing bound P3M from the backside of a 700 °C pretreated sample titrated with P3M.....149

Figure A.9: *In situ* PL spectra after P3A exposure (— . —) and after subsequent annealing at 300 °C (———) from fused silica samples pretreated at 700 °C 150

Figure A. 10: *In situ* PL spectra from fused silica samples preheated to various temperatures after P3A exposure. 150

Figure B.1: *Ex situ* emission spectra (Left) and fluorescence decay curves (Right) from 0.08 P3M / nm^2 sample collected using either no polarization (Unpolarized) or with a polarizer set at 0° between excitation monochromator and sample and a polarizer set at 55° between sample and detector monochromator (Magic Angle). Both the steady-state and time-resolved measurements appear nearly identical between the two settings. The decay curve collected using magic angle polarizer settings was scaled by a factor of two, due to the very low hit rate obtained with polarizers in place. 153

Figure B.2: Fluorescence spectra from solutions prepared by removing P3M molecules from sample surfaces that had been cleaved from the center of the sample, to ensure molecules adsorbed on the edges did not contribute. The cleaved wafers were generally approximately 0.9 cm × 0.9 cm; however, the final dimensions of each sample were measured and used in the calculations. 154

Figure B.3: *In situ* emission spectra collected before and after the backside of the sample was exposed to atomic deuterium generated on a hot tungsten filament. The low wavelength features are attributed to low densities of fluorophores (monomer emission) on the back of the sample, which are eliminated by the atomic deuterium exposure. 155

Figure B.4: *In situ* emission spectra collected with our without 425 nm long-pass filter in place, showing the artifact around 550 nm due to the filter.155

Figure B.5: **(A)** Normalized *in situ* and *ex situ* emission spectra from low density (red line) and high density (black line) samples. **(B)** *In situ* emission spectra from sample collected after P3M exposure process (*In situ*) and after reloading sample back into vacuum system after *ex situ* measurements (*In situ* reloaded). The relative *ex situ* emission spectrum is shown for comparison. 156

Figure B.6: *In situ* emission spectra from samples displaying monomer (left) and excimer-like (right) emission collected at various chamber pressures. Pressures were increased by isolating pumps and leaking in air. Monomer emission displays a slight shift in the position of the vibronic peaks when the pressure is increased to 10^{-4} torr, and the intensity decreases only slightly with pressure up to 3 torr. The position of the excimer-like peak does not change with pressure, but the intensity decreases by approximately half between the $< 10^{-8}$ torr and 2 torr measurements. However, *ex situ* measurements were performed with pressures below 15 mtorr, so that little fluorescence quenching is expected for either sample at this pressure. 157

Figure B.7: Time-resolved emission spectra from the sample with 0.03 P3A / nm^2 showing only monomer emission in all time windows. Essentially no signal is observed in the latest time window. 158

Figure B.8: Fluorescence decay profiles from samples with various fluorophore densities.....159

Figure B.9: Fluorescence decay profiles from samples with various fluorophore densities.....160

Figure B.10: Deconvoluted emission spectrum from a sample with physisorbed material (2.36 P3M / nm^2) showing large contribution from a fully relaxed (600 nm centered) emission feature. The integrated intensity is approximately two-thirds attributed to fully relaxed emission and one-third attributed to emission from a partially relaxed species. The contribution from fully relaxed species is significantly larger than from samples with chemically bound P3M (maximum density of 1.56 nm^{-2}). 161

Figure C.1: (Left) TPD spectra showing D_2^+ (m/z 4) signal from Ge(100) samples given various exposures of atomic deuterium. (Right) Plot of D_2^+ signal versus exposure for low exposures. 162

Figure C.2: TPD spectra of m/z 44 (SiO^+) from thermal oxide on Si(100) before and after exposure to 1.0 ML Si. 163

Figure C.3: Si $2p_{3/2}$ XP spectra from fused silica samples given various Si exposures. Spectra have been shifted so that the Si^{4+} peak is centered at 103.5 eV to account for charging.....163

Chapter 1: Introduction

1.1 Overview

Oxide materials have many technological applications, including supported catalysts, magnetic recording media, corrosion protection, and thermal coatings [1–3]. Certain oxides also serve a critical role in microelectronic devices. These materials are used as the gate dielectric in transistors for logic and memory applications [4–6]. For many of the applications involving oxide materials, either metal or semiconductor particles or films are deposited on the oxide. Control over this deposition process is critical to creating material structures with desirable properties.

Defect sites on oxide surfaces can trap adatoms, leading to the formation of stable clusters and eventually larger particles or films [7]. Such processes are shown in Figure 1.1. Generation or passivation of defect sites could then be used to provide additional control over deposition processes. Such control could enable selective deposition of metal or semiconductor films on specific surfaces or deposition of ultra-thin continuous metal or semiconductor films on oxide surfaces. Additionally, supported oxide catalysts with high loadings of metal particles could be generated using this approach.

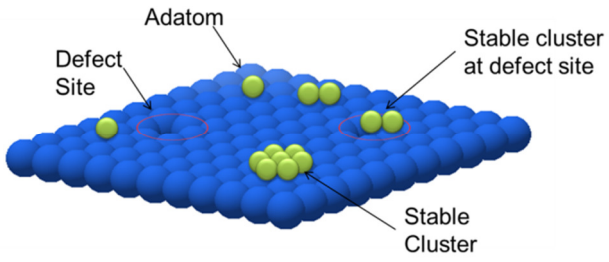

Figure 1.1: Schematic of defect mediated nucleation processes.

The ability to characterize defect sites, which trap adatoms and influence particle deposition, would provide valuable insight into the chemical nature of such sites and enable one to determine how various processes affect the density of defect sites. Unfortunately, as described below, low density surface defect sites on many oxide materials are currently experimentally inaccessible. The development of a technique to characterize low density sites on planar oxide surfaces is the primary focus of this dissertation.

1.2 BACKGROUND

Particle and film formation are governed by several competing phenomena. Nucleation of adatoms generates the initial stable clusters. Further incorporation of adatoms into a particle causes growth. Particle density decreases through either agglomeration, in which particles merge with their neighbors, or Ostwald ripening, in which smaller particles give up their constituents to larger particles [7]. Semiconductor and metal particles generally grow in a Volmer-Weber (VW), or three-dimensional, growth mode on oxide materials, due to differences between surface and interfacial energies [7]. This means that particles tend to form on these surfaces prior to film formation, so that a continuous film is only obtained when sufficient material has been deposited to cause coalescence of all the particles, as demonstrated in Figure 1.2. One strategy for achieving ultra-thin films is then to increase the nucleation density, so that each particle has to grow less to achieve a continuous film.

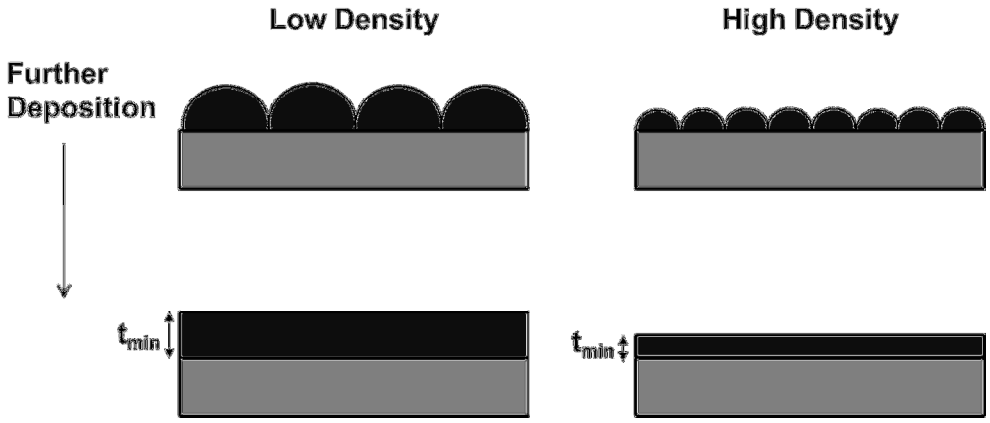

Figure 1.2: Schematic showing influence of particle density on the minimum thickness, t_{min}, of a continuous film for materials that grow in a three-dimensional growth mode.

One approach to controlling nucleation is to introduce defects on surfaces that can serve as traps for adatoms. A number of systems including Fe on Cu(100) [8], metals on MgO [9–11] and TiO_2 [1,12], and Au on SiO_2 [13] are known to possess some form of defect mediated nucleation. A critical cluster size of zero, indicating a single adatom is stable on the surface, has been observed for nucleation of germanium on SiO_2 [14] and HfO_2 [15], suggesting defects may play a role in mediating nucleation in these systems as well.

Defects are well known to govern a number of important properties of surfaces, such as catalytic activity [2]. Different oxides are known to have different defects due in large part to the differences in bonding of their constituents. Amorphous SiO_2 forms covalent bonds between Si and O atoms and forms a continuous random network (CRN) with an average oxygen coordination number of two [3,16,17]. Transition metal oxides have more ionic bond character and form random close packed (RCP) networks that result in a higher oxygen coordination number [17]. Although both silica (SiO_2) and transition metal oxides have high heats of formation, making defects energetically

unstable, the SiO_2 bonding network allows for defects to relax much better than in transition metal oxides [17]. This means that, in general, silica is expected to have a lower density of intrinsic defects compared to metal oxide materials. A particularly important class of defects that is believed to be common in most oxide systems is the oxygen vacancy defect (OVD) [2,16]. This type of defect is responsible for color, or F, centers in materials such as MgO [2,3] and has also been observed directly on TiO_2 [18]. Properties of OVDs can vary significantly between different classes of oxides, depending on types of bonding between the constituent atoms [3].

Surface defects on oxides have been studied for some time, but little direct knowledge of surface OVDs is available on silica or other wide band gap materials. This is because these materials are insulating, which limits the ability of traditional surface science techniques such as x-ray photoelectron spectroscopy (XPS) and scanning tunneling microscopy (STM) to study these structures in detail. However, Min and coworkers did use STM to study Au nucleation on thin films of SiO_2 on Mo and found defect mediated nucleation, which they attributed to oxygen vacancy clusters, although they were unable to directly identify the defects [13]. This indicates such sites may play an important role in nucleation of other materials both on silica and on other oxide materials. Additionally, such defects can be artificially introduced in oxides by irradiation with electrons [19], γ-rays [20], or ions [21,22]. Fast atom bombardment of both SiO_2 and ZrO_2 with Ar atoms was shown to reduce the oxygen content of these materials near their surface, although the effect was greater for ZrO_2 [23]. Chemical approaches can also be used to create defects. Winkenwerder and Ekerdt demonstrated enhanced trapping of germanium on SiO_2 after the surfaces was exposed to SiH_x (x = 1,2,3) fragments generated by cracking disilane on a hot tungsten filament [24]. The

enhanced nucleation was attributed to defects generated by the SiH_x exposure process, although the chemical nature of these defect sites was unclear.

The work presented in this dissertation is focused on the study of the silica surface. The surface chemistry of silica has been studied extensively due to silica's use in applications such as chromatography, absorbents, and as a catalyst support [25–28]. The primary surface sites on silica are hydroxyl sites and siloxane bridges [25,28]. Hydroxyl sites are well studied, with a fully hydroxylated surface having approximately 5×10^{14} sites / cm^2 [25]. Heating silica in a vacuum leads to condensation of adjacent hydroxyl sites and the formation of water and siloxane bridge sites [25,28]. Siloxane bridge sites are generally unreactive, however a small fraction of these sites are highly reactive strained sites that are known to react with water, ammonia, and alcohols [29]. The strained siloxane sites are believed to be edge sharing tetrahedron with densities on the order of 10^{12} sites / cm^2 [30].

As discussed above, detection of OVD sites on the surface of silica remains experimentally challenging. However, surface defects on silica have been studied computationally [31–33]. Using simulations, Kuo and Hwang identified oxygen vacancy, nonbridged oxygen, threefold coordinate Si, silanone, and dicoordinated Si (silylene) point defects on the surface of amorphous silica. Neutral oxygen vacancy defects are also predicted to convert to a structure consisting of a silylene and a silanone group [33]. Experimental detection of such sites would enable determination of their densities and also provide insight into their role in defect mediated nucleation processes.

1.3 OBJECTIVE AND OVERVIEW OF CHAPTERS

The objective of the work described herein is to demonstrate that creation of surface defects on oxides can lead to enhanced nucleation of semiconductor particles and to understand the chemical nature of both the intrinsic and generated defect sites. This work is motivated by the desire to utilize defect mediated nucleation to control deposition of metal and semiconductor films on oxide materials. The oxide used for all studies described in this work is fused silica, or amorphous SiO_2. This material was chosen for study both because it is technologically relevant and because much is already known about its surface properties. Each subsequent chapter describes a separate aspect of this project and, generally, a separate publication. The final chapter, Chapter 6, contains a summary of the work and suggestions for future research.

In Chapter 2, exposure of SiO_2 surfaces to SiH_x fragments (Si exposure process) is shown to increase the density of germanium nanoparticles deposited by how-wire chemical vapor deposition. The particle density can be increased by an order of magnitude using the exposure process, from approximately 10^{11} to 10^{12} particles / cm^2. The SiH_x fragments are presumed to generate defect sites on the SiO_2 surface, although characterization of these sites could not be accomplished using traditional surface science techniques. The content of this chapter has been published in *The Journal of Crystal Growth*.

The inability to characterize either the intrinsic defect sites or sites generated by the Si exposure process motivated the development of a new experimental technique capable of characterizing low density sites on planar oxide surfaces. This strategy involves using fluorescent probes to titrate specific surface sites, enabling both selectivity and high sensitivity. Chapter 3 describes the development the fluorescent probe technique and characterization of free hydroxyl and strained siloxane sites on planar

silica surfaces in vacuum. Perylene derivatives with either alcohol functional groups were used to titrate free hydroxyl sites and perylene derivatives with amine functional groups were used to selectively titrate strained siloxane sites. Densities of the former site were found to be approximately 0.8 – 1.5 × 10^{14} sites / cm^2, depending on the pretreatment temperature, in good agreement with literature values for high surface area silica. Strained siloxane sites were readily detected using this technique using *in situ* fluorescence emission measurements, with estimated densities of 0.5 – 2.5 × 10^{12} sites / cm^2. A detection limit of below 10^{10} sites / cm^2 was estimated for this technique, demonstrating its much higher sensitivity relative to other surface science tools, such as XPS. The content of this chapter has been published in the journal *Langmuir*.

The luminescence from surfaces with covalently attached fluorescent molecules was found to vary dramatically as a function of fluorophore density. The relationship between fluorescence emission and the density of covalently attached perylene fluorophores is examined in Chapter 4. For low fluorophore densities (below 10^{13} cm^{-2}) , only monomeric emission is observed and emission intensity is found to be linear with density. Samples with fluorophore densities above 4.4 × 10^{13} cm^{-2} display excimer-like emission. Absorbance measurements indicate preferential alignment of the long axis of the perylene moieties in the direction normal to the surface with increasing fluorophore density, leading to a non-linear change in absorbance with density. Additionally, the quantum yield from the excimer-like species is shown to be lower than monomer species. The combination of these two phenomena explains the observed relationship between emission intensity and fluorophore density. Time-resolved measurements were performed and indicate Förster-type resonance energy transfer between perylene moieties. Emission from two types of excimer states, partially and fully relaxed, is identified based on comparison with other works using Langmuir-Blodgett films

containing perylene derivatives. Little emission from the fully relaxed state is observed from samples with covalently attached fluorophores. This is attributed to the use of a one-carbon tether between the perylene moiety and the functional group, which hinders the ability of the fluorescent molecule to interact with neighboring molecules. The presence of excimer-like emission indicates the presence of adjacent fluorophores on the sample surface. The content of this chapter has been submitted for publication.

After demonstrating the feasibility of the fluorescent probe technique and understanding the nature of the luminescence, this approach is applied towards the study of oxygen vacancy defect sites on the surface of fused silica. Chapter 5 describes the use of a perylene derivative with a vinyl functional group for detecting low density sites, which are presumed to be OVDs. Intrinsic OVD sites with densities of approximately 10^{11} cm^{-2} are observed after annealing the planar silica samples in vacuum. The influence of atomic deuterium and the Si exposure process on the density of free hydroxyl, strained siloxane, and OVD sites is examined. Neither atomic deuterium nor the Si exposure process appears to change the density of free hydroxyl sites. The Si exposure process is shown to decrease the density of strained siloxane sites, and, initially, increase the density of bound vinyl derivatives of perylene. The latter result suggests the formation of OVD-like sites during the Si exposure process. Additionally, atomic deuterium exposure leads to a similar increase in bound vinyl derivative density. These results indicate that strained siloxane sites are converted to an OVD-like site upon exposure to SiH_x fragments. The density of such sites after the Si exposure process appears to be approximately 10^{12} cm^{-2}. The densities of intrinsic OVD sites and OVD-like sites correspond to the nucleation densities of germanium on SiO_2 without and with the Si exposure process, respectively. This indicates these defect sites are responsible for controlling nucleation for this particular material system.

Chapter 6 summarizes the results presented in this dissertation and makes recommendations for futures studies that leverage the knowledge and techniques developed in this work.

1.4 REFERENCES

[1] E. Wahlström, N. Lopez, R. Schaub, P. Thostrup, a. Rønnau, C. Africh, et al., Bonding of Gold Nanoclusters to Oxygen Vacancies on Rutile TiO2(110), Phys. Rev. Lett. 90 (2003) 1–4.

[2] G. Pacchioni, Oxygen Vacancy: The Invisible Agent on Oxide Surfaces, ChemPhysChem. 4 (2003) 1041–1047.

[3] F. Cinquini, C. Di, E. Finazzi, L. Giordano, Theory of oxides surfaces , interfaces and supported nano-clusters, (2007) 827–845.

[4] K. Eisenbeiser, Device Principles of High-K Dielectrics, in: A. Demkov, A. Navrotsky (Eds.), Mater. Fundam. Gate Dielectr., Springer, Dordrecht, The Netherlands, 2005: pp. 37–56.

[5] S. Guha, V. Narayanan, High-k/Metal Gate Science and Technology, Annu. Rev. Mater. Res. 39 (2009) 181–202.

[6] G.W. Burr, B.N. Kurdi, J.C. Scott, C.H. Lam, K. Gopalakrishnan, R.S. Shenoy, Overview of candidate device technologies for storage-class memory, IBM J. Res. Dev. 52 (2008) 449–464.

[7] C. Ratsch, J. Venables, Nucleation theory and the early stages of thin film growth, J. Vac. Sci. Technol. A Vacuum, Surfaces, Film. 21 (2003) S96–S109.

[8] D. Chambliss, K. Johnson, Nucleation with a critical cluster size of zero: Submonolayer Fe inclusions in Cu (100), Phys. Rev. B. 50 (1994) 5012–5015.

[9] G. Haas, A. Menck, H. Brune, J. Barth, J.A. Venables, K. Kern, Nucleation and growth of supported clusters at defect sites: Pd/MgO (001), Phys. Rev. B. 61 (2000) 105–108.

[10] A. Bogicevic, D. Jennison, Effect of oxide vacancies on metal island nucleation, Surf. Sci. 515 (2002) L481–L486.

[11] J. Venables, Nucleation and growth on defect sites: experiment–theory comparison for Pd/MgO (001), J. Physics-Condensed Matter. 18 (2006) S411–S427.

[12] J. Zhou, D. a. Chen, Controlling size distributions of copper islands grown on TiO2()-(1×2), Surf. Sci. 527 (2003) 183–197.

[13] B. Min, W. Wallace, A. Santra, D.W. Goodman, Role of defects in the nucleation and growth of Au nanoclusters on SiO2 thin films, J. Phys. Chem. B. 108 (2004) 16339–13343.

[14] Q. Li, J.L. Krauss, S. Hersee, S.M. Han, Probing Interactions of Ge with Chemical and Thermal SiO to Understand Selective Growth of Ge on Si during Molecular Beam Epitaxy Probing Interactions of Ge with Chemical and Thermal SiO 2 to Understand Selective Growth of Ge on Si during Molecular Beam E, (2007).

[15] S. Coffee, J. Ekerdt, Investigation of Volmer-Weber growth mode kinetics for germanium nanoparticles on hafnia, J. Appl. Phys. 102 (2007) 1149129.

[16] J. Robertson, P. Peacock, Atomic Structure, Interfaces, and Defects of High Dielectric Constant Gate Oxides, in: A.A. Demkov, A. Navrotsky (Eds.), Mater. Fundam. Gate Dielectr., Springer, Dordrecht, The Netherlands, 2005: pp. 179–214.

[17] G. Lucovsky, Electronic Structure and Chemical Bonding in High-K Transition Metal and Lanthanide Series Rare Earth Alternative Gate Dielectrics, in: A.A.

Demkov, A. Navrotsky (Eds.), Mater. Fundam. Gate Dielectr., Springer, Dordrecht, The Netherlands, 2005: pp. 109–178.

[18] R. Schaub, E. Wahlström, A. Rønnau, E. Lagsgaard, I. Stensgaard, F. Besenbacher, Oxygen-mediated diffusion of oxygen vacancies on the TiO2(110) surface., Science. 299 (2003) 377–379.

[19] V. Bermudez, V. Ritz, Investigation of the silica surface via electron-energy-loss spectroscopy, Phys. Rev. B. 20 (1979) 3446–3455.

[20] G. Buscarino, S. Agnello, F. Gelardi, Characterization of E′δ and triplet point defects in oxygen-deficient amorphous silicon dioxide, Phys. Rev. B. 73 (2006) 1–8.

[21] Y. Eyal, R. Evron, Y. Cohen, Defect Structure of Ion-Irradiated Amorphous SiO2, J. Appl. Crystallogr. 30 (1997) 618–622.

[22] R. Devine, The structure of SiO 2, its defects and radiation hardness, Nucl. Sci. IEEE Trans. 41 (1994) 452–459.

[23] F. Iacona, R. Kelly, G. Marletta, Regular Articles-X-ray photoelectron spectroscopy study of bombardment-induced compositional changes in ZrO2, SiO2, and ZrSiO4, J. Vac. Sci. Technol. A Vacuum, Surfaces, Film. 17 (1999) 2771–2778.

[24] W.A. Winkenwerder, J.G. Ekerdt, Germanium interactions with Si-etched silicon dioxide, Surf. Sci. 602 (2008) 2796–2800.

[25] L. Zhuravlev, The surface chemistry of amorphous silica. Zhuravlev model, Colloids Surfaces A. 173 (2000) 1–38.

[26] B. Granqvist, T. Sandberg, M. Hotokka, Adsorption of organic probes on silica through Lewis interactions: A comparison of experimental results and quantum chemical calculations, J. Colloid Interface Sci. 310 (2007) 369–376.

[27] B.A. Morrow, I.D. Gay, Infrared and NMR Characterization of the Silica Surface, in: E. Papirer (Ed.), Adsorpt. Silica Surfaces, Marcel Dekker, Inc., New York, 2000: pp. 9–34.

[28] R.K. Iler, The Chemistry of Silica : Solubility, Polymerization, Colloid and Surface Properties, and Biochemistry, 1979.

[29] B. Morrow, I. Cody, Infrared studies of reactions on oxide surfaces. 6. Active sites on dehydroxylated silica for the chemisorption of ammonia and water, J. Phys. Chem. 80 (1976) 1998–2004.

[30] B. Bunker, D. Haaland, T. Michalske, W. Smith, Kinetics of dissociative chemisorption on strained edge-shared surface defects on dehydroxylated silica, Surf. Sci. 222 (1989) 95–118.

[31] C. Wang, N. Kuzuu, Y. Tamai, Effects of charge transfer on a-SiO[sub 2] surface structure: A molecular dynamics study, J. Appl. Phys. 92 (2002) 4408.

[32] C.-L. Kuo, S. Lee, G. Hwang, Strain-Induced Formation of Surface Defects in Amorphous Silica: A Theoretical Prediction, Phys. Rev. Lett. 100 (2008) 1–4.

[33] C. Kuo, G. Hwang, Structure and interconversion of oxygen-vacancy-related defects on amorphous silica, Phys. Rev. Lett. 97 (2006) 066101.

Chapter 2: Hot-wire CVD of Ge nanoparticles on Si-etched Silicon Dioxide

2.1 INTRODUCTION

Germanium nanoparticles (NPs) have attracted attention for their possible role as a floating gate in nonvolatile memory devices [1-4]. Other researchers have explored quantum confinement-based photoluminescence from these structures [5-6]. In both cases, Ge NPs are deposited either on a SiO_2 surface or within a SiO_2 matrix. This work describes an approach to produce Ge NPs on a silica surface and control particle density based on purposefully introducing Si surface vacancies in the SiO_2.

A variety of techniques have been used to fabricate Ge NP systems including ion implantation [1], molecular beam epitaxy [5, 7-9], plasma-enhanced chemical vapor deposition (CVD) [4, 10], electron-beam evaporation [11], and radio-frequency (RF) sputtering [6]. Other researchers have used CVD to grow Si core – Ge shell NPs [2, 12-13], or grow Ge NPs over ultrathin oxide layers on a Si substrate [14-15].

Conventional CVD with GeH_4 is unable to nucleate Ge NPs directly on SiO_2 [15-17]. This is because Ge adatoms on SiO_2 are known to have low desorption activation energies [7] so that there is a significant desorption of adatoms at substrate temperatures high enough to decompose the precursor, which results in too low of an adatom concentration to facilitate nucleation. The weak adsorption and long diffusion length of Ge adatoms on silica have been exploited in selective growth techniques using a silica mask on a variety of materials, including Si [18-19] and HfO_2 [17]. Accumulation of Ge adatoms on a SiO_2 surface can be accomplished using hot-wire CVD (HWCVD), in

which the precursor gas is catalytically cracked on a hot filament to form GeH_x (x = 1, 2, 3). HWCVD with GeH_4 as a precursor has been used to deposit amorphous SiGe:H [20] and Ge:H [21] films on glass and to grow epitaxial Ge films on Si [22]. HWCVD was also used to generate high densities of Si NPs on SiO_2 [23] and the present work demonstrates that Ge NPs on SiO_2 can also be obtained using HWCVD.

To obtain Ge NPs on silica, the flux of adatoms arriving at the surface must exceed the flux desorbing from the surface, resulting in a net accumulation of adatoms. GeH_x adatoms are known to desorb from silica surfaces in two different pathways. At temperatures of 500 – 750 K recombinative desorption dominates [24]. At slightly higher temperatures, hydride ligands are removed from the GeH_x adatoms, resulting in Ge adatoms on the surface. Ge adatoms can desorb without recombining with hydrogen above 800 K [24]. To obtain particles, the surface temperature must be high enough for removal of hydride ligands but not so high that the flux of desorbing Ge adatoms exceeds the flux of impinging GeH_x. Therefore, directing a high GeH_x flux towards the sample and maintaining an optimal sample temperature are crucial for growing Ge NPs on silica.

This work also examines how defects created by etching SiO_2 with Si influence the density of Ge NPs. A schematic of this process and relevant reaction mechanisms are presented in Figure 2.1. Surface defects can serve as traps for adatoms and lead to nucleation in a variety of systems [25-28], including Ge deposition on HfO_2 [29]. Si-etching of SiO_2 has been shown to create defects through the reaction $Si(ad) + SiO_2(s) \rightarrow 2SiO(g)$ [30-31], and these defects can trap GeH_x adatoms [32]. The chemistry of the defect sites created during the etching process is presently unknown; however a structure containing adjacent germinal and vicinal hydroxyl groups has been proposed [32]. This may result from the hydration of an oxygen vacancy defect consisting of an oxygen dangling bond and silanone group proposed by Kuo and Hwang [33]. The GeH_x species

may be trapped at this site and, after losing hydride ligands, react with an additional Ge adatom or GeH_x fragment to form a stable and likely immobile cluster. Further accumulation of GeH_x species during HWCVD may then lead to an observable particle.

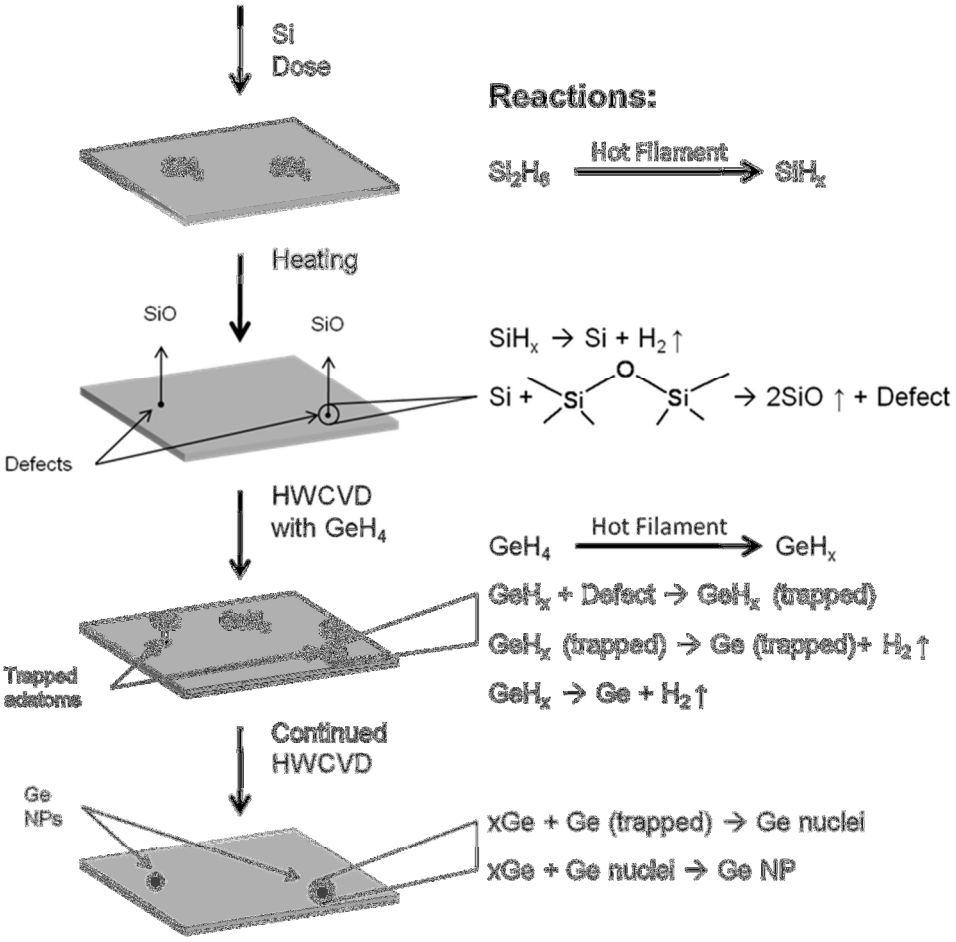

Figure 2.1: Schematic describing process used to deposit Ge NPs on fused silica surface.

Mean-field rate equations incorporating a critical cluster size can be used to model particle nucleation and growth [27, 34-36]. A critical cluster size is defined as the cluster size such that the addition of one adatom results in stable nuclei [35-36]. Researchers have determined critical cluster sizes for Ge on SiO_2 of zero [7] and one or

two [8], depending on substrate temperature. A critical cluster size of zero means that a single adatom is stable on the surface [26, 35-36]. Systems in which adatoms are strongly trapped by defects can have kinetics consistent with a critical cluster size of zero [26, 28]. Therefore, there is precedence for defect induced nucleation of Ge on SiO_2. However, the substrate temperature used to obtain a critical cluster size of zero was less than the temperature used in the experiments described here and any intrinsic defects may differ from those generated through the etching process. Regardless, since an increase in Si-etching presumably increases defect density, any positive correlation between etching and particle density would indicate the presence of defect-mediated nucleation of Ge NPs on SiO_2.

2.2 Experimental Procedure

Experiments were performed inside a multi-chamber ultra-high vacuum (UHV) system consisting of a growth chamber, a transfer chamber, and an analysis chamber equipped with a VG Microtech 8025 X-ray photoelectron spectroscopy (XPS) system and a CLAM2 cylindrical analyzer operating at pass energy of 100 eV. Al Kα radiation was used for all scans. Details of this system can be found elsewhere [31, 37]. The base pressure in all chambers was ~10^{-8} torr.

A typical experiment involved cracking Si_2H_6 on a hot-wire filament to deposit a controlled amount of SiH_x (x = 1, 2, 3) followed by rapidly heating the sample to etch the silica surface with the silane fragments [32]. From now on, the SiH_x exposure will be referred to as the Si dose for brevity. HWCVD and thermal CVD using the GeH_4 precursor were then used to grow Ge NPs. Thermal CVD was performed immediately following HWCVD using GeH_4 in order to increase the size of particles formed during

HWCVD so they could be more easily observed in scanning electron microscope (SEM) images. Control experiments were conducted to ensure no germanium particles were nucleated by thermal CVD alone. The same sample and filament configuration is used for dosing Si and for HWCVD with GeH_4 and has been described previously [29, 37-38]. Briefly, the sample is positioned 3 cm from a 250 W Osram Xenophot bulb with a section of the glass enclosure removed. A current of 4 A is supplied to the bulb, resulting in a filament temperature of ~ 1800 K [38].

Fused silica was used as the substrate to eliminate secondary sources of Si during XPS analysis. Wafers (Siegert Consulting) were diced into 16 mm x 16 mm squares and cleaned in a H_2SO_4:H_2O_2:H_2O (6:2:1) solution for 15 min. The wafers were placed on a cleaned Mo ring and loaded into the chamber through a load lock. Samples were then annealed at ~975 K for 15 min. After the sample had cooled to ~ 525 K, the sample was transferred to the analysis chamber and an XPS scan was collected to ensure the surface had minimal carbon contamination.

To deposit SiH_x, samples were transferred to the growth chamber and exposed to a calibrated dose of Si by cracking 4% Si_2H_6 in He (Voltaix) on a hot tungsten filament [37]. The partial pressure of disilane was 8×10^{-8} torr for all Si doses and the exposure time was adjusted to deposit various quantities of Si. One monolayer equivalent (ML) was deposited in 3.75 min.

After the Si exposure, an XP spectrum was collected. The Si peak associated with the deposited radicals could not be differentiated from the large peak due to the SiO_2 substrate and is therefore not shown. The samples were then heated at a linear rate of 2 K/s to ~950 K to facilitate the etching reaction and remove all Si [32]. After cooling, another XP spectrum was collected, which is again not shown. Samples were then transferred back to the growth chamber and heated to ~800 K. The wafers were allowed

to thermally equilibrate for 15 min before introducing 4% GeH_4 in He (Voltaix) at a germane partial pressure of 1.6×10^{-7} torr and turning on the cracking filament for 12.5 min. After HWCVD, the filament was turned off and the partial pressure of germane was increased to 1×10^{-4} torr for 15 min. Following thermal CVD, gas flow was stopped and the sample heater was turned off. The samples were allowed to cool before being transferred back to the analysis chamber where a final XP spectrum was collected. The sample was then removed from the system.

All samples were sputter coated with ~ 2 nm Ir to reduce charging in SEM. Images were collected with a Zeiss Supra 40VP using an accelerating voltage of 10 kV. Particles were counted in two ways. One image was selected from each sample and at least one thousand particles were counted manually in that image. The particle diameters were also measured. Additionally, four images from each sample had particles counted using the "Find Maxima" command in ImageJ. The results of both types of counting were similar.

2.3 RESULTS AND DISCUSSION

Samples were prepared with 0, 0.2, 0.4, 0.6, and 1.0 ML Si doses. Figure 2.2 shows Ge $2p_{3/2}$ XP spectra taken after HW and thermal CVD of germanium. Control experiments (not shown) have verified that the peak around 1218 eV, near the expected binding energy of the Ge^0 peak [24], is due to material deposited on the Mo foil holding the sample in place. This was observed in all samples and no further analysis was done on this peak. Because of the insulating nature of the sample, charging was significant and no attempt was made to adjust the peak positions. Only Ge^0 is expected, because Ge is thought to be unable to abstract oxygen from SiO_2 at moderate temperatures [7]. The

figure clearly shows that the peak corresponding to Ge on the sample surface increases in intensity with an increasing Si dose.

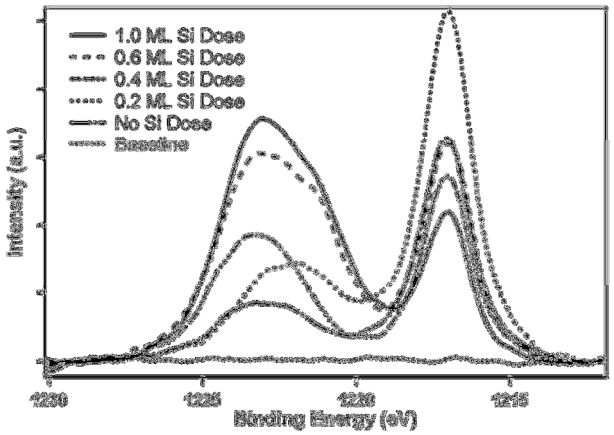

Figure 2: Ge $2p_{3/2}$ XP spectrum taken after HW and thermal CVD using GeH_4 for various samples. The higher binding energy peak (~1223 eV) is from the silica surface while the lower binding energy peak is from the Mo foil holding the sample in place.

One possible explanation for an increase in Ge NP density with increasing Si dose is that Si NPs are formed during the Si-etching process and that a Ge shell is grown on top of these structures, similar to growth techniques mentioned previously [2, 12-13]. Previous work has shown that seeding the surface with Si nuclei can affect densities of both Si NPs [37] and Ge NPs [12-13]. Although Winkenwerder and Ekerdt have shown that no Si particles were deposited during the etching process [32], additional control experiments were performed to ensure that no Ge particles were observed when only thermal CVD was used. As discussed above, thermal CVD with GeH_4 on bare silica is unable to deposit Ge [15-17], however if Si NPs are present on the surface after the etching process, a Ge shell should be deposited through thermal CVD alone [12-13]. Figure 2.3 shows the Ge $2p_{3/2}$ XP spectra for two samples exposed to only thermal CVD

with GeH_4 precursor. Both samples show a strong peak corresponding to deposition on the Mo foil, but even the sample given a 1.0 ML Si dose shows no significant Ge peak from the sample surface, indicating deposition did not occur. This is corroborated by SEM images presented below. Therefore, there is strong evidence that no Si NPs are deposited during the etching process, so the increased particle density due to increased etching is attributed solely to the creation of defects during Si-etching. Additionally, the control experiments show that all nucleation occurs during HWCVD.

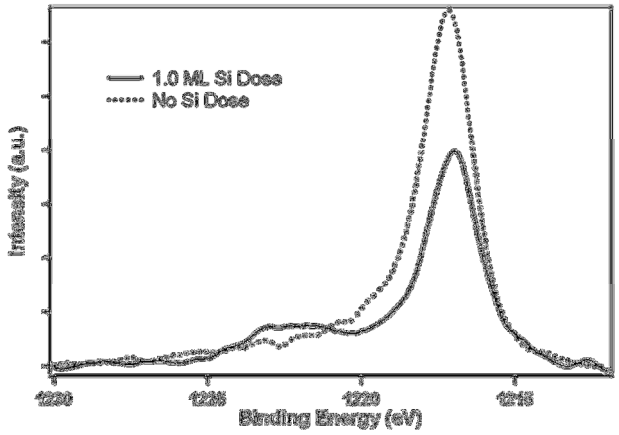

Figure 2.3: Ge $2p_{3/2}$ XP spectrum taken after exposing samples to thermal CVD with germane precursor without any HWCVD.

SEM images from each of the etched samples, including the etched control sample, are shown in Figure 2.4. The right half of each image has been enhanced to improve the contrast between particles (if present) and substrate. Particles are clearly visible in all images except (a), which is the 1.0 ML Si-etched sample given thermal CVD only. The faint structures visible in (a) and between particles in the remaining images correspond to Ir grain boundaries. The areal density of particles clearly increases with increasing Si-etching. The lack of particles in (a) is further evidence that no Ge was

deposited on the etched control sample. Therefore the presence of Si particles as a result of the Si deposition and subsequent heating is unlikely. The remaining images demonstrate that, even without Si-etching, HWCVD using the germane precursor can be used to grow high density, nanometer-sized Ge particles on SiO_2. However, the increasing particle density with increasing Si dose also provides strong evidence that the defects created by etching the silica surface with Si not only serves as traps for GeH_x radicals, as shown previously [32], but that these defects also act as nucleation sites for Ge NPs.

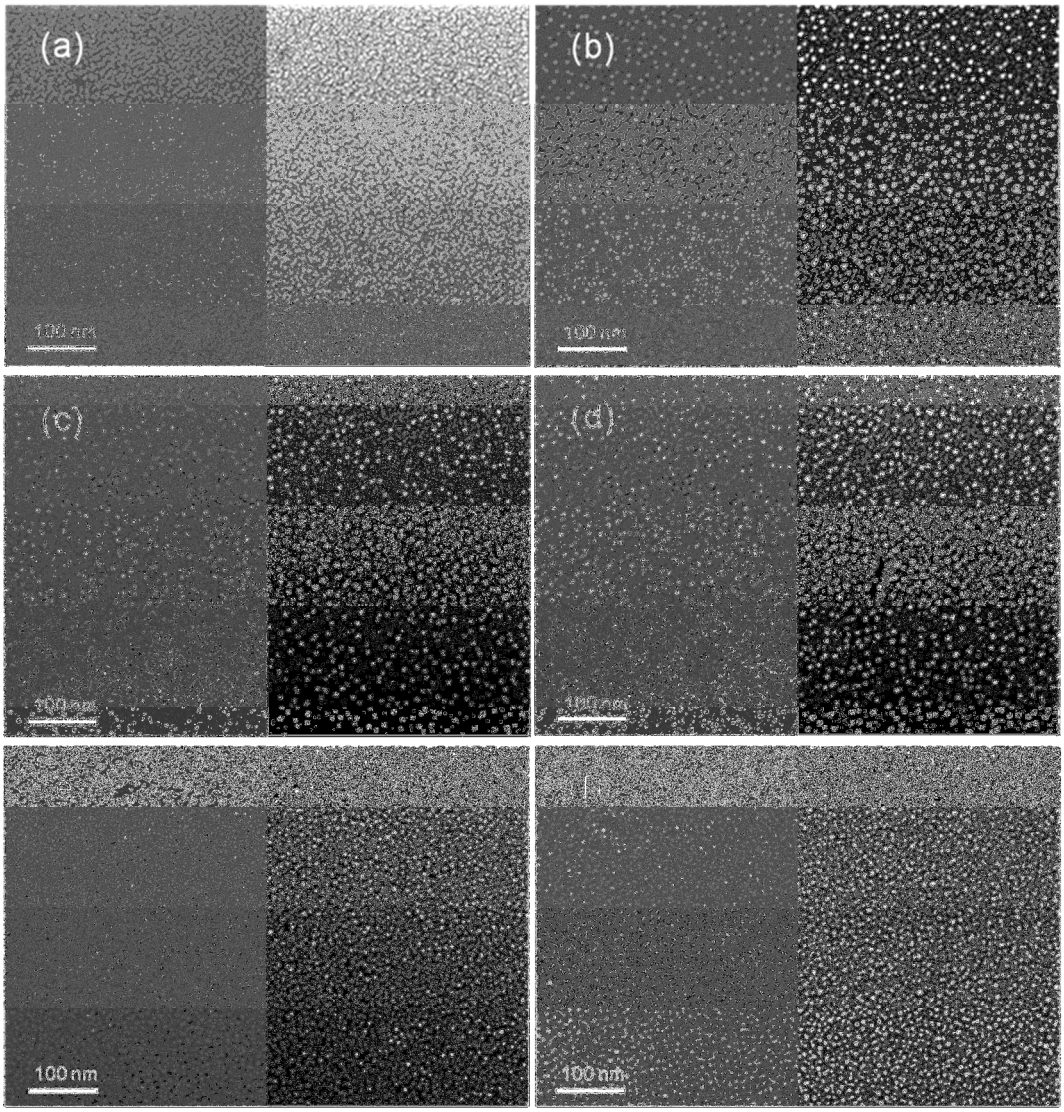

Figure 2.4: SEM images showing (a) control experiment and Ge particles on samples given (b) 0 ML, (c) 0.2 ML, (d) 0.4 ML, (e) 0.6 ML, and (f) 1.0 ML Si doses. The right half of each image has been enhanced to make particle density more obvious. The lack of contrast in (a) indicates the absence of particles.

The results of both manual and automated particle counting are shown in Figure 2.5. Areal density increases with increasing Si dose, reaching a value of over 1×10^{12} cm^{-2} at 1.0 ML etching, which is on the order deemed optimal for devices [39]. The error

bars for the automated counting corresponds to two standard deviations, showing that particle density does vary somewhat over the sample. Figure 2.6 shows the mean particle diameter for various Si exposures. The mean diameter for unetched samples is around 7 nm and decreases slightly with increasing Si dose.

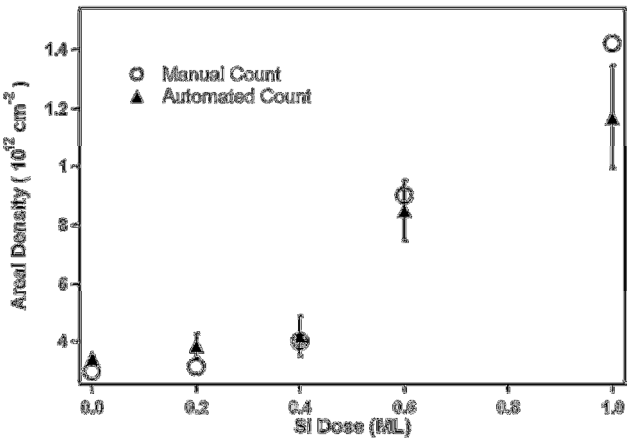

Figure 2.5: Ge particle densities for samples dosed with various amounts of Si. Particles were counted manually for one SEM image from each sample and a computer routine was used to estimate the number of particles in four images from each sample.

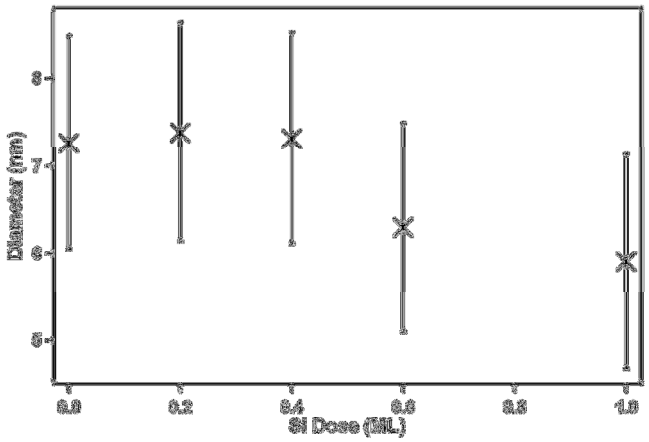

Figure 2.6: Mean particle diameter for samples given various Si doses. The error bars are two standard deviations in diameter.

Previous work had shown that defects created by etching SiO_2 surfaces with Si can trap GeH_x. (The first three surfaces in Figure 2.1.) The experiments reported here demonstrate that these same sites serve as nucleation centers for Ge NPs and that particle density can be controlled through the creation of these defect sites. Nucleation of Ge NPs on the unetched sample indicates either some type of defect is already present on the fused silica surface, possibly the same as generated by etching, or that another competing nucleation mechanism exists. One should note that Ge adatoms are unable to etch silica in the absence of Si, as the reaction is known to be $Ge + Si + 2SiO_2 \rightarrow GeO + 3SiO$ [7, 24]. Since all Si is removed during the etching process, the creation of defects during HWCVD of Ge NPs is unlikely. Further work is required to determine the chemical/structural nature of the defects created by Si-etching and whether these defects are intrinsic to silica surfaces.

In addition to achieving a high areal density, this growth technique produced a fairly uniform size distribution, which is similar to what is observed in HWCVD of Si NPs on fused silica [23]. The combination of high density, small particle size, and

narrow size distribution could make this technique valuable for the further study of non-volatile memory devices and quantum confinement photoluminescence.

2.4 CONCLUSION

Ge NPs have been grown on fused silica using a combination of HWCVD and thermal CVD with GeH_4 as the precursor gas. HWCVD was shown to nucleate Ge NPs on the silica surface while thermal CVD was used to increase the particle size to improve the quality of the data. Etching of the silica surface with Si prior to Ge deposition was shown to increase both the amount of material deposited and the areal density of NPs. Defects created during etching are believed to trap Ge adatoms and serve as nucleation sites for Ge NPs. Control over Ge particle density was demonstrated by changing the Si dose used to etch the surface. Further refinement of this technique may allow for precise control over areal density and particle size, which is necessary for device applications.

References

[1] M. Yang, T.P. Chen, J.I. Wong, C.Y. Ng, Y. Liu, L. Ding, S. Fung, A.D. Trigg, C.H. Tung, C.M. Li, Charge trapping and retention behaviors of Ge nanocrystals distributed in the gate oxide near the gate synthesized by low-energy ion implantation, J. Appl. Phys., 101 (2007) 124313.

[2] H. Liu, W. Winkenwerder, Y.R. Liu, D. Ferrer, D. Shahrjerdi, S.K. Stanley, J.G. Ekerdt, S.K. Banerjee, Core-Shell Germanium-Silicon Nanocrystal Floating Gate for Nonvolatile Memory Applications, IEEE T. Electron. Dev., 55 (2008) 3610-3614.

[3] M. Kanoun, C. Busseret, A. Poncet, A. Souifi, T. Baron, E. Gautier, Electronic properties of Ge nanocrystals for non volatile memory applications, Solid State Electron., 50 (2006) 1310-1314.

[4] T. Dürkop, E. Bugiel, I. Costina, A. Ott, R. Peibst, K.R. Hofmann, PE-CVD fabrication of germanium nanoclusters for memory applications, Mater. Sci.Eng. B, 147 (2008) 213-217.

[5] A.A. Shklyaev, M. Ichikawa, Visible photoluminescence of Ge dots embedded in Si/SiO_2 matrices, Appl. Phys. Lett., 80 (2002) 1432-1434.

[6] Y. Maeda, Visible photoluminescence from nanocrystallite Ge embedded in a glassy SiO_2 matrix: Evidence in support of the quantum-confinement mechanism, Phys. Rev. B, 51 (1995) 1658 -1670.

[7] Q.M. Li, J.L. Krauss, S. Hersee, S.M. Han, Probing interactions of Ge with chemical and thermal SiO_2 to understand selective growth of Ge on Si during molecular beam epitaxy, J. Phys. Chem. C, 111 (2007) 779-786.

[8] D. Leonhardt, S.M. Han, Energetics of Ge nucleation on SiO_2 and implications for selective epitaxial growth, Surf. Sci., 603 (2009) 2624-2629.

[9] L. Zhang, H. Ye, Y.R. Huangfu, C. Zhang, X. Liu, Densely packed Ge quantum dots grown on SiO_2/Si substrate, Appl. Surf. Sci., 256 (2009) 768-772.

[10] S. Foss, T.G. Finstad, A. Dana, A. Aydinli, Growth of Ge nanoparticles on SiO_2/Si interfaces during annealing of plasma enhanced chemical vapor deposited thin films, Thin Solid Films, 515 (2007) 6381-6384.

[11] I. Berbezier, A. Karmous, A. Ronda, A. Sgarlata, A. Balzarotti, P. Castrucci, M. Scarselli, M. De Crescenzi, Growth of ultrahigh-density quantum-confined germanium dots on SiO_2 thin films, Appl. Phys. Lett., 89 (2006) 063122.

[12] T. Baron, B. Pelissier, L. Perniola, F. Mazen, J.M. Hartmann, G. Rolland, Chemical vapor deposition of Ge nanocrystals on SiO_2, Appl. Phys. Lett., 83 (2003) 1444-1446.

[13] L. Masarotto, K. Yckache, A. Fanton, F. Aussenac, F. Fillot, Embedding of reduced pressure-chemical vapor deposition grown Ge nanocrystals in a high quality SiO_2 matrix for non-volatile memory applications, Thin Solid Films, 518 (2010) 5382-5386.

[14] C. Renard, M. Halbwax, D. Cammilleri, F. Fossard, V. Yam, D. Bouchier, Y. Zheng, Ge growth over thin SiO_2 by UHV-CVD for MOSFET applications, Thin Solid Films, 517 (2008) 401-403.

[15] M. Halbwax, C. Renard, D. Cammilleri, V. Yam, F. Fossard, D. Bouchier, Y. Zheng, E. Rzepka, Epitaxial growth of Ge on a thin SiO_2 layer by ultrahigh vacuum chemical vapor deposition, J. Cryst. Growth, 308 (2007) 26-29.

[16] S.K. Stanley, S.V. Joshi, S.K. Banerjee, J.G. Ekerdt, Surface reactions and kinetically-driven patterning scheme for selective deposition of Si and Ge nanoparticle arrays on HfO_2, Surf. Sci., 600 (2006) L54-L57.

[17] S.K. Stanley, S.V. Joshi, S.K. Banerjee, J.G. Ekerdt, Ge interactions on HfO_2 surfaces and kinetically driven patterning of Ge nanocrystals on HfO_2, J. Vac. Sci. Technol. A, 24 (2006) 78-83.

[18] Q. Li, S.M. Han, S.R.J. Brueck, S. Hersee, Y.B. Jiang, H. Xu, Selective growth of Ge on Si(100) through vias of SiO_2 nanotemplate using solid source molecular beam epitaxy, Appl. Phys. Lett., 83 (2003) 5032-5034.

[19] L.H. Nguyen, V. Le Thanh, D. Débarre, V. Yam, D. Bouchier, Selective growth of Ge quantum dots on chemically prepared SiO_2/Si(001) surfaces, Mater. Sci. Eng. B, 101 (2003) 199-203.

[20] Y. Xu, B.P. Nelson, L.M. Gedvilas, R.C. Reedy, Improving narrow bandgap a-SiGe:H alloys grown by hot-wire chemical vapor deposition, Thin Solid Films, 430 (2003) 197-201.

[21] L. Zanzig, W. Beyer, H. Wagner, High quality hydrogenated amorphous germanium prepared by the hot wire technique, Appl. Phys. Lett., 67 (1995) 1567-1569.

[22] C. Mukherjee, H. Seitz, B. Schroder, Growth of epitaxial germanium films on silicon using hot-wire chemical vapor deposition, Appl. Phys. Lett., 78 (2001) 3457-3459.

[23] N. Salivati, Y.Q. An, M.C. Downer, J.G. Ekerdt, Hot-wire chemical vapor deposition of silicon nanoparticles on fused silica, Thin Solid Films, 517 (2009) 3481-3483.

[24] W.A. Winkenwerder, J.G. Ekerdt, Interaction of germanium with silicon dioxide, Surf. Sci., 602 (2008) 2796-2800.

[25] R. Giulian, P. Kluth, L.L. Araujo, D.J. Llewellyn, M.C. Ridgway, Pt nanocrystals formed by ion implantation: A defect-mediated nucleation process, Appl. Phys. Lett., 91 (2007) 093115-093113.

[26] J.B. Wedding, G.C. Wang, T.M. Lu, Vacancy-enhanced submonolayer nucleation of Si on Si(111), Surf. Sci., 504 (2002) 28-36.

[27] J.A. Venables, L. Giordano, J.H. Harding, Nucleation and growth on defect sites: experiment–theory comparison for Pd/MgO(001), J. Phys.: Condens. Matter, 18 (2006) S411-S427.

[28] J. Zhou, D.A. Chen, Controlling size distributions of copper islands grown on TiO_2(110)-(1×2), Surf. Sci., 527 (2003) 183-197.

[29] S.S. Coffee, J.G. Ekerdt, Investigation of Volmer-Weber growth mode kinetics for germanium nanoparticles on hafnia, J. Appl. Phys., 102 (2007) 114912-114917.

[30] D.C. Streit, F.G. Allen, Thermal and Si-Beam Assisted Desorption of SiO_2 from Silicon in Ultrahigh-Vacuum, J. Appl. Phys., 61 (1987) 2894-2897.

[31] W.T. Leach, J.H. Zhu, J.G. Ekerdt, Thermal desorption effects in chemical vapor deposition of silicon nanoparticles, J. Cryst. Growth, 243 (2002) 30-40.

[32] W.A. Winkenwerder, J.G. Ekerdt, Germanium interactions with Si-etched silicon dioxide, Surf. Sci., 602 (2008) 3071-3076.

[33] C.L. Kuo, G.S. Hwang, Structure and interconversion of oxygen-vacancy-related defects on amorphous silica, Phys. Rev. Lett., 97 (2006) 066101.

[34] C. Ratsch, J.A. Venables, Nucleation theory and the early stages of thin film growth, J. Vac. Sci. Technol. A, 21 (2003) S96-S109.

[35] D.D. Chambliss, K.E. Johnson, Nucleation with a critical cluster size of zero: Submonolayer Fe inclusions in Cu(100), Phys. Rev. B, 50 (1994) 5012-5015.

[36] J.G. Amar, F. Family, Critical Cluster Size: Island Morphology and Size Distribution in Submonolayer Epitaxial Growth, Phys. Rev. Lett., 74 (1995) 2066-2069.

[37] W.T. Leach, J.H. Zhu, J.G. Ekerdt, Cracking assisted nucleation in chemical vapor deposition of silicon nanoparticles on silicon dioxide, J. Cryst. Growth, 240 (2002) 415-422.

[38] S.S. Coffee, D. Shahrjerdi, S.K. Banerjee, J.G. Ekerdt, Selective silicon nanoparticle growth on high-density arrays of silicon nitride, J. Cryst. Growth, 308 (2007) 269-277.

[39] S. Tiwari, F. Rana, H. Hanafi, A. Hartstein, E.F. Crabbe, K. Chan, A silicon nanocrystals based memory, Appl. Phys. Lett., 68 (1996) 1377-1379.

Chapter 3. Titration of Free Hydroxyl and Strained Siloxane Sites on Silicon Dioxide with Fluorescent Probes

3.1 INTRODUCTION

The detection of low density sites on oxide surfaces remains a significant challenge, hindering our understanding of the role defect sites play in processes such as catalysis and nucleation on these surfaces [1–4]. In the present work, we demonstrate a technique using fluorescent probe molecules to titrate low density sites on planar silica surfaces in vacuum. Amorphous silica was chosen as the material system for this study, both because of its widespread use and because its surface chemistry has been extensively characterized, which enables validation of the fluorescent probe titration approach.

The silica surface consists of surface hydroxyl, or silanol, sites in addition to siloxane bridge sites [5–7]. Both single (≡Si-OH) and geminal (=Si-$(OH)_2$) silanol sites exist on the silica surface, although the fraction of geminal species is low [7,8]. Silanol sites can also be classified based on hydrogen bonding. Vicinal sites are surface hydroxyl groups that are hydrogen bonded to an adjacent silanol while free silanols are not hydrogen bonded to another surface hydroxyl site [5–7]. Both single and geminal species can be either free or hydrogen bonded [8]. Free and hydrogen bonded silanols are distinguishable by both their signature in infrared (IR) spectroscopy [9] and their chemical reactivity [10,11]. Numerous amorphous silicas, including silica gels, aerosils, and porous glasses, have been studied and the surface hydroxyl densities were found to be similar among the various types of silica, with a maximum surface OH density of 4.6 – 4.9 nm^{-2} [5,7,11,12]. The distribution of the free and hydrogen bonded sites on the

surface is readily altered by heating silica in a vacuum. As the temperature increases, adjacent silanol sites begin to condense, forming water, which desorbs, and a siloxane bridge site [5,7,9,13]. Because of their close proximity, vicinal silanols undergo condensation prior to free silanol sites. The coverage of each site as a function of vacuum anneal temperature has been studied and reviewed [7]. According to Zhuravlev, physisorbed water is completely removed from the silica surface by annealing to 200°C, while dehydroxylation begins at around 150 - 180 °C [7]. Most vicinal sites are eliminated in the temperature range 200 - 400 °C, with free silanol density increasing to a maximum of 2.05 nm^{-2} at 400 °C [7,11]. Further increase in temperature causes the density of free silanols to decrease and the average distance between surface hydroxyls to increase [7,11].

Some fraction of the siloxane bridges formed while heating a silica sample exhibit markedly increased reactivity. These sites are termed reactive or strained siloxane bridges and are believed to be edge-sharing defects [7,9,14,15]. Strained siloxane sites are detected on high surface area silica using IR spectroscopy by characteristic bands at 908 and 888 cm^{-1} [9,14,15]. These IR bands were observed by annealing silica in vacuum to temperatures of at least 600 – 700 °C [9,16,17]. Room temperature chemisorption of ammonia is observed on silica annealed in vacuum at temperatures as low as 350 °C and is attributed to the presence of strained siloxane sites [17]. The density of strained siloxane sites appears to increase with increasing vacuum anneal temperatures [9,14,17], with an estimated density of 0.04 – 0.13 nm^{-2} for pretreatment at 900 °C [15]. Chemisorption of water, alcohols, methylamine, and organosiloxanes, in addition to ammonia, has been shown to occur on the strained siloxane sites at room temperature [9,14,15,17–19].

Although much has been learned about the silica surface, as evidenced in the discussion above the primary tool for characterization of this system has been infrared spectroscopy. Other workers have also utilized nuclear magnetic resonance (NMR) spectroscopy,[8,13,20,21] chemical titration methods [10,22,23], thermogravimetric analyses [7,24], or a combination of techniques. Each of these techniques, however, has certain limitations. NMR and IR spectroscopies are not surface sensitive techniques, which can lead to difficulty in distinguishing internal and surface hydroxyls [7,10,11], and cannot quantify site densities directly. Chemical titrations, such as the one we report herein, are surface specific but can lead to underestimation of site densities due to steric hindrance for high density sites and bulky chemical probes [11]. Deuterium exchange combined with Brunauer-Emmett-Teller (BET) surface area analysis is another method to quantify silanol density; this method is both surface specific and not limited by steric hindrance [5,7], although the BET measurement can introduce some uncertainty into the calculated densities [20,24].

A significant limitation all the aforementioned techniques share is the need for high surface area silica samples. The ability to observe and quantify various sites on planar surfaces could enable direct study of how these sites impact surface processes such as catalytic reactions or particle nucleation [2]. However attempts to study sites on planar surfaces have been limited. Workers have used techniques including static secondary ion mass spectrometry (SIMS) [25], X-ray photoelectron spectroscopy (XPS) analysis of derivatized sites [25], attenuated total reflectance (ATR)-IR [26], and thermal desorption of methanol [27] to study silanol sites on planar silica surfaces. None of these methods can provide direct, absolute measurements of silanol densities. Observation of strained siloxane sites on planar surfaces is even more challenging due to the much lower density of such sites. Chiang and coworkers used reflection absorption infrared spectroscopy to

study strained siloxane sites on thin SiO_2 films deposited on a highly reflecting substrate [28], but, in addition to requiring a special substrate, this method cannot quantify the site density directly.

Fluorescence spectroscopy is a highly sensitive analytical technique [29,30], enabling detection of sites with low densities. Fluorescent probes have previously been used to study various types of surfaces. Pyrene derivatives with chloro- and alkoxysilane groups have been used to study hydroxyl sites on high surface area silica [31] and alumina [32]. Strongly hydrogen bonding perylene derivatives were used to study the passivation of silanol sites on glass [33]. Additionally, self-assembled monolayers (SAMs) of covalently attached pyrene derivatives on glass were prepared by Flink and coworkers [34], while the detection of different functional groups on oxidized SAMs using fluorescent probes has been demonstrated [35]. Xing and Borguet estimated a lower detection limit of 10^{-9} cm^{-2} for fluorescent probes bound to glass slides with amine, aldehyde, and epoxide terminated surfaces [36]. All of these approaches used solution phase reactions.

In the current work, experiments are performed in an ultra-high vacuum (UHV) system to ensure the stability of surface sites generated while heating a fused silica substrate to various pretreatment temperatures. Derivatives of perylene, a high quantum yield fluorophore [37], were used as the fluorescent probes. Similar molecules, such as pyrene derivatives, may also be suitable fluorescent probes for these studies. The use of perylene derivatives over other molecules was dictated by the overlap of the perylene absorption features with the excitation source (laser) used in this work. Alcohols are known to react with free silanol sites at elevated temperatures through an esterification reaction, yielding a covalently bonded Si-O-R site and water, where R is the carbon backbone of the alcohol [5,9,38–41]. Both alcohols and primary amines can chemisorb

on strained siloxane sites [15,17]. However amines should not react with hydroxyl sites at room temperature [17,18]. This difference in reactivity between the two functional groups is exploited to enable quantification of strained siloxane sites. A perylene compound containing an alcohol functional group, perylene-3-methanol (P3M), was used to titrate primarily free hydroxyl sites, while a compound with an amine group, perylene-3-methanamine (P3A) was used to specifically titrate strained siloxane sites, as shown in Figure 3.1. Because alcohol molecules also react with strained siloxane sites, the titration with P3M is not selective towards hydroxyl sites. However, because the density of strained siloxane sites is much lower than the density of hydroxyl sites, the reaction between P3M and the strained siloxane sites causes only a minor error in the measurement of silanol densities, as demonstrated below. The titration with P3A is selective towards strained siloxane sites. *In situ* photoluminescence (PL) measurements collected from each sample after titration provides insight into the relative number of probe molecules bound to the surface, while hydrolytic cleavage of bound P3M into solution enables determination of absolute fluorophore densities.

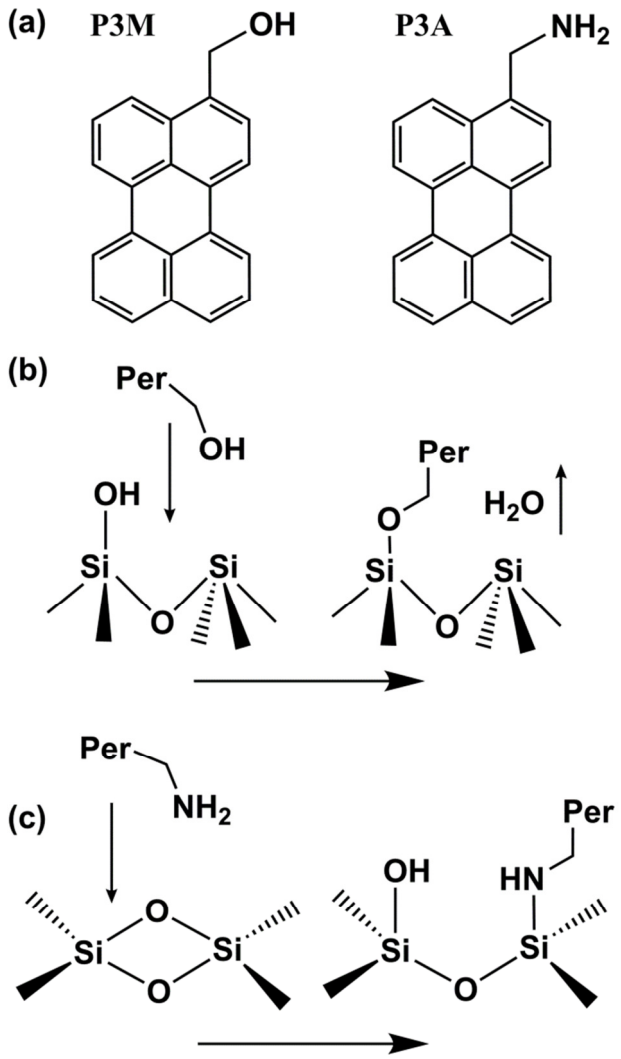

Figure 3.1: (a) Structures of perylene-3-methanol (P3M) and perylene-3-methanamine (P3A). (b) Reaction between P3M molecule and a free hydroxyl site. (c) Reaction between P3A molecule and a strained siloxane site.

3.2 EXPERIMENTAL

Synthesis of the compounds used in this work is described in Appendix A. As a final purification step, each precursor was sublimed onto aluminum foil wrapped around the cold finger in a sublimation apparatus. The material was then loaded into the evaporator immediately, as extended exposure to ambient conditions appeared to degrade

the precursor, which interfered with the experimental results. Experiments were performed in a multi-chamber (UHV) system described previously [42,43], with a base pressure of ~10^{-9} torr. Briefly, the system consists of three large chambers and one smaller chamber, all evacuated by turbomolecular pumps. A transfer chamber is connected by gate valves to a load lock, a growth chamber, and an analysis chamber. Attached to the transfer chamber is a quartz tube furnace used for pretreating and annealing samples. The transfer chamber is connected to a smaller exposure chamber by a gate valve, enabling evaporation of the organic precursors while minimizing contamination to the remaining system. The exposure chamber consists of a hook attached to a linear translator, enabling transfer of the samples between chambers, and an evaporator cell containing the appropriate compound. The evaporator cell consists of an aluminum cylinder with a cavity for holding the precursor-coated aluminum foil and is heated by a cartridge heater. A thermocouple is placed between the foil and cell walls to obtain an accurate measure of precursor temperature.

The transfer chamber also includes a viewport to which an optics assembly is mounted. This assembly consists of a set of lenses attached by fiber optics to a 405 nm continuous wave diode laser with an output power of 20 mW (CrystalLaser) and spectrometer with a wavelength range of 300 – 1050 nm (Ocean Optics QE6500). The laser and collection optics are mounted at an angle of ~30 ° from each other and focused onto the sample in the UHV system with a spot size of 1 mm^2, enabling *in situ* photoluminescence (PL) measurements. A 425 nm long pass filter was placed in line with the collection optics to prevent scattered laser light from reaching the spectrometer. Spectra were typically collected using a 1 s integration time and a three scan average. For spectra in which the intensity saturated the detector under these conditions, such as for the P3M titration experiments, an integration time of 0.25 s was used to collect the

spectra and the collected data were then multiplied by four to account for the shorter integration time and make all spectra comparable. Intensity was verified to be commensurate with integration time based on spectra from lower coverage samples.

In a typical experiment, cleaned fused silica wafers (Appendix A) are attached to a molybdenum sample holder and placed in the load lock. Samples were first moved to the tube furnace and pretreated by heating to the desired temperature. Temperature calibration was performed using an instrumented sample holder. All samples were soaked at the specified temperature for 30 min. After cooling to below 200 °C, samples were moved in front of the optics assembly for the collection of baseline PL measurements.

Samples were next moved to the exposure chamber. The evaporator containing the appropriate compound is preheated to ~100 °C or ~65 °C for P3M or P3A, respectively. The choice of temperature was based on the desire to ensure a sufficient amount of precursor reached the sample in a reasonable time, but also prevent degradation of the precursor, which was observed at higher precursor temperatures. The samples were placed ~2 cm from the evaporator and the sample was heated to ~80 °C by a cartridge heater attached to the hook assembly holding the sample puck. Exposure times of 60 min and 30 min were used for P3M and P3A exposures, respectively.

After exposing the sample to the precursor, the samples were moved in front of the optics assembly and PL spectra were collected. The samples were then moved to the tube furnace and the temperature was ramped to 300 °C at 30 °C / min. Samples were left at this temperature for 30 min to remove physisorbed molecules, leaving only chemisorbed species. After annealing, the samples were moved back in front of the optics assembly. The emission intensity gradually increased while the samples cooled. A spectrum was collected after no further changes in emission intensity were observed.

Samples exposed to P3M were removed from the system and placed with P3M exposed side face down on a silicone gasket with a 0.9 cm diameter circle cut out of the center. The gasket was then placed on a screw cap vial containing 10 ml of 0.01 M aqueous n-propylamine solution, which had been brought to a boil. The vial was flipped over to expose the selected area to the solution, ensuring that no molecules attached to the back or edges of the wafer were collected in solution. Experiments (Appendix A) indicated that minimal P3M was present on the backside of the wafers.

The fluorescence emission spectra from solutions prepared from samples were collected and the concentration of the solutions determined from the standard curve (Appendix A). From this and the area of the sample exposed to the solution, the density of P3M on the surface of each sample was determined.

3.3 Results and Discussion

The UV-Vis absorption and fluorescence emission spectra of perylene, P3M, and P3A solutions in cyclohexane are shown in Figure 2. All three compounds have similar spectra, and the 405 nm wavelength of the laser is shown to overlap with an absorption peak for all compounds. The emission spectra exhibit vibronic structure and are consistent with emission from a monomer species [44]. The similarity of the spectra demonstrates the separation of the functional group from the fluorophore by even a single carbon atom is sufficient to maintain the desired spectroscopic features.

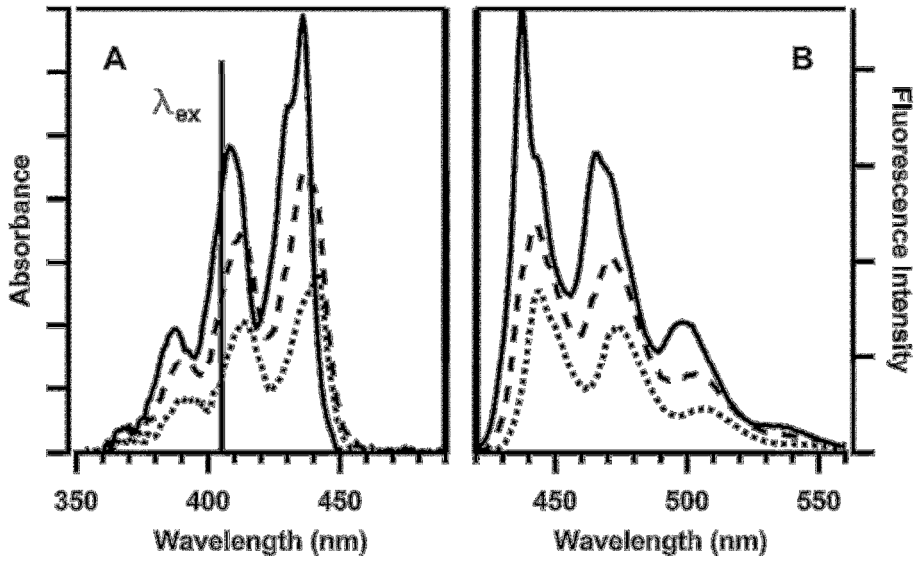

Figure 3.2: Absorption (A) and fluorescence emission (B) spectra from 1×10^{-6} M perylene (———), P3M (– – – -), and P3A (------) compounds in cyclohexane. The excitation wavelength for the emission spectra was 405 nm, the same wavelength as the laser use in *in situ* measurement.

In situ PL spectra from samples pretreated to 700 °C and then titrated with either perylene, P3M, or P3A is shown in Figure 3.3. The spectra clearly demonstrate the role the functional group, or lack thereof, plays in the binding of the fluorophore to the surface. Details of the P3M and P3A spectra are discussed below. For perylene exposure, only a very weak peak is present, and this is attributed to adventitious P3M or P3A from the chamber walls.

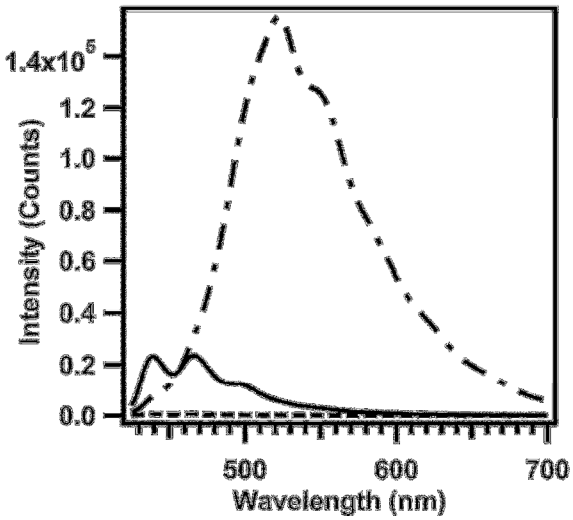

Figure 3.3: *In situ* PL spectra from fused silica wafers pretreated to 700 °C and then titrated with either perylene (------), P3M (— · —), or P3A (———).

3.2.1 Titration of silanol sites with P3M:

Surface hydroxyl sites can react with alcohol molecules, forming a covalent alkoxy group (Si-O-R) on the SiO_2 surface with the release of water [38–41]:

$$\equiv\text{Si-OH} + \text{ROH} \leftrightharpoons \equiv\text{Si-OR} + H_2O \qquad (3.1)$$

This reaction is known to be activated, typically requiring temperatures of greater than 200 °C for the vapor phase reaction [9,39,41]. Numerous attempts exposing a sample heated to such temperatures to P3M resulted in limited chemisorption of the fluorophore. The inability to titrate hydroxyl sites under these conditions can be rationalized by considering the influence of sample temperature on the overall reaction kinetics. Although the rate constant for the desired esterification reaction increases with increasing sample temperature, so too does the rate of desorption of the probe molecules. The overall degree of titration is dependent on both rates, as an increase in the desorption rate

of P3M leads to a decrease in the effective concentration of the molecule on the surface, effectively slowing the rate of titration. Increasing the flux of P3M by increasing the evaporator temperature can compensate for the increased rate of desorption, but the precursor appeared to degrade upon heating above ~150 °C in the evaporator, thus setting an upper limit on attainable flux. To overcome the limitations imposed by the reaction kinetics, a catalyst was introduced into the system to enable a lower temperature titration. Lewis bases, including ammonia and n-propylamine, have been shown to catalyze the reaction [39]. Experiments using n-propylamine did exhibit increased densities of bound P3M, however the measured densities still appeared lower than expected based on literature values.

A more effective catalyst proved to be P3A. A small sliver of P3A coated foil was added to the evaporator along with the P3M coated foil. Experiments performed using P3A catalyst resulted in bound P3M densities in good agreement with literature densities for hydroxyl sites, as discussed below. PL spectra from samples using P3A, n-propylamine, or no catalyst are provided in Appendix A and demonstrate that using P3A as a catalyst increases the amount of chemisorbed species. Control experiments (*vide infra*) verify that the chemisorbed species is primarily P3M, as P3A reacts only with strained siloxane sites and not with silanol sites, and the density of strained siloxane sites are expected to represent less than 10% of possible P3M binding sites [17]. P3A may be a more effective catalyst than n-propylamine because of the ability of the perylene group on P3A to interact with the same group on bound P3M, likely leading to an increased residence time of the P3A molecule on the surface compared with n-propylamine. Other molecules may also act as suitable catalysts for the reaction between silanol sites and P3M, however P3A was the sole catalyst used in the remainder of this work.

The *in situ* emission spectra from a 700 °C pretreated fused silica wafer after P3M exposure with P3A catalysts and after a subsequent anneal at 300 °C are shown in Figure 3.4. The spectra are clearly much different than the monomer emission observed in solution (Figure 3.2). Perylene is known to exhibit different fluorescence peaks depending on the structure in which the molecules are arranged [44]. The broad emission observed after P3M exposure is attributed to a combination of chemisorbed and physisorbed probe molecules. The 300 °C anneal step is used to remove any physisorbed molecules, leaving only chemically bound species, as depicted in Figure 3.1 B. The spectrum after the anneal step is blue shifted and displays increased intensity with respect to the spectrum prior to annealing. An anneal temperature of 300 °C was chosen both to ensure desorption of physisorbed molecules and to minimize desorption or degradation of chemisorbed species. Repeated annealing at 300 °C resulted in no change in the spectrum, indicating the bound molecules are stable at this temperature. Increasing the anneal temperature to 400 °C resulted in a decrease in emission intensity, suggesting some loss of chemisorbed fluorophores.

The broad feature at approximately 530 nm from the post anneal spectrum is similar to emission observed in β-perylene crystals, which consist of "monomeric" perylene molecules, as opposed to the broad structureless "excimer-like" emission observed in α-perylene crystals, which consist of "dimeric" perylene molecules [44]. This does not mean β-perylene crystals are present on the surface, but rather that the densely packed perylene units strongly interact with each other. Similar spectra have been observed in Langmuir-Blodgett films [45,46] and polymer films [47] containing perylene fluorophores and the broad peaks red shifted with respect to monomer emission were attributed to various forms of dimer or excimer-like emission. Atomic force microscopy (AFM) images (Appendix A) confirm that no particles are present on the

surface after titration. The sharp features at approximately 520 and 550 nm on top of the broad peak are artifacts of the interference filter used to reject scattered laser light. A more detailed consideration of the photo-physical processes of this system is beyond the scope of the present work.

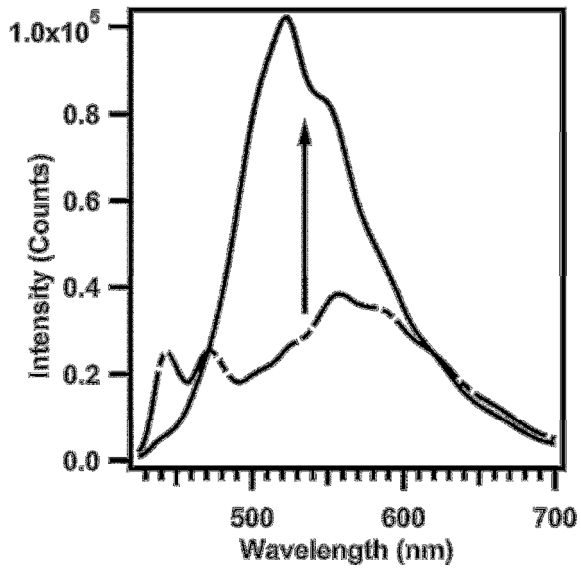

Figure 3.4: *In situ* PL spectra after P3M exposure (— · —) and after a subsequent anneal at 300 °C (——) from fused silica samples pretreated at 700 °C.

Figure 3.5 shows the post anneal emission spectra from fused silica samples pretreated to various temperatures. All samples exhibit similar spectra, with the primary difference between samples being a slight decrease in the intensity of the long wavelength shoulder of the emission feature with increasing pretreatment temperature. As discussed below, the similarity between spectra does not indicate the density of bound P3M is the same on all samples. However, the non-monomeric emission does preclude

the use of the *in situ* spectra in Figure 3.5 for directly determining the density of the bound fluorophores.

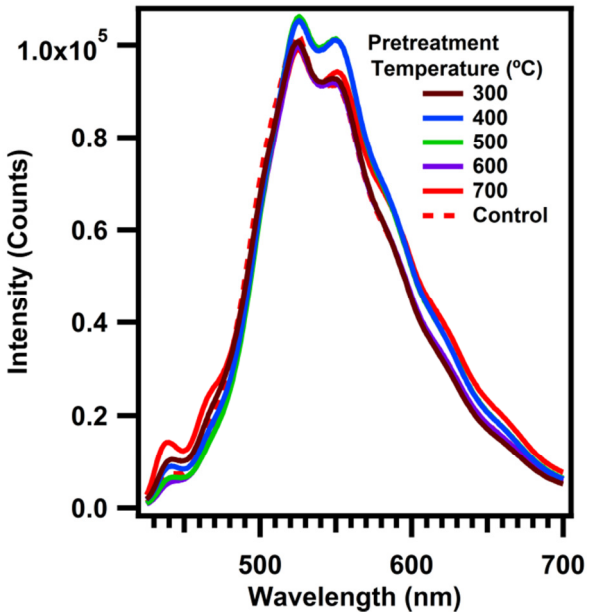

Figure 3.5. *In situ* emission spectra from fused silica samples pretreated to various temperatures after P3M exposure and annealing at 300 °C. The control sample is described in the text.

Although other workers have reported that amines do not chemisorb onto hydroxyl sites on silica [17,18], a control experiment was performed to verify this observation. A fused silica sample pretreated at 700 °C was cooled to near room temperature and then exposed to 500 mTorr n-propylamine vapor for 5 min. The sample was then annealed at 300 °C for 30 min to remove any physisorbed molecules, and subsequently exposed to P3M (with the P3A catalyst) and annealed in the same manner as other samples. The *in situ* PL spectrum, shown in Figure 3.5, is consistent with the 700 °C pretreated sample with no n-propylamine exposure, indicating the amine exposure

had little effect on the reaction between surface hydroxyl groups and P3M. No nitrogen signal was detected by XPS on a sample exposed to n-propylamine vapor (Appendix A), indicating only low densities of the amine could be bound to the surface. Additionally, the n-propylamine exposure eliminates strained siloxane sites, preventing the subsequent chemisorption of P3A molecules onto the silica surface (*vide infra*). The control experiments demonstrate that no P3A chemisorption is necessary during the P3M titration process, supporting the claim that P3A acts as a catalyst during the esterification reaction.

In order to determine the density of fluorophores on the silica surface after titration by P3M, the chemically bound fluorophores were removed through a hydrolysis reaction, which is the reverse of the reaction used to titrate the hydroxyl sites (Reaction 1). Hydrolytic cleavage of the Si-O-R structure is known to be thermodynamically favorable [41], but the hydrolysis reaction can proceed slowly for surfaces with a high coverage of organic molecules [40]. The presence of an amine has been shown to catalyze the hydrolysis reaction so an aqueous solution of n-propylamine was used to ensure a rapid and complete removal of bound probe molecules from the surface [40]. Because the reverse reaction forms P3M molecules in solution, the concentration of each solution can be directly measured using fluorescence spectroscopy by comparison with a standard curve (Appendix A). Using the concentration and the known surface area exposed to the solution, the areal density of bound P3M can be calculated. Figure 3.6 shows the P3M densities calculated for each sample based on the concentration of P3M in the solution after hydrolysis. The maximum calculated density is found to be ~1.5 nm^{-2} for the 300 °C, 400 °C, and 500 °C pretreated samples, suggesting the titration process is sterically hindered at high densities. Flink and coworkers concluded steric hindrance limits the maximum coverage of similar molecules, such as pyrene, covalently attached to

a surface [34]. The densities of bound P3M on the 500 °C, 600 °C, and 700 °C pretreated samples are consistent with literature values for the free silanol densities, as opposed to total silanol densities [7]. This is in agreement with prior work showing that vapor phase alcohol primarily reacts with free silanol sites and not with hydrogen bonded sites [39].

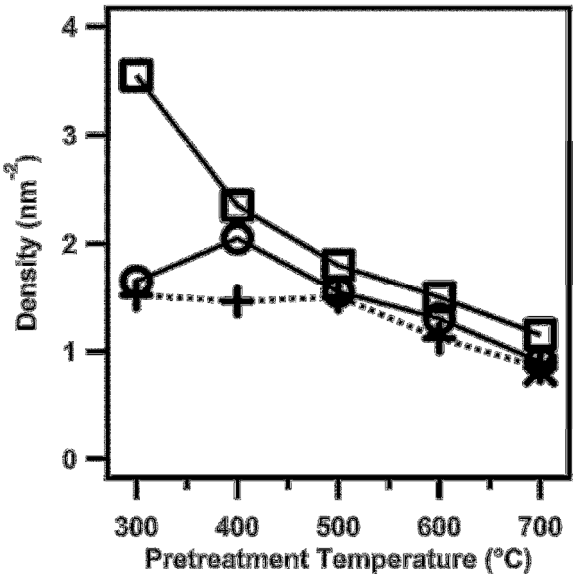

Figure 3.6: Plot of P3M density (+) versus sample pretreatment temperature and total (□) and free (○) hydroxyl densities from Zhuravlev [7]. The P3M density on the control sample (×) is slightly lower than the density on the 700 °C pretreated sample.

Alcohol molecules are also known to react with strained siloxane sites [15,17], therefore the total measured density (Figure 3.6) also includes these sites. The reaction between an alcohol molecule and a strained siloxane site forms both a chemisorbed alkoxy group and a new hydroxyl site. The newly formed hydroxyl site may subsequently react with a P3M molecule, leading to two chemisorbed P3M molecules per strained siloxane site. As discussed in the following section, the ratio of strained siloxane sites to

free hydroxyl sites is very low (< 0.03) for all pretreatment temperatures studied in this work, so correcting for the reaction between P3M and strained siloxane sites would lead to only a minor change in the calculated densities. Additionally, other techniques used to quantify hydroxyl densities in literature, such as deuterium exchange using D_2O vapor, should result in similar additional hydroxyl sites due to reactions with strained siloxane sites. Therefore, no attempt was made to correct for the presence of strained siloxane sites when comparing the calculated P3M densities to the literature values for hydroxyl densities.

The PL emission from the 700 °C pretreated sample has nearly the same intensity as the 400 °C pretreated sample, despite having significantly lower P3M density. This is another consequence of the high density of fluorophores on the surface. The overall intensity of the spectrum is not expected to be linear with density at such high coverage due to the presence of non-monomeric emission bands. The inability to obtain linear relationships between PL intensity and fluorophore density at high coverages is one limitation to the current technique; however, for this particular system the ability to readily remove the bound molecules by hydrolysis and determine the densities from solution measurements overcomes this problem. The density of the 700 °C sample exposed to n-propylamine vapor (0.82 nm^{-2}) was similar to, but slightly less than the density for the sample with the same pretreatement temperature but no amine exposure (0.85 nm^{-2}), indicating amine adsorption on strained siloxane sites does not significantly impact the chemisorption of P3M on hydroxyl groups in the presence of the P3A catalyst.

Additional experiments were performed without the P3A catalyst and using lower evaporator temperatures and shorter times in order to follow the evolution of the emission spectra as a function of bound P3M density. The *in situ* PL spectra from samples with various P3M densities, as determined by solution fluorescence measurements, are shown

in Figure 3.7. This figure shows that monomer emission is observed for low densities of chemisorbed P3M, with a shoulder centered ~520 nm forming for densities of ~0.1 nm^{-2}. The presence of additional bound P3M molecules appears to build up the ~520 nm peak at the expense of the monomer bands. This suggests that attempts to correlate PL intensity directly with fluorophore density must be restricted to fluorophore densities below 0.1 nm^{-2}.

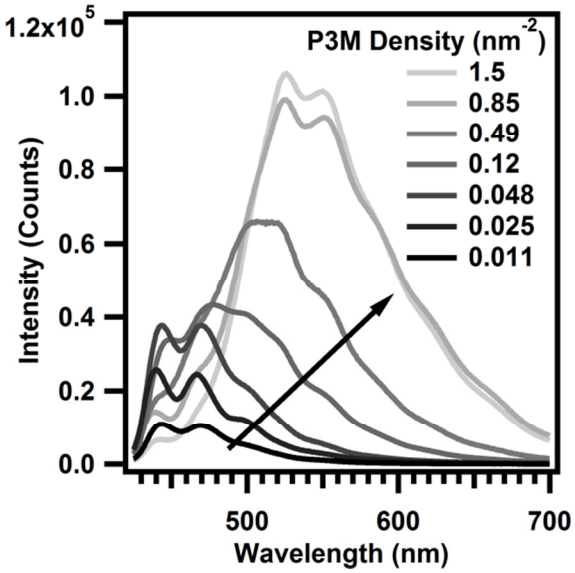

Figure 3.7: *In situ* PL spectra from fused silica samples with various densities of chemically bound P3M, showing the transition from monomer to high density emission.

3.3.2 Titration of strained siloxane sites with P3A

An amine functional group was chosen to selectively titrate strained siloxane sites, as amines do not react with hydroxyl sites under the conditions used in this work [17,18]. Unlike the reaction between alcohols and silanol sites, the reaction between

amines and strained siloxane sites proceeds readily at room temperature [15,17]. The same strategy of exposure followed by annealing at 300 °C used for P3M titrations was also employed for the P3A titrations; however no catalyst was required. A broad feature is observed in the *in situ* PL spectra (Appendix A) after the exposure step, which is attributed to physisorbed probe molecules.

Figure 3.8 shows the *in situ* PL emission spectra from samples pretreated at various temperatures after P3A titration. Emission bands are readily observable for all samples, with a monotonic increase in peak intensity with increasing pretreatment temperature. The PL spectra exhibit only monomer emission, with well-defined vibronic peaks. Repeating the anneal step at 300 °C did not alter the spectra, indicating the chemisorbed fluorophores are stable at this temperature. The monomeric nature of the emission spectra indicates the sites do not occur in close proximity to each other. Interaction between adjacent bound fluorophores would likely give rise to new spectral features, as observed with P3M titration of free hydroxyls.

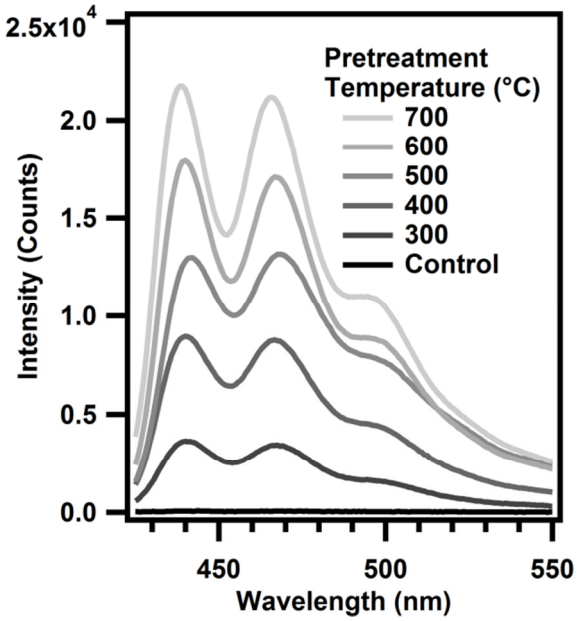

Figure 3.8: *In situ* emission spectra from fused silica samples pretreated to various temperatures after P3A titration.

A control experiment was performed in which a fused silica sample was pretreated to 700 °C and then exposed to 500 mTorr of n-propylamine vapor for 5 min at room temperature to ensure the elimination of all strained siloxane sites. The sample was next annealed at 300 °C to remove any physisorbed molecules, then titrated with P3A using the same conditions as other experiments. Very low emission intensity is observed in the spectrum collected after P3A titration (Figure 3.8, control), indicating that n-propylamine exposure eliminated the sites with which P3A reacts. As discussed previously, exposing a pretreated sample to n-propylamine vapor prior to P3M exposure has little influence on the resulting bound P3M density, indicating the amine does not react with surface silanol sites. Therefore, the sites eliminated during the n-propylamine vapor exposure are strained siloxane sites, verifying the expected selectivity of this titration.

Attempts were made to determine the P3A densities on titrated samples using an approach similar to the method of hydrolytic cleavage and solution measurements used for determining P3M densities. However, the results were largely inconsistent, possibly because the bond anchoring the P3A molecule to the surface is less reactive toward hydrolytic cleavage than the alkoxy bond for bound P3M. The density of chemisorbed P3A was instead determined by comparing the intensity of the 440 nm emission peak of the *in situ* PL measurements for P3A titrated surfaces with similar spectra from the low coverage limit of P3M exposed surfaces. A standard curve was generated from the P3M density versus *in situ* PL intensity for P3M exposed samples displaying only monomeric emission. Because the emission is monomeric, the emission intensity should be directly proportional to the number of fluorophores on the surface in the low coverage limit. The density of chemisorbed P3A, and therefore strained siloxane sites, was then estimated using the same linear relationship. The assumption that both fluorophores display similar emission intensities for a given density was tested by exposing a sample pretreated at 700 °C to a low flux of P3M by lowering the evaporator temperature to 60 °C and reducing the exposure time to 15 min. Because the strained siloxane sites are more reactive than the hydroxyl sites, P3M is expected to react with these sites first. The spectra from fused silica surfaces exposed to either P3M or P3A are shown in Figure 3.9, demonstrating similar emission intensities are observed from both samples. This indicates that the fluorescence quantum yields of the two molecules are similar, which is consistent with the spectra from solutions of these molecules shown in Figure 3.2. Perylene adsorbed on silica was shown to have a similar quantum yield as in solution [48].

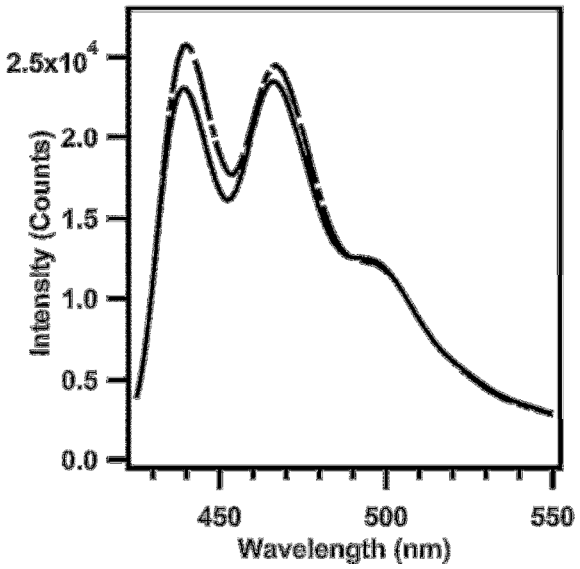

Figure 3.9: Comparison of *in situ* PL spectra from 700 °C pretreated fused silica samples either titrated with P3A (——) or exposed to a low quantity of P3M (— · —).

Figure 3.10 shows a plot of the estimated densities of bound P3A molecules versus sample pretreatment temperature. The estimated densities range from 0.004 nm^{-2} – 0.024 nm^{-2} over the span of pretreatment temperatures used in this study. Comparison of these results with literature is difficult because most studies of strained siloxane sites were performed on silica pretreated at higher temperatures than are possible in our experimental system. Bunker and coworkers estimated a strained siloxane density of 0.04 – 0.13 nm^{-2} for 900 °C pretreated silica based on relative changes in IR band intensities [15]. Morrow and Cody estimated a density of 0.15 nm^{-2} for strained siloxane sites on 1200 °C pretreated silica, also based on the relative change in the silanol IR band [17]. As a reference for the measurement, they assumed the silanol density was 1.5 nm^{-2} on silica pretreated to 800 °C, which appears too high based on other literature and the

results of hydroxyl titrations described above. Using a silanol density of 0.7 nm^{-2} [7], the Morrow-Cody estimated strained siloxane density would then be 0.07 nm^{-2}.

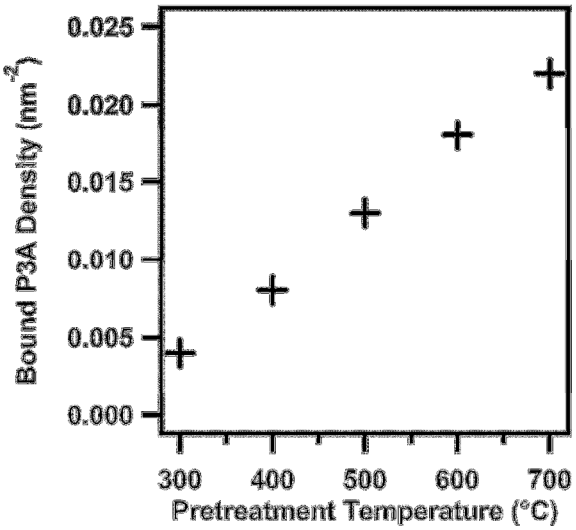

Figure 3.10: Estimated densities of chemisorbed P3A on samples pretreated to various temperatures.

The estimated strained siloxane densities (Figure 3.10) show the presence of these reactive sites on the surface of SiO_2, after even a moderate vacuum pretreatment. The steady increase in strained siloxane density with increasing pretreatment temperature is interesting, especially since the surface hydroxyl coverage changes much more dramatically with temperature. Further work is necessary to determine the mechanism behind strained siloxane formation. The results obtained from P3A titration of strained siloxane sites demonstrate the inherent sensitivity of the fluorescent probe titration technique. Based on the low noise level of the current experimental setup (< 20 counts) and the correlation between *in situ* PL intensity and fluorophores density, we estimate a lower detection limit of below 0.0001 nm^{-2} (10^{10} cm^{-2}). The high sensitivity of this

technique may enable the detection of ultra-low density sites that are currently experimentally inaccessible. Additionally, the use of fluorescent molecules to titrate surface sites could readily be extended to other oxide materials, providing a new tool for the characterization of these technologically important materials.

3.4 CONCLUSIONS

A technique utilizing fluorescent probe molecules to titrate free hydroxyl and strained siloxane sites on planar SiO_2 surfaces in vacuum has been demonstrated. A fluorescent probe containing an alcohol functional group was used to titrate the free hydroxyl sites, with the aid of a catalyst. The density of free hydroxyl sites on surfaces pretreated to various temperatures in vacuum was determined directly by removing the chemically bound probe molecules in solution and then obtaining the concentration of the solution using fluorescence spectroscopy. For high sample pretreatment temperatures, the calculated densities of bound P3M molecules are in good agreement with values for free hydroxyl site densities obtained from measurements on high surface area silica.

Strained siloxane sites were selectively titrated using a fluorescent probe with an amine functional group. Comparison of *in situ* PL measurements from surfaces titrated using P3A with surfaces with low densities of chemically bound P3M molecules enables an estimate of strained siloxane density. Chemisorption of the amine probe was observed on surfaces pretreated at 300 °C, indicating strained siloxane sites exist at lower temperatures than previously recognized.

The results of this work demonstrate that fluorescent probes can be a useful tool for the study of oxide surfaces. The remarkable sensitivity of such a technique should enable detection of ultra-low density defect sites, with a lower detection limit estimated

to be below 0.0001 nm^{-2} (10^{10} cm^{-2}), far lower than most traditional surface science techniques.

3.5 REFERENCES

[1] G. Pacchioni, Oxygen Vacancy: The Invisible Agent on Oxide Surfaces, ChemPhysChem. 4 (2003) 1041–1047.

[2] F. Mazen, T. Baron, G. Bremond, N. Buffet, N. Rochat, P. Mur, et al., Influence of the chemical properties of the substrate on silicon quantum dot nucleation, J. Electrochem. Soc. 150 (2003) G203–G208.

[3] J.M. McCrate, N. Salivati, J.G. Ekerdt, Hot-wire CVD of Ge nanoparticles on Si-etched silicon dioxide, J. Cryst. Growth. 321 (2011) 131–135.

[4] K. Vikulov, G. Martra, S. Coluccia, D. Miceli, F. Arena, A. Parmaliana, et al., FTIR spectroscopic investigation of the active sites on different types of silica catalysts for methane partial oxidation to formaldehyde, Catal. Letters. 37 (1996) 235–239.

[5] R.K. Iler, The Chemistry of Silica : Solubility, Polymerization, Colloid and Surface Properties, and Biochemistry, 1979.

[6] E.F. Vansant, P. Van Der Voort, K.C. Vrancken, Characterization and Chemical Modification of the Silica Surface, Elsevier B.V., Amsterdam, 1995.

[7] L. Zhuravlev, The surface chemistry of amorphous silica. Zhuravlev model, Colloids Surfaces A. 173 (2000) 1–38.

[8] I. Chuang, G.E. Maciel, Probing Hydrogen Bonding and the Local Environment of Silanols on Silica Surfaces via Nuclear Spin Cross Polarization Dynamics, J. Am. Chem. Soc. 118 (1996) 401–406.

[9] E.A. Wovchko, J.C. Camp, J.A. Glass, J.T. Yates, Active Sites on SiO_2: Role in CH_3OH Decomposition, Langmuir. 11 (1995) 2592–2599.

[10] C.H. Lochmuller, M.T. Kersey, Effect of thermal pretreatment on the surface reactivity of amorphous silica, Langmuir. 4 (1988) 572–578.

[11] B. Morrow, A. McFarlan, Infrared and gravimetric study of an aerosil and a precipitated silica using chemical and hydrogen/deuterium exchange probes, Langmuir. (1991) 1695–1701.

[12] L.T. Zhuravlev, Concentration of hydroxyl groups on the surface of amorphous silicas, Langmuir. 3 (1987) 316–318.

[13] C. Liu, G. Maciel, The fumed silica surface: a study by NMR, J. Am. Chem. Soc. 118 (1996) 5103–5119.

[14] B.A. Morrow, I.A. Cody, An Infrared Study of Some Reactions with Reactive Sites on Dehydroxylated Silica, J. Phys. Chem. 79 (1975) 761–762.

[15] B. Bunker, D. Haaland, T. Michalske, W. Smith, Kinetics of dissociative chemisorption on strained edge-shared surface defects on dehydroxylated silica, Surf. Sci. 222 (1989) 95–118.

[16] B. Morrow, I. Cody, Infrared studies of reactions on oxide surfaces. 5. Lewis acid sites on dehydroxylated silica, J. Phys. Chem. 80 (1976) 1995–1998.

[17] B. Morrow, I. Cody, Infrared studies of reactions on oxide surfaces. 6. Active sites on dehydroxylated silica for the chemisorption of ammonia and water, J. Phys. Chem. 80 (1976) 1998–2004.

[18] G. Blomfield, L. Little, Chemisorption of ammonia on silica, Can. J. Chem. 51 (1973) 1771–1781.

[19] A. Grabbe, T. Michalske, W. Smith, Strained siloxane rings on the surface on silica: their reaction with organosiloxanes, organosilanes, and water, J. Phys. Chem. 99 (1995) 4648–4654.

[20] V.M. Bermudez, A Proton Nuclear Magnetic Resonance Technique for Determining the Surface Hydroxyl Content of Hydrated Silica Gel, J. Phys. Chem. 74 (1970) 4160–4161.

[21] C. Bronnimann, R. Zeigler, G. Maciel, Proton NMR study of dehydration of the silica gel surface, J. Am. Chem. Soc. 110 (1988) 2023–2026.

[22] J. Peri, A.H. Jr, The surface structure of silica gel, J. Phys. Chem. 2 (1968) 242–247.

[23] R. Mueller, H. Kammler, K. Wegner, OH Surface Density of SiO_2 and TiO2 by Thermogravimetric Analysis, Langmuir. 19 (2003) 160–165.

[24] J. Gallas, J. Goupil, A. Vimont, J. Lavalley, Quantification of Water and Silanol Species on Various Silicas by Coupling IR Spectroscopy and in-Situ Thermogravimetry, Langmuir. 57 (2009) 5825–5834.

[25] A. D'Souza, C. Pantano, K. Kallury, Determination of the surface silanol concentration of amorphous silica surfaces using static secondary ion mass spectroscopy, J. Vac. Sci. Technol. A Vacuum, Surfaces, Film. 15 (1997) 526–531.

[26] V. Dugas, Y. Chevalier, Surface hydroxylation and silane grafting on fumed and thermal silica, J. Colloid Interface Sci. 264 (2003) 354–361.

[27] O. Sneh, S. George, Thermal stability of hydroxyl groups on a well-defined silica surface, J. Phys. Chem. 99 (1995) 4639–4647.

[28] C. Chiang, B. Zegarski, L. Dubois, First observation of strained siloxane bonds on silicon oxide thin films, J. Phys. Chem. 97 (1993) 6948–6950.

[29] J. Lakowicz, Princples of Fluorescence Spectroscopy, 2nd ed., Kluwer Academic / Plenum Publishers, New York, 1999.

[30] B. Valeur, Molecular Fluorescence, Wiley-VCH Verlag, Weinheim, 2002.

[31] C.H. Lochmuller, A.S. Colborn, M.L. Hunnicutt, J.. Harris, Bound Pyrene Excimer Photophysics and the Organization and Distribution of Reaction Sites on Silica, J. Am. Chem. Soc. 106 (1984) 4077–4082.

[32] R. Métivier, I. Leray, M. Roy-Auberger, N. Zanier-Szydlowski, B. Valeur, Characterization of alumina surfaces by fluorescence spectroscopy. Part 1. Grafting a pyrene derivative on γ- and δ-alumina supports, New J. Chem. 26 (2002) 411–415.

[33] L. Crowe, L. Tolbert, Silica Passivation Efficiency Monitored By a Surface-Bound Fluorescent Dye, Langmuir. 24 (2008) 8541–8546.

[34] S. Flink, F.C.J.M. van Veggel, D.N. Reinhoudt, Functionalization of self-assembled monolayers on glass and oxidized silicon wafers by surface reactions, J. Phys. Org. Chem. 14 (2001) 407–415.

[35] E. a McArthur, T. Ye, J.P. Cross, S. Petoud, E. Borguet, Fluorescence detection of surface-bound intermediates produced from UV photoreactivity of alkylsiloxane SAMs., J. Am. Chem. Soc. 126 (2004) 2260–2261.

[36] Y. Xing, E. Borguet, Specificity and sensitivity of fluorescence labeling of surface species., Langmuir. 23 (2007) 684–688.

[37] I. Berlman, Handbook of Fluorescence Spectra of Aromatic Molecules, 2nd ed., Academic Press, New York, 1971.

[38] W.K. Lowen, E.C. Broge, Effects of dehydration and chemisorbed materials on the surface properties of amorphous silica, J. Phys. Chem. 65 (1961) 16–19.

[39] R. Azrak, C. Angell, Study of alcohol-silica surface reactions via infrared spectroscopy, J. Phys. Chem. 77 (1973) 3048–3052.

[40] G.C. Ossenkamp, T. Kemmitt, J.H. Johnston, New Approaches to Surface-Alkoxylatd Silica with Increased Hydrolytic Stability, Chem. Mater. 13 (2001) 3975–3980.

[41] C. Ballard, E. Broge, R. Iler, D.S. St. John, J.R. McWhorter, Esterification of the surface of amorphous silica, J. Phys. Chem. 65 (1961) 20–25.

[42] W. Leach, J. Zhu, J. Ekerdt, Thermal desorption effects in chemical vapor deposition of silicon nanoparticles, J. Cryst. Growth. 243 (2002) 30–40.

[43] W.T. Leach, J. Zhu, J.G. Ekerdt, Cracking assisted nucleation in chemical vapor deposition of silicon nanoparticles on silicon dioxide, J. Cryst. Growth. 240 (2002) 415–422.

[44] J. Tanaka, The electronic spectra of aromatic molecular crystals. II. The crystal structure and spectra of perylene, Bull. Chem. Soc. Jpn. 36 (1963) 1237–1249.

[45] A. Vitukhnovsky, M. Sluch, J. Warren, M. Petty, The Fluorescence of Perylene-Doped Langmuir—Blodgett Films, Chem. Phys. Lett. 173 (1990) 425–429.

[46] J. Mahrt, F. Willig, W. Storck, D. Weiss, R. Kietzmann, K. Schwarzburg, et al., Luminescence and configurations of perylene dimers in a Langmuir-Blodgett film, J. Phys. Chem. 98 (1994) 1888–1894.

[47] H. Tachikawa, L. Faulkner, Anomalous luminescence from perylene in thin polymer films, Chem. Phys. Lett. 39 (1976) 436–441.

[48] S. Ruetten, J. Thomas, Fluorescence and triplet quantum yields of arenes on surfaces, J. Phys. Chem. B. 102 (1998) 598–606.

Chapter 4: Coverage Dependent Luminescence from Two-Dimensional Systems of Covalently Attached Perylene Fluorophores on Silica

4.1 INTRODUCTION

Two-dimensional systems of fluorescent molecules have been extensively studied, both for applications including sensors [1,2] and in order to understand fundamental aspects of intermolecular interaction and energy transfer in such systems [3]. We recently demonstrated a method to titrate specific sites on the surface of planar silica with fluorescent probe molecules having various functional groups, resulting in two-dimensional systems of covalently attached fluorophores [4]. In the present work, we explore the nature of the luminescence from such systems as a function of fluorophore density. The results provide insight into both the molecular organization of the fluorophores and to the proximity of sites at which the fluorophores are covalently attached. The latter information is crucial for developing a characterization method of low density surface sites using fluorescent probes.

In the previous work, perylene derivatives with an alcohol functional group, perylene-3-methanol (P3M), were used to titrate free hydroxyl sites while perylene derivatives with an amine functional group, perylene-3-methanamine (P3A), were used to titrate strained siloxane sites selectively [4]. Surfaces were prepared and experiments performed in an ultra-high vacuum (UHV) environment to ensure the stability of surface sites. Chemisorbed fluorophore densities of over 1.5 and 0.02 nm^{-2} were found for surfaces titrated with either P3M or P3A, respectively. Emission from the chemically bound fluorophores depended dramatically on coverage, with monomeric emission observed for low fluorophore densities (below 0.1 nm^{-2}) and a broad emission feature

appearing at higher densities. The current work uses both steady-state and time-resolved measurements to study how the density of the perylene moieties influences luminescence in these systems. Comparison of these results with studies of other two-dimensional perylene systems indicates that covalent attachment to a surface can influence the luminescence, particularly at high fluorophore densities.

The electronic properties of perylene have been studied in solution and crystalline phases [5,6], in glass forming mixtures [7], in thin polymer films [8], and in Langmuir-Blodgett films [9–13]. The perylene monomer displays absorption features with maxima around 430 and 290 nm corresponding to the $S_0 \rightarrow S_1$ and $S_0 \rightarrow S_2$ transitions, respectively [14]. The transition to the S_1 state is polarized along the long axis of the molecule, while the transition to the S_2 state is polarized along the short axis. Monomer emission exhibits vibronic features with maxima at 445, 470, and 500 nm in cyclohexane, with a quantum yield near unity and a lifetime of approximately 6 ns [15]. The electronic structure of crystalline perylene is dependent on the crystal structure, with monomeric β-perylene displaying structured emission with a maximum at 530 nm [5]. Emission from the dimeric α-perylene crystal is dependent on temperature [5,6]. At room temperature, E-type excimer emission is observed, with a broad structureless feature with a maximum around 620 nm. At temperatures below 35 K, Y-type emission is observed with structured features and a maximum around 530 nm. In the α-perylene crystal, the Y state is a precursor for E excimer state [6]. E-type emission is also observed in glass forming mixtures containing high concentrations of perylene, and is attributed to the emission from sandwich dimers, or a pair of fully overlapping perylene molecules [7]. This type of perylene dimer also has a distinct absorption spectra characterized by a weak peak around 375 nm [7]. Polymer films loaded with perylene displayed monomer emission at

low loadings and an emission feature at 527 nm at higher loadings attributed to an excimer-like species [8].

Langmuir-Blodgett films provide a convenient method for fabricating two-dimensional systems containing various luminescent molecules. Vitukhnovsky et al. have prepared such films containing perylene in a fatty acid matrix and showed that these films exhibited both monomer emission and a broad emission centered at 545 nm for high perylene loadings [9]. Langmuir-Blodgett films containing a perylene derivative with a long fatty acid tail in a fatty acid matrix have also been studied [10,11]. In these films the perylene molecules are aligned with their long axis perpendicular to the surface. Langmuir-Blodgett films with mole fraction greater than 0.25 exhibited E-type emission at room temperatures, and a combination of E- and Y-type emission below 2 K [10,11]. Akimoto and coworkers studied the spectral properties of Langmuir-Blodgett films containing perylene derivatives with a long fatty acid tail in a fatty acid matrix as a function of perylene loading at room temperature [13]. For low perylene concentrations, only monomer emission was observed. Increasing the perylene mole fraction to 0.1 resulted in the appearance of a peak at 535 nm, along with monomer features. Higher perylene mole fractions exhibited a combination of monomer, 535 nm, and 600 nm emission features (see below) [13]. The presence of two types of excimer-like emission features was attributed to subtle changes in the orientation of perylene dimers in the film. Excitation spectra collected at 535 nm showed predominantly monomeric features, while spectra collected at 600 nm also displayed a feature at 375 nm, consistent with sandwich dimer absorption [13]. The emission feature at 535 was therefore attributed to emission from partially overlapping perylene molecules, while emission at 600 nm was attributed to emission from fully overlapping molecules. Langmuir-Blodgett films containing perylene-4-octadecanon up to a molar ratio of 100% have been prepared and exhibited

both monomer and dimer emission, but not excimer emission [12]. However, the presence of the carbonyl group close to the fluorophore appears to alter the electronic properties of the moiety, as the shape and position of the monomer absorption and emission features are different than for perylene and perylene derivatives with a long alky chain. Two dimensional systems of pyrene chromophores, which share much similarity with perylene, have also been studied. Langmuir-Blodgett films containing pyrene derivatives exhibit both monomer and excimer emission, depending on the fluorophore concentration [16,17]. Additionally, pyrene derivatives have been covalently attached to high surface area and planar silica by solution phase reactions and were observed to emit both monomer and excimer emission, depending on fluorophore density [1,18–20].

Time-resolved fluorescence measurements can provide additional insight into intermolecular interactions. Such measurements have been employed to study energy migration and trapping processes occurring in two-dimensional geometries in Langmuir-Blodgett films [13,16,21,22] and for molecules adsorbed on surfaces [23,24]. Förster type resonance energy transfer can occur between fluorophores in close proximity, allowing for rapid energy migration between sites [3]. Energy transfer from monomer species to dimers or higher aggregates can result in the appearance of complex decay kinetics. By fitting the observed decays to appropriate physical models, one can extract relevant physical parameters, such as lifetimes and the concentration of trap sites.

Although Langmuir-Blodgett films containing perylene derivatives provide much insight into how structural changes influence the electronic properties of perylene systems, these films generally require a matrix to stabilize the film [11,13]. Additionally, the perylene moieties in these films appear to have a high propensity for forming sandwich dimers, suggesting the fluorophores are not uniformly distributed in the matrix. In the present work, the two-dimensional systems contain only perylene fluorophores that

are covalently attached to the silica surface by a one-carbon tether. The electronic properties of these systems have many similarities to Langmuir-Blodgett films containing perylene, but also significant distinctions, which we attribute to constraints imposed by attaching the fluorophore to the surface.

4.2 EXPERIMENTAL METHODS

A complete description of the technique and system used to covalently attach perylene fluorophores to fused silica surfaces in a UHV environment is given elsewhere [4]. Briefly, cleaned 1.6 cm × 1.6 cm fused silica wafers are attached to a Mo sample holder and loaded into a multi-chamber UHV system with a base pressure of ~10^{-9} torr. Samples are transferred to a quartz tube furnace and pretreated by heating to the desired temperature for 30 min. After cooling to below 100 °C, samples were moved to an exposure chamber. Samples were heated to ~60 °C and positioned ~2 cm from an evaporator containing the perylene-3-methanol (P3M) precursor, along with a small amount of perylene-3-methanamine (P3A) catalyst, which is necessary to obtain high bound fluorophore densities [4]. The evaporator was heated to from ~60 – 100 °C, depending on the desired fluorophore coverage. Exposure times of 30 – 90 min were used, again depending on the desired fluorophore coverage. The highest evaporator temperatures and longest exposure times were used to achieve nearly complete titration of free hydroxyl sites using the P3M precursor. At the end of the exposure time, the evaporator was turned off and the sample temperature was increased to ~100 °C for ~15 min, in an attempt to remove some of the physisorbed material and reduce contamination in the rest of the vacuum system.

After the exposure step, samples were moved in front of the photoluminescence (PL) assembly for *in situ* emission measurements. Samples were then moved into the tube furnace and annealed at 300 °C for 30 min to remove any residual physisorbed molecules. After cooling, a second emission measurement was collected.

The *in situ* PL assembly consists of a 405 nm continuous wave diode laser with an output power of 20mW (CrystalLaser) and a spectrometer (Ocean Optics QE6500) attached to separate lenses using fiber optics. The lenses are mounted in front of a viewport and are focused on the sample inside the UHV system with a spot size of ~1 mm^2. Spectra were collected with a 0.25 s integration time and averaged over three scans.

Although only very low densities of fluorophores are attached to the backside of the samples [4], these low densities can still produce fluorescent emission that contributes to the signal. In order to eliminate the signal from the back of the sample, samples were moved to a separate chamber in which a tungsten filament was positioned ~2 cm from the back of the sample. Atomic deuterium was generated by introducing 1×10^{-6} torr deuterium into the chamber and heating the tungsten filament to ~1500 K for 15 min [25]. Sample temperatures were estimated to reach ~150 °C during this process. After the atomic deuterium exposure, an additional *in situ* emission measurement was collected. This final *in situ* measurement is used for the spectra presented herein.

Samples were then transferred to a vacuum vessel through the load lock. The vacuum vessel consists of a stainless steel cube with four glass viewports around the side, a base with a hook attached for holding the sample, and a gate valve for isolating the vessel. The entire transfer process was completed under vacuum, so that the sample was not exposed to ambient conditions prior to *ex situ* measurements. Once the sample was mounted on the hook in the vacuum vessel, the gate valve was closed and the vessel was

removed from the system. The pressure inside the vessel remained below 15 mtorr during the all measurements.

Ex situ fluorescence emission, excitation, and lifetime measurements were performed using a Fluorolog3 Fluorimeter (Horiba Jobin Yvon). The vacuum vessel was placed inside the instrument so that viewports were facing the excitation source (Xenon lamp) and the detector (photomultiplier tube), at a right angle from each other. The sample inside the vessel was positioned ~30° from the detector normal. All measurements were performed using a 5 nm spectral bandwidth and an integration time of 0.5 s. Corrected spectra were recorded by dividing the photomultiplier tube signal by the excitation reference signal and applying the correction factors supplied by the manufacturer. Time-correlated single photon counting was used to measure the decay profiles and record time-resolved emission spectra. A 405 nm pulsed light-emitting diode (LED) with a 1 MHz repetition rate and pulse width < 250 ps was used as the excitation source. After all fluorescence measurements were complete, the sample was removed from the vacuum vessel. An absorption spectrum was collected using a Cary 5000 UV-Vis Spectrometer with the beam normal to the sample surface. A 2 nm spectral bandwidth and 0.5 s dwell time were used during the collection and baseline subtraction was performed using a clean fused silica wafer.

Both steady-state and fluorescence decay measurements collected using a magic angle polarizer configuration were nearly identical to unpolarized measurements (Appendix B). The use of polarizers greatly reduces the intensity of light reaching the detector, requiring significantly longer measurement times, which introduces greater noise levels in the measurements. As no differences were observed between the magic angle polarized and unpolarized measurements, only unpolarized measurements are presented herein.

An ~0.9 cm × 0.9 cm specimen was obtained from the center of each sample by scoring and cleaving off the edges. This center piece was placed in 10 ml 0.1 M aqueous propylamine solution and brought to boil. The fluorescence spectrum of the solution was collected (Appendix B) and compared to a standard curve to determine the concentration, and therefore calculate the areal density of bound fluorophores on the sample.

4.3 RESULTS

A schematic of the process used to attach P3M to the silica surface is shown in Figure 4.1. The titration process leads to covalently attached perylene fluorophores with a density dependent on the pretreatment conditions. A small amount of P3A was added to the P3M precursor in order to catalyze the reaction between P3M and the hydroxyl sites [4]. Samples with lower fluorophore densities were prepared using lower P3M exposures than necessary for titration. In this manner, samples with bound fluorophore densities ranging from approximately 0.02 – 1.5 nm^{-2} could be prepared. Samples pretreated to 300, 500, and 700 °C were prepared with 1.58, 1.53, and 0.86 P3M / nm^2, respectively, corresponding to nearly complete titration of free hydroxyl sites on these surfaces [4]. Additionally, one sample was exposed only to P3A precursor, resulting in the titration of strained siloxane sites by this molecule [4]. The density of bound P3A on this sample was estimated to be approximately 0.03 nm^{-2} based on comparison of emission spectra between this sample and samples with low densities of bound P3M [4].

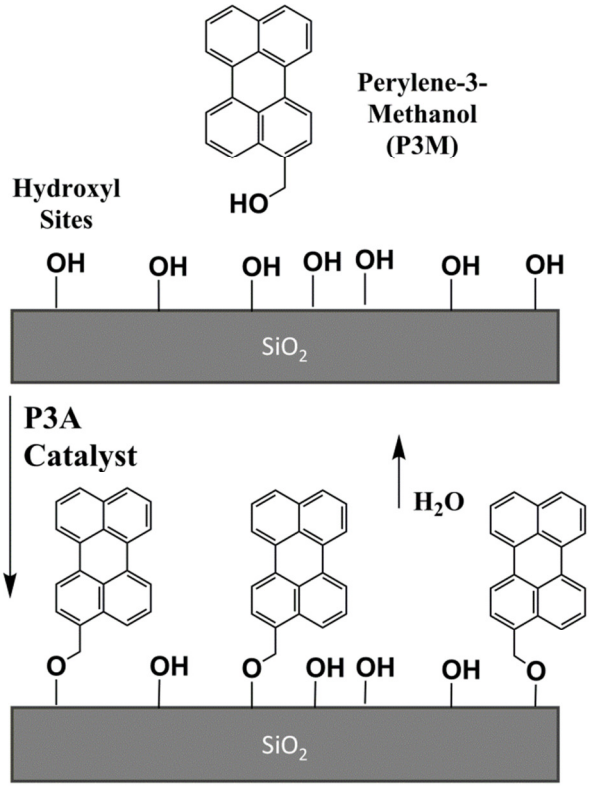

Figure 4.1: Schematic of reaction between perylene-3-methanol (P3M) molecule and hydroxyl sites on silica surface leading to covalently attached perylene fluorophores.

4.3.1 Emission Spectra

In situ and *ex situ* emission spectra from samples pretreated at 700 °C and prepared with various bound P3M coverages are shown in Figure 4.2. For very low densities of bound fluorophores, the emission spectrum is monomeric, with well-defined vibronic peaks. As coverage increases, the intensity of the spectrum past 500 nm increases. With increasing coverage, a broad peak centered around 530 nm appears at the expense of the monomeric peaks. This feature is shown to result from excimer-like emission (*vide infra*). With a bound fluorophore density of 0.44 P3M / nm^2, virtually no

monomeric emission is observed and only a broad feature around 530 nm is present. For the sample with density of 0.86 P3M / nm^2, the peak is again centered around 530 nm but is more intense.

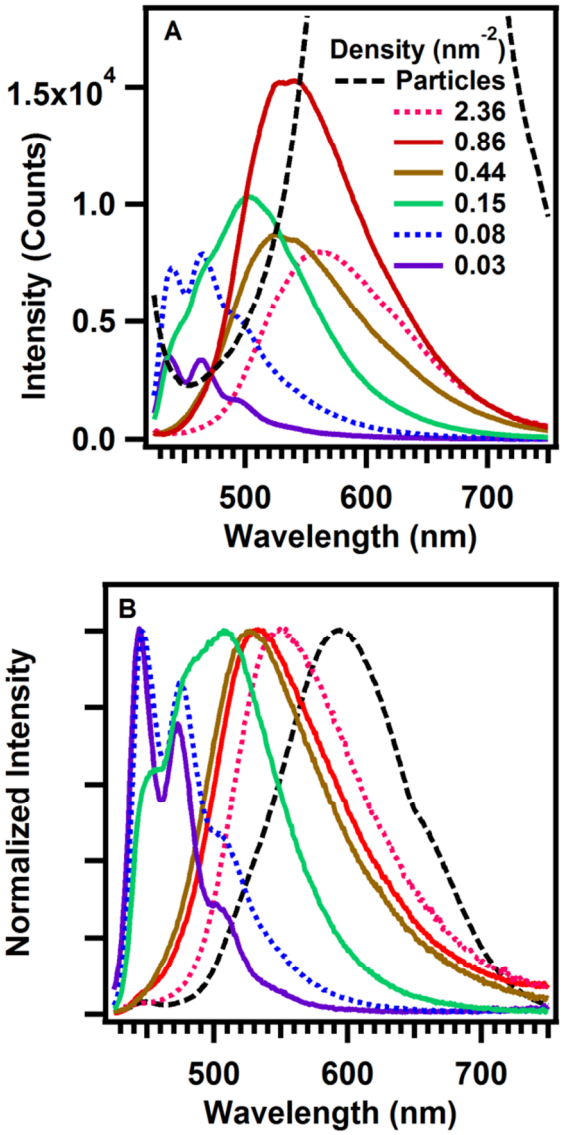

Figure 4.2: Emission spectra from 700 °C pretreated samples with various bound P3M densities. **(A)** *In situ* spectra showing the change in both intensity and position of the spectra as a function of fluorophore density. **(B)** Plot of normalized intensities of *ex situ* spectra showing clear changes in peak positions as a function of bound P3M density. The excitation wavelength was 405 nm.

The *in situ* measurements presented here are in general agreement with our previous work [4]; however, there are two important distinctions. First, no filter was

used to reject scattered laser light for the *in situ* measurements in Figure 4.2. The filter was found to introduce an artifact in the shape of the long wavelength features. Additionally, the low wavelength monomeric features observed in the emission spectra from high fluorophore density samples in the previous work were eliminated by the backside atomic deuterium exposure used in this work. Spectra showing the influence of both of these changes are included in the Appendix B.

Two other samples were prepared in which additional, non-covalently attached fluorophores were present. One sample was prepared in the same manner as the 0.86 P3M / nm^2 sample (nearly complete titration of free hydroxyl sites), but with no post exposure anneal step. A brief atomic deuterium exposure of ~ 3 min was used to eliminate the signal from the back of the sample without heating the sample so much that desorption of the physisorbed molecules occurred. The measured density from this sample was found to be 2.36 P3M / nm^2, significantly higher than the density of hydroxyl sites on silica pretreated in vacuum at 700 °C [4,26], indicating physisorbed molecules remained on the surface. A sample with deposited P3M was prepared in the same manner as the 0.86 P3M / nm^2 sample, but the sample was not heated during the exposure process and no anneal step was performed. A brief atomic deuterium exposure was again used to eliminate signal from the back of the sample. A much more intense feature due to scattered laser light was observed, indicating particles are present on the surface. No density measurement was performed on this sample.

The sample with physisorbed fluorophores (2.36 nm^{-2}) exhibited a similar spectrum as the sample with a high density of covalently attached fluorophores (0.86 nm^{-2}), but the feature was red-shifted by approximately 20 nm and was less intense relative to the latter sample. A much more dramatic distinction was observed between the 0.86 P3M / nm^2 sample and the sample with deposited P3M. The latter sample exhibited a broad

feature centered past 600 nm and with much greater intensity relative to the sample with chemically bound fluorophores.

Although none of the samples were exposed to ambient conditions prior to collecting the *ex situ* measurements, there does appear to be some slight differences between the *in situ* and *ex situ* emission measurements, primarily for low P3M density samples. The *ex situ* emission peaks from samples displaying monomeric emission features are red-shifted by approximately 10 nm with respect to the *in situ* peaks from the same samples. No change in feature position was observed between *in situ* and *ex situ* emission measurements for samples displaying excimer-like emission. Transferring a sample back into the UHV system after *ex situ* measurements were complete and collecting another *in situ* measurement confirmed the red-shift is a result of changes to the sample, and not an instrumental artifact (Appendix B). Additional experiments in which the *in situ* emission was monitored as a function of chamber pressure show that a change in the peak positions are observed at pressures as low as 10^{-4} torr for samples with monomer emission, although virtually no change was observed for high fluorophore density samples at pressures up to 1 torr (Appendix B). This indicates some change occurs to the fluorophore environment for low fluorophore density samples, even at pressures in a medium vacuum range.

To explore the influence of the local environment on emission further, two additional samples were prepared. One sample was pretreated at 300 °C and then given a very low exposure of P3M so that a low density of bound fluorophores was present (0.02 nm^{-2}). The different pretreatment temperatures in vacuum cause substantial differences in the densities of surface sites between the samples, with an estimated total hydroxyl density of 3.55 and 0.90 nm^{-2} for the 300 and 700 °C pretreated samples, respectively [26]. Additionally, a sample was prepared in which a 700 °C pretreated fused silica

wafer was exposed to the amine derivative of perylene (P3A) and then annealed. The P3A molecules titrate the strained siloxane sites selectively, and do not react with the hydroxyl sites [4]. *In situ* emission spectra from these two samples and from a low fluorophore density 700 °C pretreated sample are shown in Figure 4.3. No difference in peak position or relative shape is observed between the three samples. These results suggest that the density of hydroxyl sites does not significantly influence fluorescence emission. Both the ≡Si-O-R and ≡Si-NH-R species, where R is the remainder of the probe molecule, appear to yield similar emission spectra. This indicates the presence of the one-carbon tether effectively decouples the electronic properties of the perylene moiety from the functional group used to bind to the surface. A similar conclusion was reached for pyrene covalently attached to silica with a one-carbon tether [19].

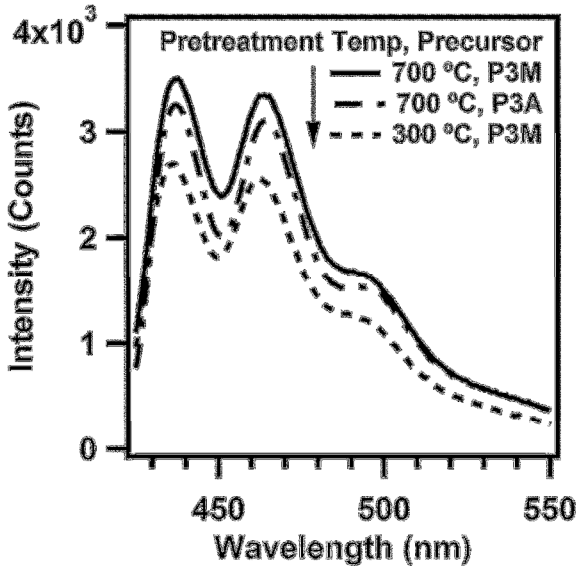

Figure 4.3: *In situ* emission spectra from samples pretreated at either 300 or 700 °C with low densities of bound P3M or P3A molecules.

In situ emission spectra from samples pretreated to various temperatures and then given high P3M exposures are shown in Figure 4. The spectra from 300 and 500 °C pretreated samples are virtually identical and are only slightly red-shifted with respect to the 700 °C pretreated sample. The densities of the 300 and 500 °C samples are 1.53 and 1.58 P3M / nm^2, respectively. This shows that even though the density of fluorophores increases substantially between the 700 °C pretreated sample (0.86 P3M / nm^2) and the lower pretreatment temperature samples, the intensities are nearly identical. The non-linear relationship between fluorophore density and emission intensity is discussed in detail below.

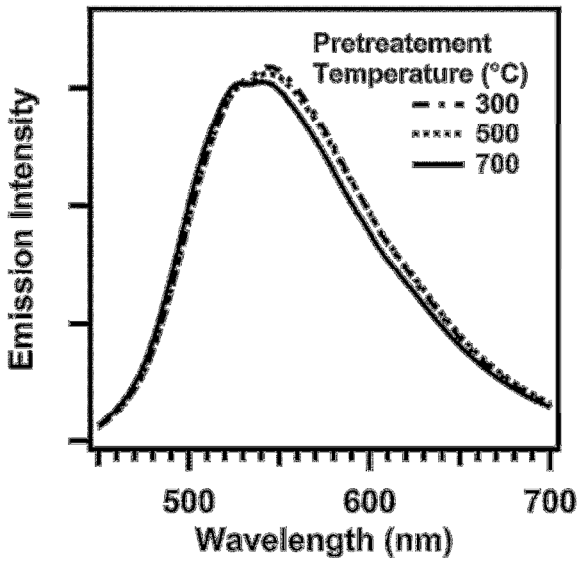

Figure 4.4: *In situ* emission spectra from samples pretreated to various temperatures and then given high P3M exposures. Densities of 1.58, 1.53, and 0.86 P3M / nm^2 were found for the 300, 500, and 700 °C pretreated samples, respectively.

4.3.2 Absorption and Excitation Spectra

Absorption and excitation spectra from the various samples are shown in Figure 4.5. For the lowest P3M densities, no features are detectable in the absorption measurements. With increasing coverage, both $S_0 \rightarrow S_1$ and $S_0 \rightarrow S_2$ features increase. However, virtually no change in absorbance is observed for the $S_0 \rightarrow S_1$ absorption feature between the sample with 0.44 P3M / nm^2 and higher fluorophore density samples while the $S_0 \rightarrow S_2$ absorption feature continues to increase with increasing density. Similar changes have been observed in the ratio of absorption features in Langmuir-Blodgett films and are attributed to the preferential alignment of the long axis of the molecule in a direction normal to the sample surface [10,13]. The sample with physisorbed material (2.36 P3M / nm^2, top curve) displays a slightly stronger and red-shifted $S_0 \rightarrow S_1$ feature with respect to the remaining samples and a much stronger $S_0 \rightarrow S_2$ feature. The excitation spectra collected from all samples using an emission wavelength of 520 nm are presented in Figure 4.5 (B). These spectra show a gradual broadening and red-shift of the absorption features with increasing density; however, no feature corresponding to the sandwich dimer was observed in any sample. The broadening of peaks and red shift of the long wavelength absorption edge with increasing fluorophore density seen in Figure 4.5 B has been observed previously in both perylene systems [10,11,13], as well as systems containing other fluorescent molecules [23,27]. The broadening with increased fluorophore density has previously been attributed to the formation of a combination of H- and J-like dimers due to the random orientation of fluorophores on the surface, leading to a superposition of blue- and red-shifted absorption features [23,27]. Importantly, the shape of the absorption and excitation spectra are mirror images of the emission spectra for samples with low fluorophore densities (below 0.15 nm^{-2}), as expected for absorption and emission from a monomer species [14,28].

However, for samples with higher fluorophore densities, the emission spectra become broad and structureless and display a much larger Stokes shift than for the monomeric samples, indicating emission from an excimer-like state [14,28]. The designation excimer-like, or alternatively pre-formed excimer, is used to distinguish excimer formation in bound fluorophores (present work) with excimer formation due to diffusion of species in solution.

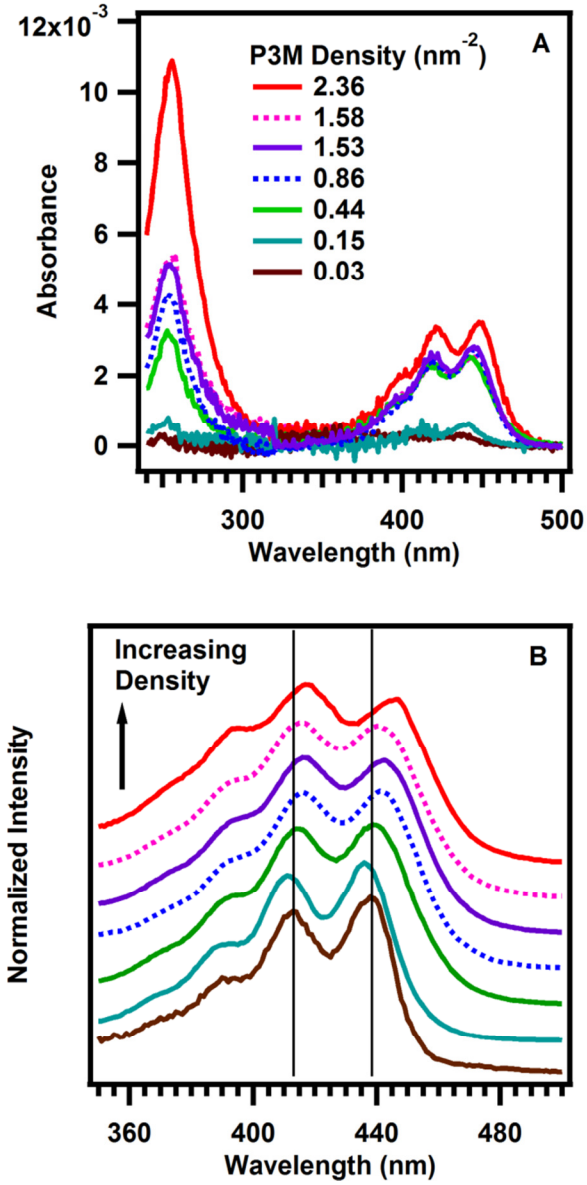

Figure 4.5: **(A)** Absorption spectra from samples with various densities of P3M. **(B)** Excitation spectra from the same samples as in (A). The emission wavelength was 520 nm.

Figure 4.6 shows excitation spectra collected from the 700 °C pretreated sample with 0.86 P3M / nm^2 from various emission wavelengths. The spectra are similar regardless of the emission wavelength. No significant differences between excitation

spectra collected with different emission wavelengths were identified for any sample prepared in this work. This observation indicates that only one type of absorbing species is present in the current systems, which differs from Langmuir-Blodgett films containing perylene derivatives in which a shoulder attributed to sandwich dimer absorption was observed in the excitation spectrum at long emission wavelengths [13]. Time-resolved emission spectra collected from the P3A titrated sample are presented in Appendix B.

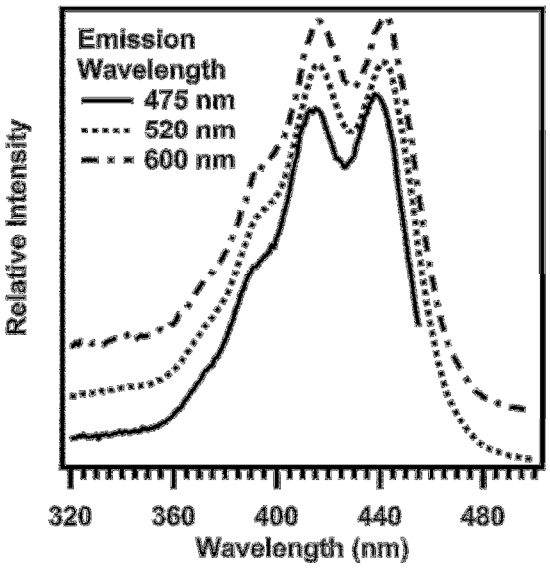

Figure 4.6: Excitation spectra at various emission wavelengths from sample with P3M density of 0.86 nm^{-2}.

4.3.3 Time-Resolved Emission Spectra

Normalized time-resolved emission spectra from samples with various P3M densities are shown in Figure 4.7. The spectra have been corrected to account for wavelength dependence of the photomultiplier tube signal. For the lowest P3M density,

monomer emission is observed in all time windows. As the density increases to 0.08 P3M / nm^2, emission changes from monomer to excimer-like at later times. At 0.15 P3M / nm^2, the transition from excimer-like emission is dominant for all but the earliest time windows. For even higher P3M densities, a broad feature is observed in all time windows; however, this feature shifts to longer wavelengths with increasing time. The sample with physisorbed P3M (2.36 nm^{-2}) displays a similar emission as the other high density samples, although the peak is further red shifted in all time windows with respect to the high bound fluorophore density (0.86 nm^{-2}) sample.

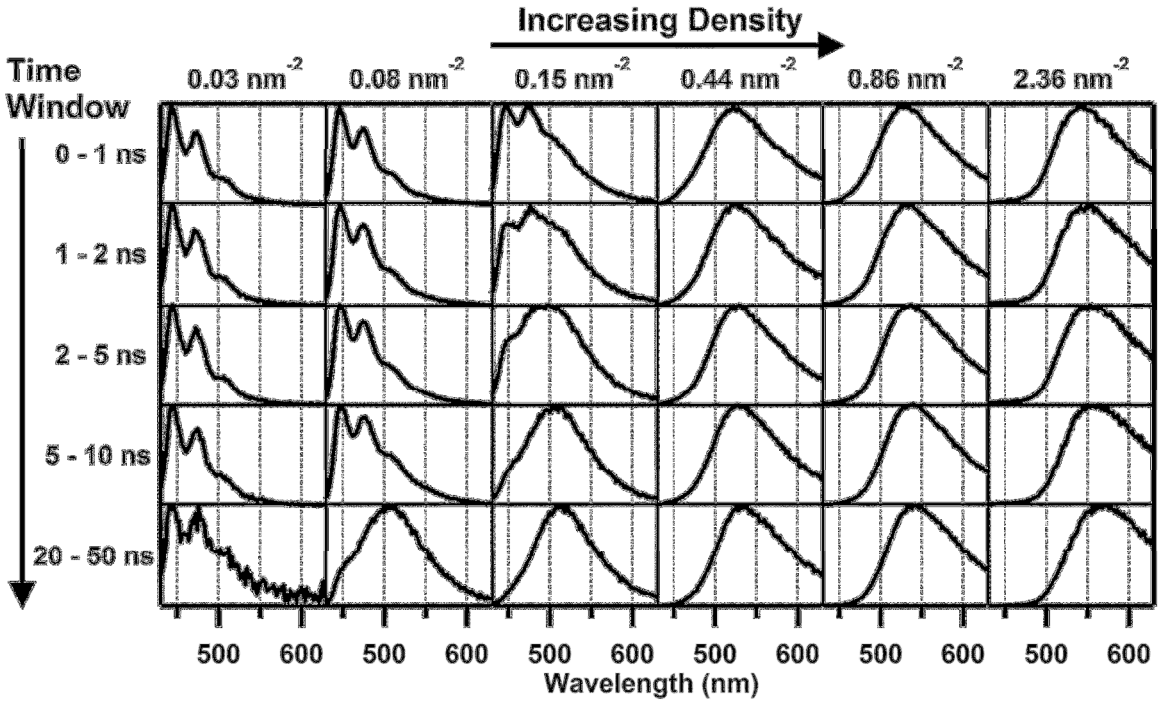

Figure 4.7: Normalized time-resolved emission spectra from samples pretreated at 700 °C with various P3M densities.

Figure 4.8 shows normalized time-resolved emission spectra at several time windows for samples preheated to various temperatures and subsequently given high P3M exposures. The profiles are nearly identical for the 300 and 500 °C pretreated samples (1.58 and 1.53 P3M / nm^2, respectively), and are slightly red shifted with respect to the 700 °C sample (0.86 P3M / nm^2), in agreement with the steady-state emission spectra. For all three samples, the peak maximum shifts to longer wavelengths by approximately 20 nm between the early and late time windows.

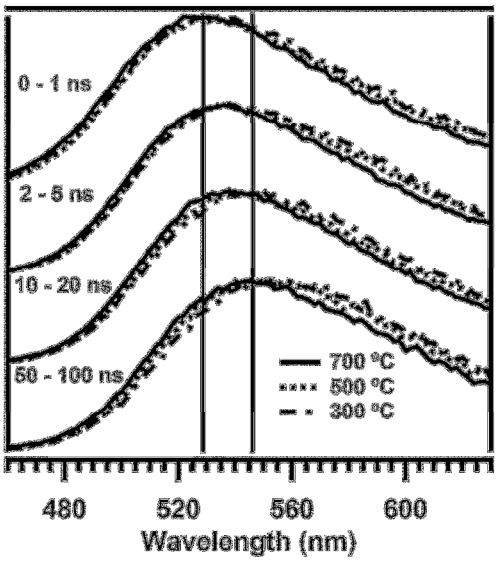

Figure 4.8. Normalized time-resolved emission spectra from samples pretreated to various temperatures and given high P3M exposures. The densities of the 300, 500, and 700 °C pretreated samples were found to be 1.58, 1.53, and 0.86 P3M / nm^2, respectively.

4.3.4 Fluorescence Decays

Fluorescence decay profiles for 700°C pretreated samples with very low and high P3M coverages are presented in Figure 4.9 (A) and (B), respectively. For low fluorophore densities the decay profiles are nearly identical for emission wavelengths near the two predominant vibronic peaks, indicating only one emitting species is present. The decay profiles appear very close to single exponential, although an improved fit is obtained using a more complex model accounting for energy transfer and quenching, as discussed below. The fluorescence decay from a solution of P3M in cyclohexane is shown for comparison in (A). The fluorescence decay from the monomer in solution is very similar to that observed from the low density sample. The lifetime for the solution was found to be 4.3 ns, which is similar to the literature value for perylene in solution (6.4 ns) [15]. In contrast to the low P3M density sample, the decay profiles from the high P3M density samples are clearly not single exponential and are wavelength dependent. Fluorescence decays quickly over the first 10 ns at 475 nm, followed by a slowly decaying tail. Emission at other wavelengths displays a similar shape, although the contribution of the slowly decaying tail becomes more significant at longer wavelengths. Fluorescence decay profiles for other samples are provided in Appendix B.

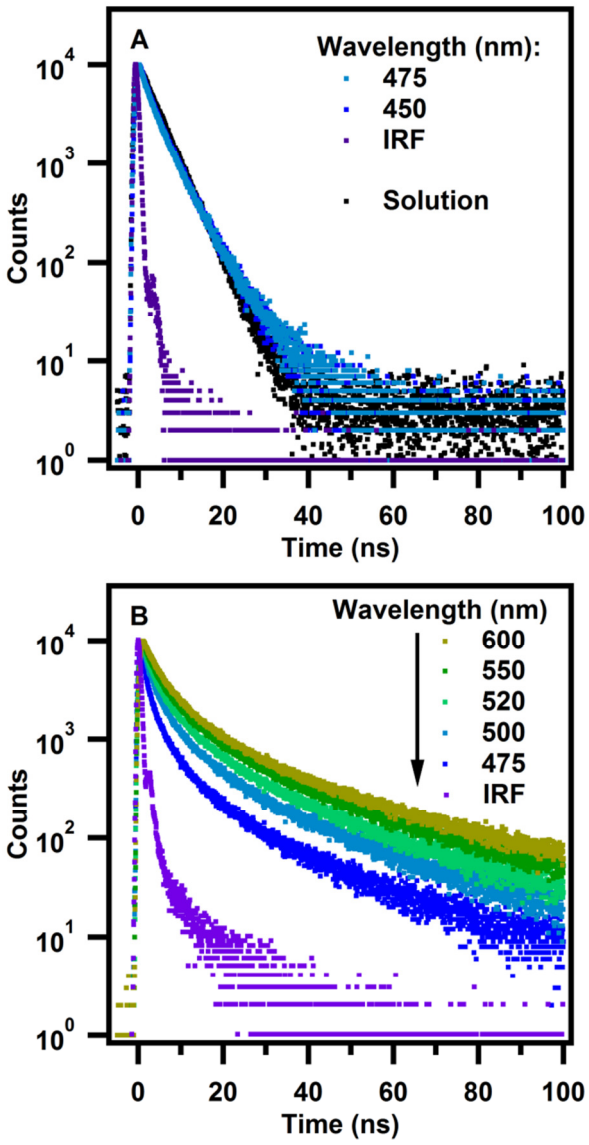

Figure 4.9: Fluorescence decay profiles collected at various emission wavelengths from 700 °C pretreated samples with P3M densities of 0.03 nm^{-2} (A) and 0.86 nm^{-2} (B). The decay labeled solution in (A) is from a 1×10^{-6} M P3M solution in cylcohexane collected at an emission wavelength of 475 nm. IRF is the instrument response.

Decay profile dependence on P3M density is demonstrated in Figure 4.10. Decays collected using emission wavelengths of 475, 520, and 600 nm are shown to illustrate the differences between samples and between emission wavelengths from the

same samples. Additionally, the 600 nm emission decay curve collected from the sample containing P3M particles deposited on fused silica is shown in part (C) to distinguish the fluorescence decay of particles with that of the bound fluorescent molecules. For 475 nm emission, the initial decay rate increases as intensity increases and a slowly decaying tail forms. For 520 nm emission, the decay curves are all similar and have a rapid decaying component and a slowly decaying tail. For 600 nm emission, the fluorescence decay profiles again display a fast decaying component and a slowly decaying tail, although the fraction of the profile associated with the fast decaying component is lower than for 520 nm emission. Emission from P3M particles is single exponential, with a lifetime of 17 ns.

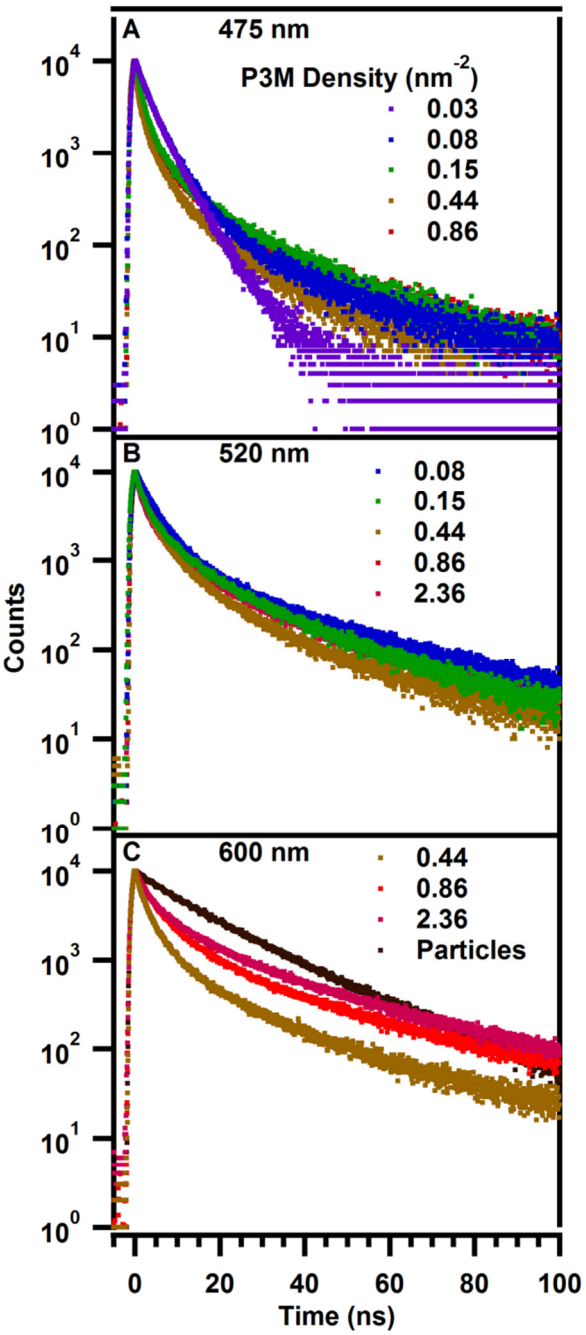

Figure 4.10: Decay profiles from samples with various P3M densities collected at emission wavelengths of (A) 475 nm, (B) 520 nm, and (C) 600 nm. The curve in (C) labeled "particles" is the decay from P3M particles deposited on fused silica.

4.3.5 Decay Analysis

The complexity of the observed decay profiles is a result of the various processes occurring in the two-dimensional perylene system upon photo-excitation. Due to their close proximity, perylene fluorophores are capable of resonance energy transfer with each other [29]. During this process, energy migration from donor to acceptor sites occurs. The observed decays in many two-dimensional systems can be modeled using the following function [3]:

$$\rho(t) = A_1 exp\left[-{}^{t}/_{\tau_1} - \gamma\left({}^{t}/_{\tau_1}\right)^{1/3}\right] + A_2 exp\left[-{}^{t}/_{\tau_2}\right] \quad (4.1)$$

where $\tau_1$is the lifetime of the donor species, $\tau_2$is the lifetime of a possibly different species that does not participate in energy migration, A_1 and A_2 are relative amplitudes of the emitting species and γ is a dimensionless constant depending on the density of acceptor sites and a term accounting for the distance over which energy transfer occurs. The left term of Equation 4.1 accounts for Förster-type energy transfer in two dimensions between randomly distributed donor and acceptor molecules, while the right term accounts for emission for sites that do not participate in resonance energy transfer. For two-dimensional systems, γ is given by:

$$\gamma = \Gamma\left(\frac{2}{3}\right)\pi n_A R_0^2 \quad (4.2)$$

where n_A is the areal density of acceptor sites and R_0 is the distance where the rate constant for energy transfer is equal to the rate constant of donor fluorescence in the absence of acceptors [3]. Based on the steady-state emission spectra shown above, there are at least two distinct emitting species. Monomeric emission is observed for low fluorophore densities (below 0.15 nm^{-2}), while a broad excimer-like emission is observed at higher densities. The decays from each sample were fitted using emission wavelengths corresponding to the predominant species for that sample. Because the model has several adjustable parameters, a global analysis using multiple emission wavelengths was

employed. The results of this analysis are presented in Table 4.1. For low fluorophore density samples (less than 0.15 nm^{-2}), lifetimes of 6 – 8 ns are observed for the primary emitting species, corresponding to monomer emission. A small fraction (A_2 / A_1) of emitting species with a lifetime of nearly 20 ns was observed for the monomeric samples with densities of 0.02 (300 °C pretreatment) and 0.08 P3M / nm^2. As the emission shifts to longer wavelength features with increasing bound perylene density, lifetimes of around 17 ns are observed for the primary species and a small fraction of species with a lifetime of over 30 ns are observed. The fraction of longer lifetime species increases with increasing emission wavelength, suggesting this species is responsible for the shift of the emission peak maxima to longer wavelengths at later times in the time-resolved emission spectra from Figures 4.8 and 4.9. Fitted values for γ range from 2 – 4.2, despite the large range of fluorophore densities examined. In fact, the limiting values were observed in two different low density samples. However, caution must be exercised when examining these quantities, as τ_1 and γ in particular are strongly correlated during the fitting routine, so that a change in one quantity can be compensated for by a change in the other with only a small change in the reduced chi-squared value, χ_r^2, which describes how well the model fits the data. Values of χ_r^2 close to unity represent good agreement between the model and experimental data. Although the global χ_r^2 values indicate less than perfect fits, using this approach yields parameters that are in agreement between samples.

Table 4.1: Results of global analysis of Equation 1 using decays from specified wavelengths. All samples were pretreated at 700 °C and exposed to P3M, unless indicated otherwise.

Fluorophore density (nm^{-2})	Emission wavelengths (nm)	A_2 / A_1	τ_1 (ns)	τ_2 (ns)	γ	Global χ_r^2
0.02[a]	450	0.0005	8.4	19.7	2.0	1.57
	475	0.0018				
0.03[b]	450	0.0016	6.4	8.5	4.2	2.43
	475	0.0018				
0.03	450	0.0001	7.2	7.4	3.8	1.47
	475	0.0008				
0.08	450	0.004	6.1	19.1	3.1	1.92
	475	0.029				
0.15	500	0.023	17.3	31.6	3.0	2.67
	520	0.019				
	550	0.049				
0.44	520	0.009	16.3	33.3	3.4	1.43
	550	0.012				
	600	0.013				
0.86	520	0.020	15.0	36.4	2.5	1.97
	550	0.030				
	600	0.040				
1.53[c]	520	0.014	17.0	35.4	3.0	1.88
	550	0.021				
	600	0.027				
1.58[d]	520	0.016	15.2	37.3	2.6	1.95
	550	0.026				
	600	0.032				
2.36[e]	520	0.016	21.0	35.6	3.4	2.87
	550	0.032				
	600	0.054				

[a]300 °C pretreatment
[b]P3A exposure
[c]500 °C pretreatment
[d]300 °C pretreatment
[e]No anneal step (physisorbed material)

The accuracy and physical meaning of the fitted parameters deserves further consideration. The model used to fit the data assumes at most two distinct emitting species, and assigns one lifetime to each species. However, the surface of amorphous silica is not homogeneous, in that sites are not uniformly spaced [18,20,30]. Therefore the distance between adjacent bound perylene moieties is not a single number for a given sample, but rather is a distribution. As discussed previously, the broadening of the absorption spectra can be attributed to the presence of various orientations of weakly bound dimers, providing further evidence for the non-uniform interactions between fluorophores. The distribution of intermolecular distances likely causes some spread in the lifetimes from each type of species, and possibly in the position of the emission maxima. The high χ_r^2 value for the 0.15 P3M / nm^2 sample is likely due to the presence of both substantial monomer and excimer-like features from this particular sample. Fluorescence decay profiles from emission wavelengths corresponding to the excimer-like species were fitted for this sample, resulting in parameters in agreement with higher fluorophore density samples. However, monomer emission also contributes to the decay profiles, particularly at shorter emission wavelengths, which is likely the cause of the worse fit relative to other samples. Similarly, the relatively worse fitting of the sample with physisorbed P3M may be due to the presence of additional emitting species or a more heterogeneous distribution of fluorophores. The interpretation of the γ term is discussed in more detail below.

4.4 DISCUSSION

4.4.1 Intensity of Emission Features

Perylene fluorophores covalently attached to planar silica surfaces exhibit unique properties compared to other systems containing the same fluorophore. The samples prepared in this work vary in fluorophore densities by nearly two orders of magnitude (0.02 – 2.36 nm^{-2}), and yet the intensities only vary by less than one order of magnitude (~2,700 – 15,200 counts). The non-linear relationship between fluorophore density and emission intensity is attributed to several phenomena. First, as the density increases, emission from excimer-like species competes with monomer emission. Because the excimer-like emission occurs from lower energy states (longer wavelengths) compared with monomer emission, such sites likely serve as acceptor states or energy traps for monomer excitation. The quantum yield from perylene monomers is near unity [15], but the quantum yield from the excimer state is likely lower, as discussed below. Therefore, for a given number of absorbed photons, less light would be reemitted from a sample with excimer-like emission than for a sample with monomeric emission. The second factor contributing to the non-linear relationship between density and emission intensity is the absorption of light by the different samples. The absorption spectra from the samples (Figure 4.5 (A)) shows that the higher density samples (greater than 0.44 nm^{-2}) all have a similar absorbance for the $S_0 \rightarrow S_1$ transition, while the $S_0 \rightarrow S_2$ feature absorbance increased with fluorophore density. This observation was explained by noting that the different transitions were polarized along different axes of the molecule. Preferential alignment of the long axis of the perylene molecule normal to the surface would decrease light absorption in the wavelength range of the $S_0 \rightarrow S_1$ transition for a given fluorophore density relative to a random molecular orientation. Therefore, although the density changes from 0.44 – 1.58 nm^{-2}, the number of photons absorbed by

these samples is very similar, explaining the similar emission intensity. The drawing in Figure 4.11 shows how fluorophore position and orientation affects the observed emission. The lower emission intensity of the sample with physisorbed P3M (2.36 nm^{-2}) relative to the high P3M density (0.86 nm^{-2}) sample is considered below.

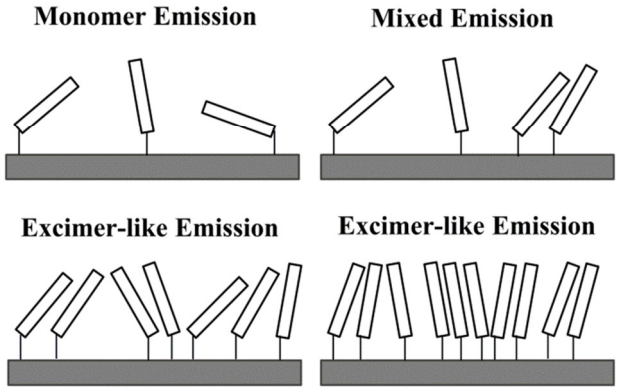

Figure 4.11: Schematic of molecular organization of fluorophores bound to the silica surface as a function of density leading to various observed emission features.

The ratio of the excimer quantum yield to the monomer quantum yield can be estimated by comparing the intensities of samples exhibiting only monomer emission and only excimer-like emission. In the limit of low absorbance, the integrated fluorescence intensity, $I_F(\lambda_E)$, is given by:

$$I_F(\lambda_E) \cong 2.3k\Phi_F I_0(\lambda_E)A(\lambda_E) \tag{4.3}$$

where Φ_F is the quantum yield, $I_0(\lambda_E)$ is the intensity of the exciting light with wavelength λ_E, $A(\lambda_E)$ is the absorbance of the system, and k is a factor accounting for the configuration of the detector [28]. The ratio of the excimer fluorescence quantum yield to the monomer fluorescence quantum yield can be obtained from Equation 4.3:

$$\frac{\Phi_F^{Ex}}{\Phi_F^{M}} = \frac{I_F^{Ex}(\lambda_E)}{I_F^{M}(\lambda_E)} \frac{A^{M}(\lambda_E)}{A^{Ex}(\lambda_E)} \tag{4.4}.$$

In order to estimate this ratio, spectra from the 0.08 and 0.44 P3M / nm2 samples were used. These samples were chosen because the former exhibited only monomeric emission and the latter only excimer emission. The *in situ* emission spectra from each sample were integrated, providing the relative intensities in Equation 4.4. The absorbance ratio requires further consideration. As shown in Figure 4.5, both monomer and excimer emission exhibit very similar absorbance features. In principle, the relative absorbance term should be equal to the ratio of fluorophore densities for such a dilute system of absorbers; however, caution must be exercised in this analysis as the preferential alignment of molecules leads to a limiting value of absorbance in this system. Although the absorbance from the 0.08 P3M / nm^2 sample was too low to be detected, the absorbance of the weak feature from the 0.15 P3M / nm^2 sample, which exhibits a combination of monomer and excimer-like emission, can be compared with the absorbance of the 0.44 P3M / nm^2 sample to determine if a linear relationship between fluorophore density and absorbance is valid for the latter sample. The ratio of the absorbance features from the 0.15 and 0.44 P3M / nm^2 samples is close to the ratio of their densities, suggesting that the absorbance ratio in Equation 4.4 can be approximated by the ratio of fluorophore densities for the 0.08 and 0.44 P3M / nm^2 samples. Based on this analysis, the estimated ratio of the excimer fluorescence quantum yield to the monomer fluorescence quantum yield, Φ_F^{Ex}/Φ_F^M, is approximately 1/3, demonstrating that the excimer quantum yield is significantly lower than the monomer quantum yield, as anticipated.

4.4.2 Identification of Emission Features

Comparing and contrasting the change from monomer-like to excimer-like emission in the present system to similar observations from Langmuir-Blodgett films containing perylene derivatives yields several important insights. Akimoto and coworkers observed monomer emission features for Langmuir-Blodgett films containing a perylene derivative at a mole fraction of 0.01, monomer emission and a feature centered around 530 nm for a mole fraction of 0.1, and emission centered around 600 nm with some monomer features for a mole fraction of 0.5 [13]. Based on the area per molecule given in that work, the densities of fluorophores range from approximately 0.05 nm^{-2} in the 0.01 mole fraction film to approximately 2.0 nm^{-2} in the 0.5 mole fraction film [13], which are similar in range to the fluorophore densities studied in this work. The two main distinctions between the Langmuir-Blodgett films and the present work are the lack of a distinct feature around 600 nm in the emission spectra of the present work and the presence of monomer features at high densities in the Langmuir-Blodgett films. We attribute both of these differences to the different nature by which the perylene fluorophores are bound to the surface in the two systems. For the Langmuir-Blodgett films, perylene moieties are attached to long carbon chains with carboxylic acid tail groups and non-fluorescent amphiphilic molecules are used as a matrix to stabilize the films. Because the fluorophores are not anchored to a specific location, they may organize during film formation. This organization may lead to domains containing multiple fluorophores and regions where isolated fluorophores exist, explaining the presence of both excimer-like and monomer emission features [13]. For the system in the present work, perylene moieties are covalently attached to sites distributed over the silica surface without the need for non-fluorescent spacer molecules, making the formation of domains of bound molecules and regions of isolated molecules unlikely.

The emission feature centered past 600 nm in the Langmuir-Blodgett films is attributed to excimer-like (E-type) emission from a sandwich dimer, consisting of two fully overlapping perylene groups, while the emission centered around 530 nm is attributed to excimer-like emission (Y-type) from partially overlapping perylene groups [7,10,11,13]. The predominance of the sandwich excimer emission in Langmuir-Blodgett films at high fluorophore densities indicates that the perylene structures have sufficient structural freedom to relax to this low energy state. Conversely, the lack of a well-defined feature corresponding to sandwich dimer absorption or emission from any sample in the present work indicates that such structures are not predominant in these systems, even for high fluorophore densities. Emission from the sandwich excimer species is predominant in the Langmuir-Blodgett films containing perylene derivatives at a fluorophore density of approximately 0.9 nm^{-2} [13], significantly lower the density of bound fluorophores on the 300 and 500 °C pretreated samples (1.58 and 1.53 P3M / nm^2, respectively) in this work. This demonstrates the lack of a distinct emission feature corresponding to the fully overlapping perylene excimer is not due solely to fluorophore density. We suggest the difference in emission between the two types of perylene systems is due to the attachment of molecules on a surface in the present samples. The use of a one-carbon tether to anchor the fluorophore to the silica surface likely constrains the motion of the perylene structure, preventing full relaxation between neighboring molecules and leading primarily to emission from partially overlapping structures, centered near 530 nm in the spectra. Pyrene fluorophores covalently bound to surfaces by longer chains than used here were shown to exhibit sandwich excimer emission in aqueous solutions, but some emission from partially overlapping excimer states was observed in dry samples [1]. The authors attributed the presence of the partially overlapping species in dry samples to a collapse of the flexible carbon chain, preventing

relaxation of excited molecules. Further work is necessary to determine the minimum chain length needed to observe full relaxation.

Although no distinct feature was observed past 600 nm in any emission spectrum in this work, evidence for some formation of fully relaxed excimer-like species exists. The emission features from high fluorophore density samples in Figures 4.2 and 4.4 are centered around 530 nm; however, careful inspection reveals that the peak is not symmetric about the maximum, with a more intense tail toward longer wavelengths. Fluorescence decay curves from high fluorophore density samples also suggest the presence of a small fraction of fully relaxed species. As shown above in Table 4.1, the results of fitting the decay curves to Equation 4.1 indicate two distinct species; one with a lifetime of approximately 17 ns and the other with a longer lifetime of greater than 33 ns. Since the faster decaying species represents the bulk of the sites, the dominant emission feature near 530 nm is associated with this species. Based on the relative pre-exponential factors, the intensity of emission from the slower decaying site increases at longer wavelengths relative to the emission intensity from faster decaying site. The longer lifetime species is then attributed to a small number of fully relaxed excimer-like species, which are expected to display an emission feature around 600 nm. This assumption also explains the red-shift of the peak location at later time windows in time-resolved measurements shown in Figures 4.7 and 4.8. A lifetime of nearly 30 ns was observed for fully relaxed (E-type) emission in Langmuir-Blodgett films, providing further evidence for the nature of this species [10].

Emission from the fully relaxed excimer-like species cannot be clearly distinguished from the partially relaxed excimer-like emission in time-resolved measurements because the fraction of the former is much less than the latter and the lifetimes are too similar. However, deconvolution of the steady-state emission spectra

can provide additional insight into the relative amounts of each component. The contributions from the partially and fully relaxed species to the overall emission for samples with various P3M densities are shown in Figure 4.12. Peaks centered at 535 and 600 nm were used for the partially and fully relaxed components, respectively. The fully relaxed component is observed in all cases, but, unlike for Langmuir-Blodgett films [13], the contribution from this component increases with increasing P3M density and is always less than the contribution from the partially relaxed component. Although peaks centered at 535 and 600 nm were used to fit the observed emission for all samples in Figure 4.12, better fits were obtained if the peak positions were allowed to vary between samples. This observation may be explained by considering the heterogeneous nature of the silica surface, as discussed above. Because the hydroxyl sites are not uniformly distributed, the distances between bound fluorophores and therefore the interactions leading to excimer formation are not the same between sites. The presence of a small fraction of fully relaxed species can be attributed to closely spaced hydroxyl sites on the silica surface, leading to closely packed bound fluorophores. However, instead of dividing emitting species into only two distinct classes, partially and fully relaxed excimers, a more appropriate description would consider distributions of emitting species based on the local environments of the fluorophores.

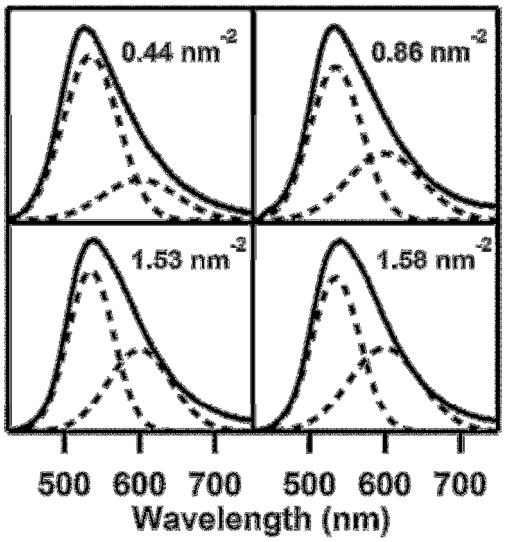

Figure 4.12: *Ex situ* emission spectra from samples with various P3M densities resolved into partially relaxed (centered at 535 nm) and fully relaxed (centered at 600 nm) excimer-like features.

The sample with physisorbed P3M (2.36 nm^{-2}) exhibits emission that is less intense and clearly red-shifted with respect to the sample with high densities of covalently attached fluorophores (0.86 nm^{-2}), as shown in Figure 4.2. The red-shift in both steady-state and time-resolved measurements from the sample with physisorbed material indicates a greater fraction of fully relaxed, or overlapping, excimer species are present in this sample relative to the 0.86 P3M / nm^{-2} sample. This assessment is supported by the relative A_2 / A_1 ratios in Table 4.1 for the two samples and by deconvolution of the emission spectrum (Appendix B). The presence of a more substantial fraction of fully relaxed excimer-like species in the sample with physisorbed P3M (2.36 nm^{-2}) is likely the cause of the lower emission intensity from this sample relative to the 0.86 P3M / nm^2 sample. The same argument used above to explain why emission intensity does not continue increasing linearly with density once excimer-like

emission is observed is applicable to this situation as well. Assuming the quantum yield from the fully relaxed state is lower than that of the partially relaxed state, energy migration from the partially relaxed (donor) to the fully relaxed (acceptor) states would result in less emitted light relative to a sample where no fully relaxed species were present. Also, although the absorbance does increase slightly between the 0.86 and 2.36 P3M / nm^2 samples, this increase is certainly not proportional to the relative change in fluorophore density. Therefore, although slightly more photons are absorbed by the 2.36 P3M / nm^2, the number of photons emitted, and hence emission intensity, is less than for the 0.86 nm^{-2} sample due to presumably lower quantum yield of the fully relaxed excimer-like state.

The time-resolved measurements in Figures 4.7 and 4.8 of samples with fluorophore densities greater than 0.44 P3M / nm^2 do not display monomer emission, even for the earliest time windows. Excimer formation occurs by association of an excited monomer and a ground state monomer, which typically requires movement of the molecules, resulting in a characteristic rise-time in the fluorescence decay curves from excimer species [28]. The rise-time in the excimer decay curve corresponds to an accelerated decay in the monomer decay curves. In systems where the monomers are already in close proximity to each other, the rate of the association process can be very rapid. In Langmuir-Blodgett films containing perylene fluorophores, this process occurs within 100 ps [13]. Such rapid process cannot be resolved by the instrument used in the present work, which explains why no monomer emission was observed for high fluorophore density samples even in early time windows.

4.4.3 Analysis of γ Term in Decay Model

The γ term contained in the model for intensity decay in a two-dimensional system (Equation 1) is related to the number of acceptor sites, n_a, and the critical transfer distance, R_0, by Equation 4.2. For energy transfer between perylene monomers in solution, R_0 is 37.85 Å; however, accounting for the alignment of the molecules in the present systems, this value would increase to 40.5 Å [29]. Using this value for R_0, one finds that the density of acceptor sites range from approximately 0.02 – 0.05 nm^{-2}. These densities are roughly the same as the entire fluorophore density for the monomer emission samples. Although similar values for γ, and therefore similar acceptor site densities based on the above R_0 value, were observed for perylene derivatives in Langmuir-Blodgett films containing the same range of fluorophore densities [13], such high acceptor site densities do not appear to be physically reasonable. Assuming Equation 4.1 is a reasonable model for this system, this observation suggests either values of γ or R_0 are inaccurate.

As explained previously, because the parameters τ_1 and γ can change simultaneously with minimal change in χ_r^2 over some range of values, some error in both values may be present. However, γ ranges from 2 – 3.8 over all samples and the $\tau_1$values for the low density samples are consistent with monomer lifetimes from solution. This suggests that even if some of the values of γ obtained from fitting of the decay profiles were overestimated, the true values cannot be sufficiently different from the fitted values to yield a physically reasonable number of acceptor sites. Alternatively, the value of R_0 for perylene in solution may not accurately reflect the efficiency of energy transfer processes on the surface. Values of R_0 for Rhodamine B derivatives in Langmuir-Blodgett films were estimated at up to 70 Å, compared to 44 Å for Rhodamine B in solution [27]. A similar increase in the present case would reduce the calculated densities

of acceptor states to values below the total fluorophore densities for all samples; however, the fraction of acceptor sites relative to total fluorophores is still quite large for the low density samples.

An alternative explanation is that Equation 1 does not accurately reflect the photo-physical processes occurring at low fluorophore densities. Equation 1 applies only to the case where excitation energy is transferred directly from the donor to the acceptor, and not between donor molecules [27]. Transfer between donors could result in an apparent increase in acceptor densities when using Equation 4.1. Alternative models have been proposed to account for this phenomenon [31,32], but they are generally more complex and have not been evaluated for the low fluorophore density samples prepared in this work.

For the higher fluorophore density samples, for which the emission is predominantly excimer-like, using an R_0 value of 40.5 Å results in calculated acceptor densities of 0.04 – 0.05 nm^{-2}. This could be interpreted as the density of fully relaxed, or sandwich, excimer species present on the samples, as the predominant (donor) emission is attributed to partially overlapping excimer species. However, the R_0 value above, which is based on energy transfer from a monomeric species, likely does not reflect the critical transfer distance from excimer-like species. Therefore, instead of focusing on numerical values for acceptor densities, we suggest that the γ term itself be used as an indication to the extent of excitation migration in the system. Based on this simplified analysis, the fluorescence decay results suggest that excitation migration occurs effectively for all samples examined in this work.

4.4.4 Influence of Coverage on Luminescence

The discussion above illustrates that many factors contribute to the luminescence observed from a surface with covalently attached perylene moieties. Interactions between fluorophores are ultimately responsible for all of the processes in this system. For low fluorophore densities (below 0.08 nm^{-2}), monomeric emission indicates that perylene molecules are in general not close enough to interact at close range; however, time-resolved emission spectra from the 0.08 P3M / nm^2 sample show the appearance of excimer-like features at late time windows. This suggests that P3M molecules do not preferentially adsorb on sites in close proximity to existing fluorophores. Deviations from single exponential fluorescence decay demonstrate long range (relative to molecular dimensions) interactions occur between bound fluorophores, leading to excitation migration between molecules.

At higher fluorophore densities (above 0.15 nm^{-2}), emission from partially relaxed excimer-like species is observed. This indicates perylene moieties are attached at sites in sufficiently close proximity so that, after absorption of a photon, a molecule in an excited state can interact with an adjacent ground state molecule. Broadening of features in the excitation spectra (Figure 4.5 (B)) also indicates the presence of fluorophores that interact at close range. In addition to the close range interactions, long range interactions are again detected by examining the fluorescence decay profiles samples exhibiting excimer-like emission.

At even higher fluorophore densities (above 0.44 nm^{-2}), emission from partially relaxed excimer-like species still dominates, although some emission from fully relaxed excimer-like species is also detected. The presence of the latter species suggests that some surface sites are sufficiently close to allow perylene molecules attached by a one-carbon tether to these sites to fully overlap; however, the fraction of such sites must be

low as no sandwich dimer absorption features is observed in the excitation spectra. In addition, the short range interactions between adjacent molecules influence the orientation of the molecules, leading to vertical alignment of the perylene moieties with respect to the surface. This effect leads to a saturation of the emission intensity as a function of bound fluorophore density, because essentially no further absorption of light occurs with increasing density.

The presence of only monomer emission in the time-resolved emission spectra from the sample titrated with P3A indicates that strained siloxane sites are spatially separated from each other on the silica surface. Additionally, comparison of both time-resolved and steady-state measurements from this sample and low density P3M samples demonstrates that separating the functional group from the perylene moiety by one carbon atom is sufficient to maintain the electronic properties of perylene. This suggests that other fluorescent probe molecules with different functional groups could be used to titrate other surface sites on silica and the same interpretation of emission spectra developed herein would apply to those systems as well, potentially providing insight to both the density of such sites and their proximity to each other or different sites. The combination of high sensitivity and spatial information should make such a technique valuable towards the characterization of ultra-low density surface sites on oxides, which remain elusive to study [33].

4.5 CONCLUSIONS

The density of covalently attached perylene fluorophores determines both the intensity and structure of emission spectra from these two-dimensional systems. For fluorophore densities below 0.08 nm^{-2}, only monomeric emission is observed. Samples

with fluorophore densities above 0.44 nm^{-2} exhibit predominantly excimer-like emission. Preferential orientation of fluorophores with increasing density results in samples with densities of 0.86 – 1.58 nm^{-2} having nearly identical absorption spectra in the wavelength range of the $S_0 \rightarrow S_1$ transition. This in turn causes nearly identical emission intensities between these samples.

Two-dimensional systems of perylene fluorophores covalently attached to silica surfaces exhibit distinct luminescence relative to other perylene containing systems. Unlike for perylene derivatives in Langmuir-Blodgett films, little emission attributed to a fully relaxed excimer-like species is observed in any sample. The short carbon chain used to attach the fluorophore to the surface is assumed to inhibit adjacent molecules from reaching a fully relaxed state. Future studies examining the influence of chain length on the formation of fully relaxed excimer species could provide additional insight into this phenomenon.

Fluorescence decay profiles are not single exponential, even for the lowest fluorophore density samples. A model accounting for energy migration and trapping in two dimensions was used to fit the decay profiles. Lifetimes of monomer species were found to be approximately 6 ns, in agreement with the lifetime of perylene monomers in solution. The lifetime of the partially relaxed excimer-like species was approximately 17 ns, while a lifetime of approximately 33 ns was found for the small fraction of fully relaxed excimer-like species.

This work demonstrates that covalent attachment of fluorophores can be used to generate systems with unique properties. The ability to tune the degree to which excimer-like species relax may prove useful for tailor the luminescence for specific applications. This is especially true for systems containing perylene, for which the various emission features span nearly the entire visible light region.

4.6 REFERENCES

[1] L. Gao, Y. Fang, X. Wen, Y. Li, D. Hu, Monomolecular layers of pyrene as a sensor to dicarboxylic acids, J. Phys. Chem. B. 108 (2004) 1207–1213.

[2] S. Zhang, F. Lü, L. Gao, L. Ding, Y. Fang, Fluorescent sensors for nitroaromatic compounds based on monolayer assembly of polycyclic aromatics, Langmuir. (2007) 1584–1590.

[3] I. Yamazaki, N. Tamai, T. Yamazaki, Electronic excitation transfer in organized molecular assemblies, J. Phys. Chem. 94 (1990) 516–525.

[4] J. McCrate, J. Ekerdt, Titration of Free Hydroxyl and Strained Siloxane Sites on Silicon Dioxide with Fluorescent Probes, Langmuir. 29 (2013) 11868–11875.

[5] J. Tanaka, The electronic spectra of aromatic molecular crystals. II. The crystal structure and spectra of perylene, Bull. Chem. Soc. Jpn. 36 (1963) 1237–1249.

[6] B. Walker, H. Port, H. Wolf, The two-step excimer formation in perylene crystals, Chem. Phys. 92 (1985) 177–185.

[7] J. Ferguson, Absorption and Emission Spectra of the Perylene Dimer, J. Chem. Phys. 44 (1966) 2677.

[8] H. Tachikawa, L. Faulkner, Anomalous luminescence from perylene in thin polymer films, Chem. Phys. Lett. 39 (1976) 436–441.

[9] A. Vitukhnovsky, M. Sluch, J. Warren, M. Petty, The Fluorescence of Perylene-Doped Langmuir—Blodgett Films, Chem. Phys. Lett. 173 (1990) 425–429.

[10] D. Weiss, R. Kietzmann, J. Mahrt, B. Tufts, W. Storck, F. Willig, E-excimer and Y-type luminescence of perylene dimers in a Langmuir-Blodgett film at 1.5 K, J. Phys. Chem. 96 (1992) 5320–5325.

[11] J. Mahrt, F. Willig, W. Storck, D. Weiss, R. Kietzmann, K. Schwarzburg, et al., Luminescence and configurations of perylene dimers in a Langmuir-Blodgett film, J. Phys. Chem. 98 (1994) 1888–1894.

[12] M. Sluch, A. Vitukhnovsky, L. Ande, Fluorescence of perylene-4-octadecanon in Langmuir-Blodgett films, Thin Solid Films. 248 (1994) 230–233.

[13] S. Akimoto, A. Ohmori, I. Yamazaki, Dimer Formation and Excitation Relaxation of Perylene in Langmuir-Blodgett Films, J. Phys. Chem. B. 101 (1997) 3753–3758.

[14] J.B. Birks, Photophysics of Aromatic Molecules, Wiley-Interscience, New York, 1970.

[15] I. Berlman, Handbook of Fluorescence Spectra of Aromatic Molecules, 2nd ed., Academic Press, New York, 1971.

[16] I. Yamazaki, N. Tamai, T. Yamazaki, Picosecond Fluorescence Spectroscopy on Excimer Formation and Excitation Energy Transfer of Pyrene in Langmuir-Blodgett Monolayer Films, J. Phys. Chem. 91 (1987) 3572–3577.

[17] M. Sluch, A. Vitukhnovsky, M. Petty, Pyrene excimer formation in Langmuir-Blodgett films, Thin Solid Films. 285 (1996) 622–626.

[18] C.H. Lochmuller, A.S. Colborn, M.L. Hunnicutt, J.. Harris, Bound Pyrene Excimer Photophysics and the Organization and Distribution of Reaction Sites on Silica, J. Am. Chem. Soc. 106 (1984) 4077–4082.

[19] M. Mazur, G. Blanchard, Probing intermolecular communication with surface-attached pyrene, J. Phys. Chem. B. 109 (2005) 4076–4083.

[20] C. Lochmuller, A. Colborn, M. Hunnicutt, Organization and distribution of molecules chemically bound to silica, Anal. Chem. 55 (1983) 1344–1348.

[21] N. Tamai, T. Yamazaki, I. Yamazaki, Two-dimensional excitation energy transfer between chromophoric carbazole and anthracene in Langmuir-Blodgett monolayer films, J. Phys. Chem. 91 (1987) 841–845.

[22] N. Tamai, T. Yamazaki, I. Yamazaki, Excitation energy relaxation of rhodamine B in Langmuir-Blodgett monolayer films: Picosecond time-resolved fluorescence studies, Chem. Phys. Lett. 147 (1988) 25–29.

[23] K. Kemnitz, N. Tamai, I. Yamazaki, N. Nakashima, K. Yoshihara, Fluorescence decays and spectral properties of rhodamine B in submono-, mono-, and multilayer systems, J. Phys. Chem. 90 (1986) 5094–5101.

[24] P. Anfinrud, R.L. Crackel, W.S. Struve, Excitation transport and trapping in a two-dimensional disordered system: cresyl violet on quartz, J. Phys. Chem. 88 (1984) 5873–5882.

[25] N. Salivati, J.G. Ekerdt, Temperature programmed desorption studies of deuterium passivated silicon nanocrystals, Surf. Sci. 603 (2009) 1121–1125.

[26] L. Zhuravlev, The surface chemistry of amorphous silica. Zhuravlev model, Colloids Surfaces A. 173 (2000) 1–38.

[27] P. Ballet, M. Van der Auweraer, F. De Schryver, H. Lemmetyinen, E. Vuorimaa, Global analysis of the fluorescence decays of N, N'-Dioctadecyl rhodamine b in Langmuir-blodgett films of diacylphosphatidic acids, J. Phys. Chem. 100 (1996) 13701–13715.

[28] B. Valeur, Molecular Fluorescence, Wiley-VCH Verlag, Weinheim, 2002.

[29] I. Berlman, Energy Transfer Parameters of Aromatic Compounds, Academic Press, New York, 1973.

[30] H. Wang, J. Harris, Origins of bound-probe fluorescence decay heterogeneity in the distribution of binding sites on silica surfaces, J. Phys. Chem. 99 (1995) 16999–17009.

[31] G. Zumofen, A. Blumen, Energy trapping in mixed molecular crystals, Chem. Phys. Lett. 98 (1983) 393–397.

[32] J. Klafter, A. Blumen, Fractal behavior in trapping and reaction, J. Chem. Phys. 80 (1984) 875–877.

[33] G. Pacchioni, Oxygen Vacancy: The Invisible Agent on Oxide Surfaces, ChemPhysChem. 4 (2003) 1041–1047.

Chapter 5: Detection of Oxygen-Vacancy Defect Sites on the Silica Surface using Fluorescent Probes

5.1 INTRODUCTION

Oxygen vacancy defects (OVDs) are believed to be present on the surfaces of many oxides, although detection of these sites has proven challenging for many material systems [1]. Such sites may play an important role in many surface processes, including catalysis and nucleation. The ability to detect low density OVD sites may provide new insight into such fundamental processes.

We have previously demonstrated the detection of both free hydroxyl and strained siloxane sites on planar silica surfaces in vacuum using a technique in which specific sites are titrated by fluorescent probes [2]. With this approach, perylene derivatives with particular functional groups are used to titrate specific sites, forming chemically bound fluorophores on the surface. The detection limits of this technique have been estimated to be below 10^{10} sites / cm^{-2} [2], making this technique suitable for detection of ultra-low density surface sites. A more detailed study on the nature of luminescence from surfaces as a function of fluorophore density has also been performed [3].

Several types of point defects are known to exist in bulk amorphous silica [4]. Paramagnetic defects including E', or silyl (≡Si•), centers, non-bridging oxygen hole (NBOH) centers (≡Si-O•), and peroxy radicals (≡Si-O-O•) have been detected using electron paramagnetic resonance (EPR) techniques [4]. Defect sites can be generated on the silica surface using various methods including ion-bombardment [5], mechanical activation [6], and chemical treatments [7–11]. Several types of defect sites can be

generated from “reactive silica”, or silica in which the surface hydroxyl sites are substituted with methoxy groups (≡Si-O-CH_3), followed by vacuum pyrolysis to form silyl (≡Si•) and silylene (≡Si:) centers [7,8,11,12]. Dioxasilirane (>Si(O2)) [8,10], silanone (>Si=O) [8,10], and non-bridging oxygen hole center (≡Si-O•) sites [9] could subsequently be formed from the silylene centers. Using this approach, sufficient densities of various defect sites could be prepared on high surface area silica to enable characterization of these sites using infrared (IR) and photoluminescence (PL) spectroscopies [7–12]. Because of the challenge of experimentally detecting low density intrinsic defect sites on the silica surface, computational studies of such sites have been performed [13–15]. Kuo and Hwang found that a surface OVD is capable of transforming from a Si-Si dimer to other reactive structures, including silylene and silanone sites [13].

In order to detect OVD sites, a fluorescent probe molecule must be chosen that will react with these sites but not with either hydroxyl or strained siloxane sites. Alkenes, such as ethylene, have been shown to be non-reactive towards both strained siloxane and hydroxyl sites [16]. Additionally, Cerofolini and Meda demonstrated that high energy ion bombardment of high surface area silica in an ethylene environment resulted in the chemisorption of ethylene molecules on defect sites [5]. Infrared spectroscopy and density functional theory calculations were used to show that the ethylene molecules added across the defect site, at least after annealing the sample. Therefore, a perylene derivative with a vinyl functional group, 3-vinyl perylene (3VP), was chosen as the probe molecule for titrating OVD sites.

In addition to characterizing intrinsic OVD sites on the silica surface, this work explores the relationship between these sites and other surface sites. Specifically, we examine how a Si exposure process, in which SiH_x (x = 1, 2, 3) fragments are generated

by cracking disilane on a hot tungsten filament, influences the distribution of surface sites. This process has previously been demonstrated to lead to enhanced nucleation of germanium (Ge) nanoparticles on the Si surface [17]. Understanding how the Si exposure process affects various surface sights may provide new insight into defect mediated nucleation processes.

5.2 EXPERIMENTAL

Details of the synthesis of perylene-3-methanol (P3M) and perylene-3-methanamine (P3A) have been described previously [2]. 3-Vinyl perylene (3VP) was obtained from the University of Florida. All compounds were purified over a silica gel column and then sublimed onto aluminum foil, which was subsequently loaded into a thermal evaporator cell in the vacuum chamber.

Details of the multi-chamber UHV chamber used in this work are described elsewhere [2]. Briefly, this system consists of a load lock, a transfer chamber with a quartz tube furnace, a chamber for exposure of samples to the fluorescent probe molecules, a chamber containing a hot filament for cracking either deuterium or disilane gases, and an analysis chamber containing an x-ray photoelectron spectrometer (XPS) and a mass-spectrometer for temperature programmed desorption (TPD) measurements. All chambers operate with a base pressure approximately 10^{-9} torr or below.

In situ emission measurements are performed using a photoluminescence setup consisting of a 405 nm diode laser with an output power of 20 mW, a spectrometer (Ocean Optics), and optics to focus both the laser beam and the spectrometer onto the sample through an optical window with a spot size of ~1 mm^2. The laser and

spectrometer were connected to the optics assembly via fiber optics. All measurements were performed using a 1s integration time and averaging three measurements.

A typical experiment involved loading cleaned fused silica wafers (Sydor Optics) onto a molybdenum sample holder [2]. The sample transferred into the system through the load lock and could then be moved to the desired chamber. Unless otherwise noted, all samples were pretreated by heating to 700 °C for 30 min in the tube furnace. After cooling, samples were then either moved to the chamber used for gas exposure or to the chamber for exposure to the desired fluorescent precursor.

Cracking of disilane on a hot tungsten filament to generate SiH_x fragments has been described previously [17]. The sample was positioned approximately 3 cm from a 250 W Osram Xenophot bulb with part of the glass enclosure removed. 4% Disilane in a helium balance (Voltaix) was introduced through a leak valve to bring the partial pressure of disilane to 8×10^{-8} torr. A current of 4 A was then applied to the bulb, resulting in filament temperatures of ~1800 K [18]. The flux of SiHx fragments was calibrated based on the attenuation of the Si^{4+} feature in XPS after a 60 min exposure (Appendix C). One monolayer (ML) equivalent was deposited in 3.33 min.

Atomic deuterium was generated by introducing deuterium gas (99.999%; Matheson) through a leak valve to bring the total chamber pressure to 10-6 torr. The same filament and current settings used to crack disilane was also used to generate atomic deuterium. The flux of atomic deuterium generated in this manner was calibrated using temperature programmed desorption of D2 from a Ge(100) sample. The clean, oxygen free surface was given various exposures of atomic deuterium followed by TPD measurements in the analysis chamber. Saturation of the monohydride feature was observed, so that the area of this feature in TPD corresponds to a surface with 5.8×10^{14} D / cm^2. TPD measurements collected after much lower exposures were then used to

calculate the flux (Appendix C). The areas of the TPD features were linear with exposure in the low exposure range, and a sticking coefficient of unity at low coverages was assumed. A flux of 5×10^{14} D/cm^2/s was found using this analysis.

Samples exposed to various Si exposures were subsequently transferred to the analysis chamber and ramped to ~700 °C at ~2 °C/s. This step was done to replicate the procedure used previously that was assumed to remove surface Si as SiO through an etching process [17]. The latter assumption will be reevaluated below. Samples were allowed to cool to below 100 °C before transferring out of the analysis chamber.

After samples had received the appropriate pretreatment, including heating in the tube furnace exposure to either atomic deuterium or SiHx fragments, they were then moved to the exposure chamber containing the desired precursor. The evaporator cell containing the precursor was heated to 60 °C for the P3A and 3VP precursors and exposure times of 30 min were found to be sufficient to titrate all reactive sites for the particular molecule. For titration of free hydroxyl sites with P3M, a small amount of P3A precursor was added to the P3M in order to catalyze the reaction, as described previously [2]. The evaporator was heated to 100 °C for this precursor and an exposure time of 60 min was used to ensure nearly complete titration. All samples were heated to ~80 °C during the exposure processes to minimize the amount of physisorbed material.

After samples were exposed to the desired precursor, they were then moved in front of the photoluminescence setup to collect an in situ emission spectrum. The samples were then transferred into the tube furnace and annealed at 300 °C for 30 min. This step is critical for removing any physisorbed material, thereby ensuring only chemically bound species are present on the surface. After cooling, a final in situ emission spectrum was collected. This spectrum represents emission from chemically

bound fluorophores. Unless otherwise noted, all spectra presented in this work were collected after the anneal step.

5.3 Results and Discussion

5.3.1 Titration of sites using 3-vinyl perylene

Samples pretreated to various temperatures were exposed to the vinyl derivative of perylene, 3VP. The emission spectra collected after annealing to remove physisorbed molecules is presented in Figure 5.1. An emission feature is clearly visible on all samples, with roughly double the intensity between the 300 and 700 °C pretreated samples. The emission appears primarily monomeric, although the nature of the emission features is examined further below. Repeated exposure and anneal steps on the same sample resulted in very little change to the resulting emission spectrum, indicating the chemisorption process is truly due to titration of specific sites and not a slow and incomplete reaction with higher density sites.

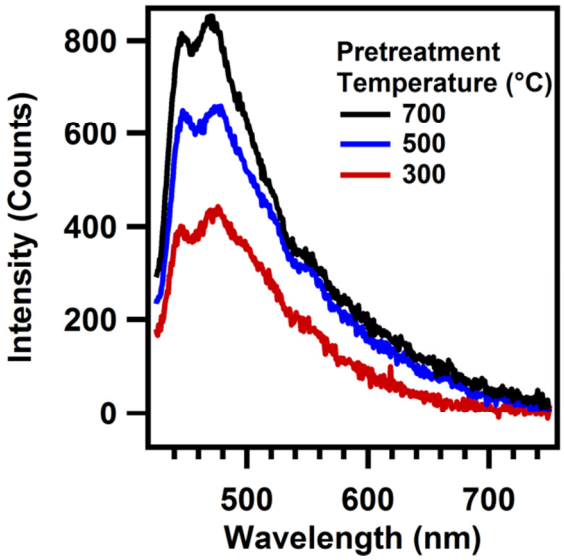

Figure 5.1: *In situ* emission spectra from samples pretreated to various temperatures and titrated with 3VP.

The chemisorption of 3VP suggests the presence of a low density site that is different than the previously identified free hydroxyl and strained siloxane sites. This is because alkenes, such as ethylene, are known not to react with either of the aforementioned sites [16]. Comparison of the emission spectra from 3VP titrated surfaces with that of P3A titrated surfaces provides additional insight into both the density and nature of sites at which 3VP is bound. Such a comparison is presented in Figure 5.2 for samples pretreated to 700 °C. The emission intensity from the P3A sample is over one order of magnitude more intense than that of the 3VP sample. The density of bound P3A molecules present on a 700 °C pretreated sample has been estimate to be approximately 2.5×10^{12} cm^{-2} [2]. Based on the relative intensities between samples, the density of bound 3VP molecules is estimated to be approximately 10^{11} cm^{-2}. However, as shown in the bottom part of Figure 5.2, emission from the 3VP titrated sample is not purely monomeric. Additional features appear to be present at longer wavelengths, indicating excimer-like emission also occurs [3]. Therefore, the estimated density of 10^{11} cm^{-2} represents a lower bound for the actual density of bound 3VP. Because the emission is primarily monomeric, this estimated value should be reasonable [3].

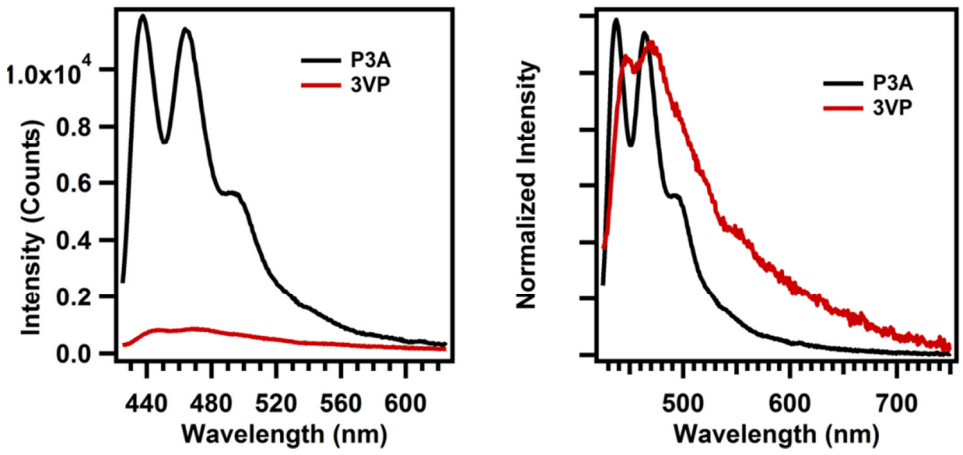

Figure 5.2: **(Left)**: *In situ* emission spectra collected from 700 °C pretreated samples titrated with either P3A or 3VP. **(Right):** Normalized spectra from the top figure showing the differences between emission features.

The chemical nature of the adsorption site deserves further consideration. As explained above, the vinyl functional group is not anticipated to react with either the hydroxyl sites or the strained siloxane sites [16]. The much lower density of bound 3VP molecules relative to bound P3A molecules after the titration process provides evidence that the 3VP is reacting with a lower density surface site than even the strained siloxane sites. Repeated exposure and anneal steps resulted in virtually no change in the observed emission, providing further evidence that the 3VP molecules were not simply slowly reacting with strained siloxane sites.

An explanation for the reaction between 3VP and the silica surface can be found by examining the adsorption of ethylene on ion-bombarded high surface area silica [5]. This work demonstrated that ethylene can chemisorb at either oxygen vacancy or silicon vacancy sites on the silica surface. Adsorption on the oxygen vacancy sites were found to occur by addition across the adjacent silyl radicals (≡Si•), at least after annealing. Density functional theory calculations showed that such structure should be thermodynamically favorable [5]. A similar structure is anticipated to form by reaction

of the vinyl group on 3VP with the oxygen vacancy site, as shown in Figure 5.3. Additionally, the presence of hydrogen may lead to the formation of hydride (≡SiH) sites on the surface. Such sites could potentially react with 3VP in either the same manner as the silyl sites. However, strong relaxation of the hydride site could lead to the chemisorption of two 3VP molecules on the OVD site, with one bound to each ≡SiH site. This latter reaction could then presence of the weak excimer-like features observed in the emission spectra form 3VP titrated surfaces. Such a feature must be due to perylene moieties in close proximity to each other, and is not typically observed for fluorophore densities below 10^{13} cm^{-2} [3].

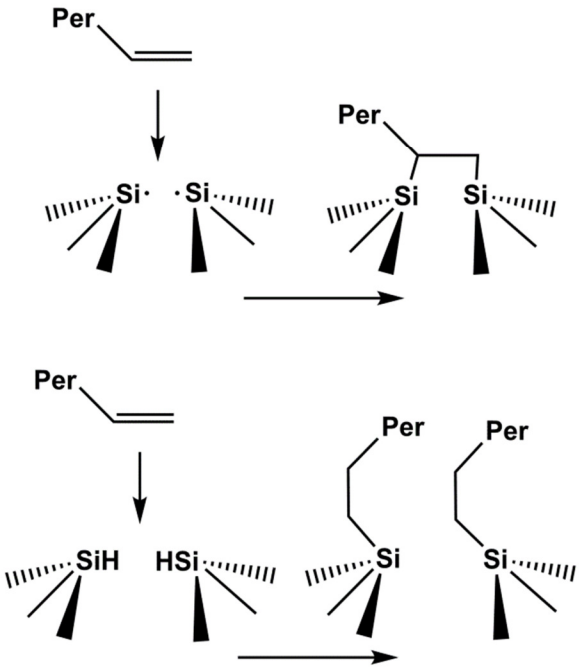

Figure 3: Proposed reactions between 3VP and possible surface sites.

Alternative adsorption sites for the 3VP molecule include other defect sites, such as the silylene (=Si:), silanone (=Si=O), or non-bridging oxygen hole sites (≡Si-O•) sites.

Diamagnetic silylene centers can be generated by converting hydroxyl sites to methoxy sites, followed by pyrolysis in vacuum [11]. The interaction of ethylene with these sites has been studied, and essentially no chemical bonding between the ethylene molecule and the silylene center was detected using infrared spectroscopy [19]. This suggests the silylene center also will be unreactive towards the 3VP molecule, if such sites exist on the silica surface prepared in this work. Silanone sites are very reactive [6,12], and could potentially react with 3VP molecules. However, the interaction of such sites with atomic deuterium is known to result in the formation of hydroxyl sites (≡Si-OH) [6], which would then be unreactive towards the 3VP molecule. As shown below, atomic deuterium does not appear to passivate the reactive sites, but rather creates additional sites. This observation suggests that if silanone sites are present and do react with 3VP, they must not be the dominant surface site.

Adsorption of 3VP on NBOH centers may also be possible. The reaction between ethylene and Si vacancy sites, which are essentially four adjacent NBOH sites which may relax to form O-O bonds, has been studied on ion-bombarded silica using IR spectroscopy [5]. This reaction was found to be complex, with evidence of ethylene insertion followed by bond rearrangement leading to the formation of structures with either C=C or C=O bonds [5]. These sites are believed to react with molecular hydrogen readily at room temperature, forming a silanol (≡Si-OH) site and atomic hydrogen [20]. However, exposure to molecular deuterium prior to 3VP titration (*vide infra*) does not appear to change the density of bound 3VP, indicating the majority of sites at which the fluorescent probe is attached in this work are not NBOH centers. The sites are also unlikely to be peroxy radicals, as such sites are known to thermally decompose at temperatures above 650 K to form NBOH centers and molecular oxygen [12].

The results thus far provide experimental evidence for the existence of intrinsic low density sites, likely oxygen vacancy defects. Due to their extremely low density (~10^{11} cm^{-2}), such sites have not previously been detectable, even on high surface area silica. The detection of such sites by titration with fluorescent probes demonstrates the high sensitivity of this technique and opens up the possibility of studying the reactivity of these and other sites.

5.3.2 Influence of atomic deuterium on surface sites

Having demonstrated the detection of presumably oxygen-vacancy defect sites, along with previous work on the titration of strained siloxane and free hydroxyl sites [2], we now examine the reactivity of these sites in the presence of atomic deuterium. Such information is necessary to determine the mechanism by which the Si exposure process leads to enhanced nucleation of Ge particles on a SiO_2 surface, as atomic hydrogen is almost certainly generated during that process.

Exposure of 700 °C pretreated samples to various amounts of atomic deuterium followed by titration with P3M results in the spectra shown in Figure 5.4. Although the emission intensity does decrease with increasing atomic deuterium fluence, measurements of bound P3M densities obtained by hydrolytically cleaving off the molecules into a solution [2] reveal the densities are very similar between samples. Additionally, previous work has demonstrated that a decrease in density leads not only to a decrease in emission intensity, but also a change in the emission features [3]. This suggests that the decrease in intensity with increasing atomic deuterium exposure must be due to a quenching of the luminescence. Atomic deuterium may migrate into the bulk and form electrically active defect sites, which may act as the fluorescence quenchers .

Regardless of the nature of quenching, the external solution measurements confirm that virtually no change in hydroxyl density is observed with atomic deuterium exposure. Previous studies have also reached the same conclusion [21].

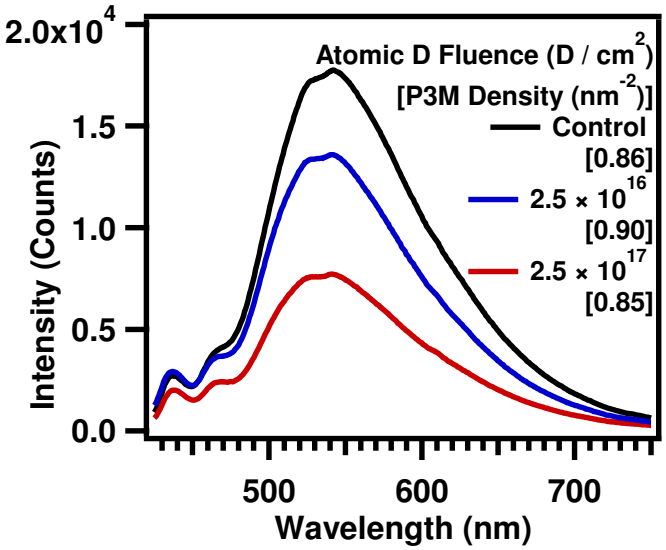

Figure 5.4: *In situ* emission spectra collected from 700 °C pretreated samples exposed to various quantities of atomic deuterium and then titrated with P3M. The bound P3M densities measured by hydrolytic cleavage of the molecules into solution are shown in brackets.

Samples pretreated to 700 °C were also exposed to various amounts of atomic deuterium and subsequently titrated with P3A to determine the influence of atomic deuterium exposure on these sites. The spectra from samples subjected to various atomic deuterium exposures are presented in Figure 5.5. In this case, virtually no change in intensity is observed with increasing atomic deuterium fluence. This suggests that either atomic deuterium does not react with strained siloxane sites or that any site generated by such a reaction also reacts with the P3A molecule in a similar fashion as the strained siloxane site itself. The latter conclusion is shown to be most probable (*vide*

infra). The observation that no quenching of the emission is observed with increasing atomic deuterium fluence is in contrast to the results of the P3M titrations shown above. This observation can be explained by noting that emission from species with longer lifetimes is more likely to be quenched compared with emission from shorter lifetime species. Due to the high fluorophore denisty, the emission from the P3M titrated samples is excimer-like, with a lifetime on the order of tens of nanoseconds, while the emission from the low fluorophore density P3A titrated samples is monomeric, with a lifetime of approximately 5 ns [3]. Therefore, emission from the P3A titrated samples is expected to be less prone to quenching relative to the P3M titrated samples.

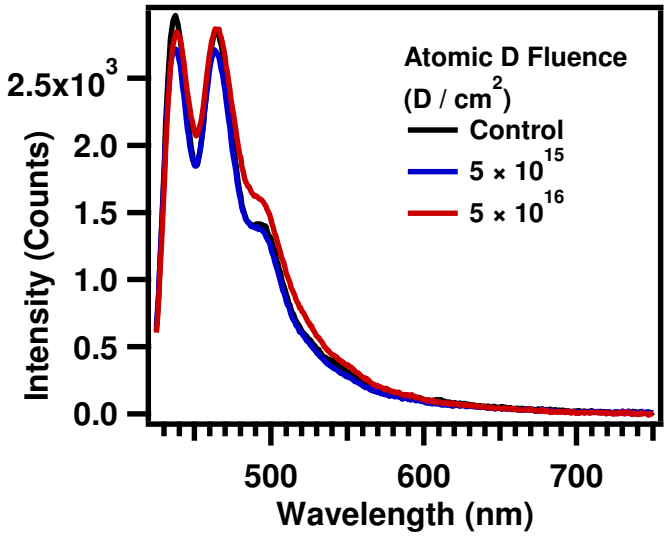

Figure 5.5: *In situ* emission spectra from 700 °C pretreated samples exposed to various amounts of atomic deuterium and subsequently titrated with P3A.

The influence of atomic deuterium exposure on the density of bound 3VP molecules is shown in Figure 5.6. Exposure to deuterium gas (D_2) only causes no change in the observed emission intensity. However, exposure to a fluence of 5×10^{14} D/cm^2 causes a significant increase in the emission intensity. Increasing the fluence by an order

of magnitude causes a further increase in emission intensity, but further increases in the atomic deuterium exposure result in no further increase in emission intensity. This suggests that the atomic deuterium exposure creates new sites at which 3VP can chemically bind; however, only a certain number of these sites can be generated. The emission intensity increases by nearly one order of magnitude between the sample with no atomic deuterium exposure and the sample with 5 x 10^{15} D/cm^2 exposure. The emission also remains primarily monomeric, so that a bound fluorophore density of approximately 10^{12} cm^{-2} is estimated for samples with the two highest atomic deuterium exposure.

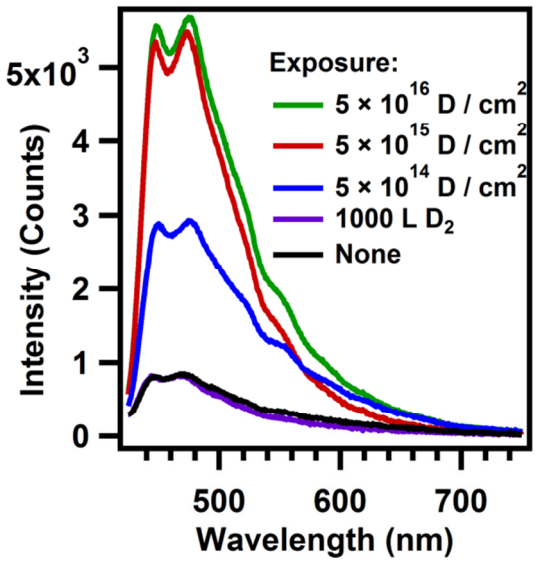

Figure 5.6: *In situ* emission spectra from 700 °C pretreated samples exposed to various amounts of atomic deuterium and subsequently titrated with 3VP.

In order to examine the thermal stability of the sites generated by the atomic deuterium exposure, a 700 °C pretreated sample was given a 5 × 10^{15} D / cm^2 exposure and then heated to 700 °C at 2 °C/s prior to titration with 3VP. The emission spectra

from both this sample and a sample with the same atomic deuterium exposure but without the additional heating step are shown in Figure 5.7. The intensity of the emission feature from the sample heated to 700 °C after atomic deuterium exposure decreases by about half relative to the sample without the heating step; however, the intensity is still greater than emission from a sample without any atomic deuterium exposure. This indicates that some fraction of the sites generated by atomic deuterium exposure are stable even at high temperatures. Importantly, this same heating step is used in the Si exposure process, so that sites generated by atomic hydrogen during the Si exposure process may also be chemisorbing 3VP, in addition to any sites generated by the SiH_x fragments.

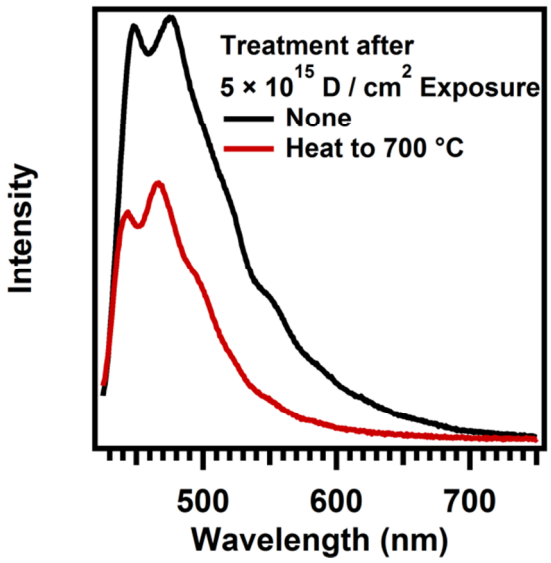

Figure 5.7: *In situ* emission spectra collected from 700 °C samples given an atomic deuterium exposure and titrated with 3VP with and without a heating step between the atomic deuterium exposure and titration process.

5.3.3 Influence of Si exposure on surface sites

In order to understand the chemical nature of the enhanced nucleation of Ge particles on SiO_2 after the Si exposure process, the fluorescent probe titration technique was used to examine how the densities of each type of site changed with increasing Si exposure. The calibration of the Si exposure is described above. One monolayer equivalent (ML) corresponds to 5 x 10^{14} Si / cm^2. As explained in the experimental section, after the Si exposure, the sample was rapidly heated to approximately 700 °C and subsequently cooled to below 100 °C prior to titration with the desired precursor.

Figure 5.8 shows the emission spectra from a 700 °C pretreated sample exposed to various Si exposures and then titrated with P3M. As in the case of atomic deuterium exposure, the emission intensity from P3M titrated samples decreases with increasing exposure. However, once again, the density measurements performed by hydrolytically cleaving the bound P3M molecules from the sample surface into a solution demonstrate that no change in bound P3M density, and therefore hydroxyl density, is observed. Quenching of the emission with increasing Si exposure is once again attributed to generation of defects in the bulk due to hydrogen.

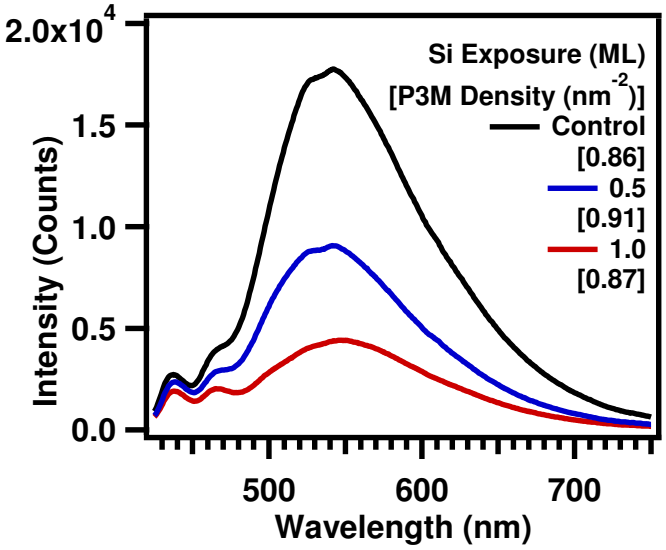

Figure 5.8: *In situ* emission spectra from 700 °C pretreated sample given various Si exposures and then titrated with P3M. Densities measured by hydrolytic cleavage of bound P3M into solution are given in brackets.

Unlike atomic hydrogen exposure, the Si exposure process causes a dramatic change in both the emission intensity and shape from samples titrated with P3A, as shown in Figure 5.9. The lowest (0.1 ML) exposure causes a dramatic decrease in the observed emission intensity relative to a sample with no Si exposure, but the feature still appears to be monomer emission. Surprisingly, the sample given an 0.5 ML exposure shows a feature indicative of both monomer and excimer-like emission [3]. The intensity of this feature is similar to the 0.1 ML exposure feature, but the presence of excimer-like emission indicates that the density of bound P3A is actually higher than for the 0.1 ML Si exposed sample. A sample exposed to 1.0 ML Si shows very little emission, indicating little P3A is chemisorbed on the surface of this sample. The changes in the emission spectra for samples given various Si exposures and titrated with P3A are complex and additional results discussed below must be considered to explain this phenomenon.

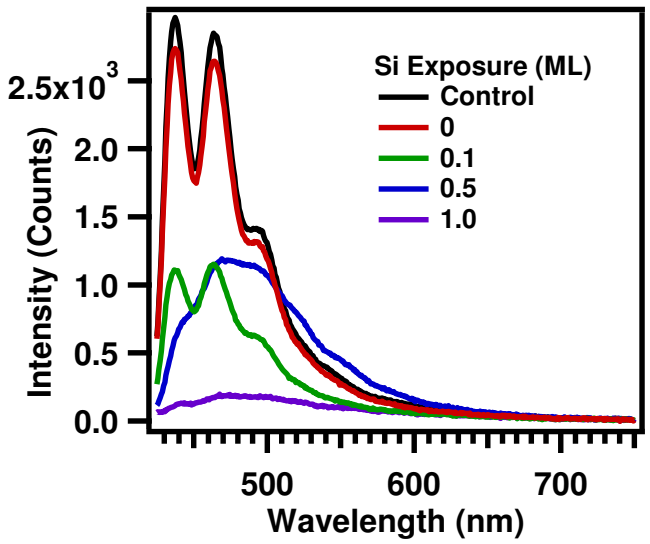

Figure 5.9: *In situ* emission spectra from 700 °C pretreated samples given various amounts of Si exposure and then titrated with P3A.

The Si exposure process also significantly influences the density of bound 3VP, as shown in Figure 5.10. For the lowest exposure (0.1 ML Si), the emission intensity increases by approximately a factor of ten relative to a sample with no Si exposure. The emission appears primarily monomeric, although some excimer-like emission is clearly present. The density of sites generated by this low exposure appears to be approximately 10^{12} cm^{-2}, based on the intensity alone. After an 0.5 ML Si exposure, titration with 3VP results in emission that is still higher than the sample with no Si exposure, but lower than the 0.1 ML Si exposure sample. The emission is now clearly due to a combination of monomeric and excimer-like species. A Si exposure of 1.0 ML and subsequent 3VP titration results in even lower emission. Exposure of the sample to only disilane gas prior to 3VP titration also causes an increase in the density of bound 3VP.

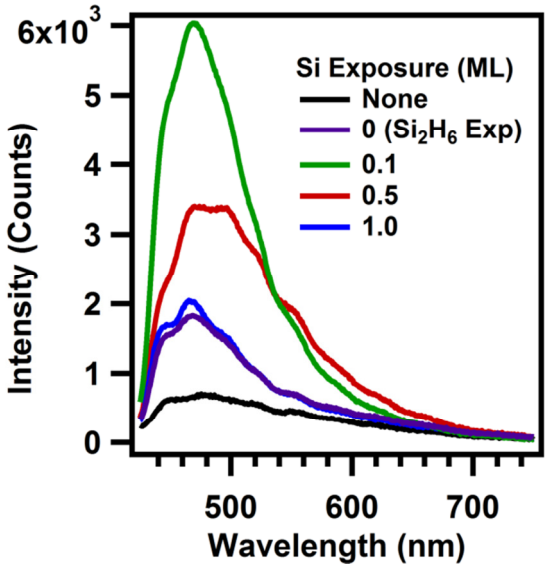

Figure 5.10: *In situ* emission spectra from 700 °C pretreated samples given various Si exposures and subsequently titrated with 3VP.

Based on the results of the P3A and 3VP titrations after Si exposure, one possible explanation for the observed spectra in both cases is that the Si exposure converts some strained siloxane sites to sites which are capable of chemisorbing 3VP. In order to test this hypothesis, an experiment was perforemed in which a 700 °C pretreated sample was exposed to n-propylamine prior to the Si exposure process. Such an exposure has previously been shown to eliminate strained siloxane sites, forming Si-NH-R sites [2,16,22]. After titration with 3VP, this sample exhibits an emission spectrum that is consistent with no Si exposure as shown in Figure 5.11, suggesting that the strained siloxane sites are in fact the sites at which the Si exposure reacts. Additionally, as mentioned above, the density of bound 3VP appears to increase to approximately 10^{12} fluorophores / cm^2, which is consistent with the density of strained siloxane sites.

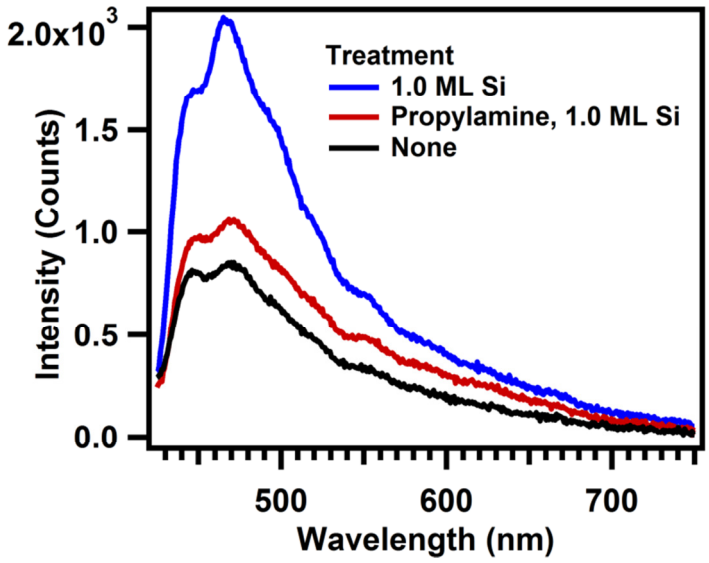

Figure 5.11: *In situ* emission spectra showing influence of n-propylamine exposure prior to Si exposure.

The above results strongly suggest that the strained siloxane sites react with SiH_x fragments, leading to new sites capable of 3VP chemisorption. However, atomic deuterium was also shown to generate sites capable of binding 3VP molecules. In order to acertain the relationship between the various sites, an experiment was perfomed in which sites were titrated sequentially. First, a sample pretreated to 700 °C was titrated with 3VP, which results in titration of the intrinsic sites. A subsequent 1.0 ML Si exposure eliminates emission from the sample, likely by hydrogenation of the perylene moiteies, rending these molecules non-fluorescent. An additional 3VP exposure and anneal step results in the titration of sites generated during the Si exposure process. A subsequent atomic deuterium exposure once again eliminates virtually all emission. A final 3VP exposure and anneal step results in the titration of sites generated during the atomic deuterium exposure. Spectra collected over the course of this experiment are presented in Figure 5.12. Emission collected after titration of intrinsic sites is consistent

with previous experiments. The emission spectrum after the Si exposure and subsequent titration with 3VP is similar, but slightly higher, in intensity when compared with the sample in which the same Si exposure was performed prior to any 3VP titration. Additionally, less excimer-like emission is observed from the sample which had been titrated with 3VP prior to Si exposure compared with the sample that was not titrated with 3VP prior to Si exposure. Emission collected after a subsequent atomic deuterium exposure shows only a weak feature relative to a sample in which only atomic deuterium exposure was performed prior to 3VP titration. This suggests that the sites with which atomic deuterium typically reacts were already largely consumed by this point in the experiment.

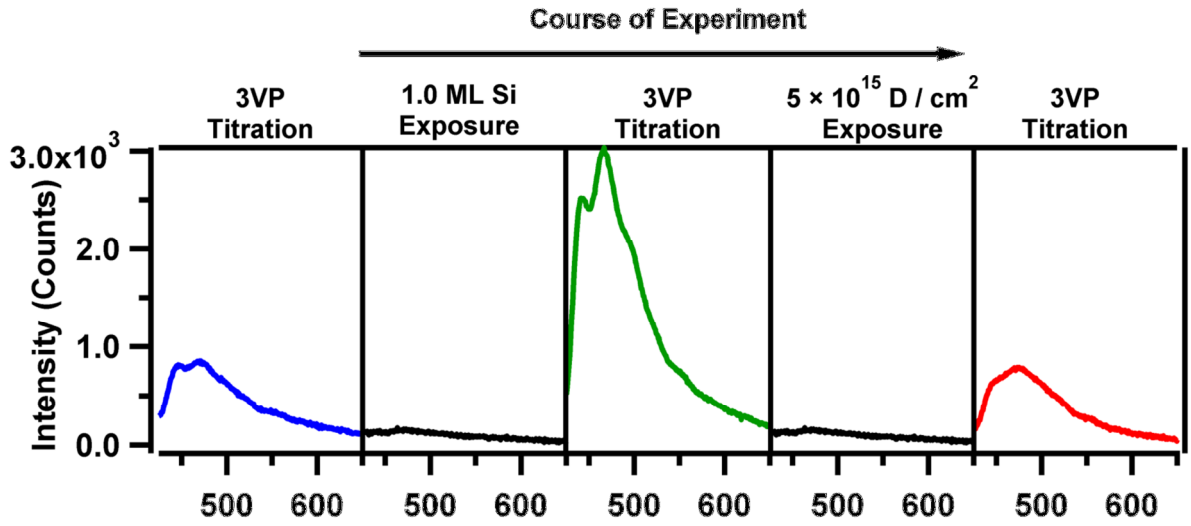

Figure 5.12: *In situ* emission spectra collected after various exposure steps showing relationship between sites.

5.3.4 Nature of Si exposure process

The generation of defect sites due to the Si exposure process has previously been attributed to etching of the SiO_2 surface by Si, forming volatile SiO [23]. This

conclusion was reached based on observation of a m/z 44 signal in TPD measurements. However, when a Si coated sample holder was used to eliminate contributions from the sample holder to the TPD signal, only a very weak m/z 44 feature was observed in TPD, as shown in Appendix C. The previous observation of a m/z 44 signal attributed to SiO^+ is likely due instead to CO_2^+, which could result from carbon contamination on the sample holder. Further insight was obtained about the nature of the Si exposure process by monitoring the amount of deposited Si as a function of Si exposure using XPS (Appendix C). The plot of Si^0 2p area versus Si exposure is shown in Figure 5.13. For exposures below 1.0 ML, very little Si^0 signal is observed. At higher exposures, the peak area, and hence amount of deposited material, increases linearly with exposure. This indicates an induction period exists in which little deposition occurs.

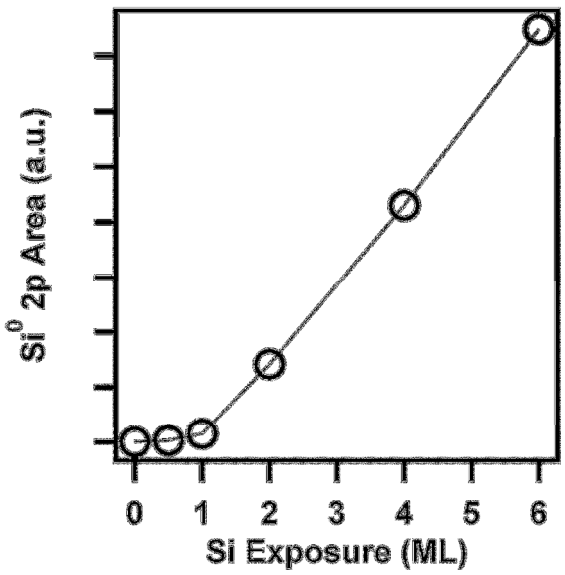

Figure 5.13: Plot of Si^0 2p peak area versus Si exposure.

5.3.5 Proposed mechanism for atomic deuterium and SiH_x interaction with strained siloxane sites

Based on the above results, we propose that atomic deuterium interacts with strained siloxane sites as depicted in Figure 5.14, forming a ≡SiD and ≡SiOD species. Computational studies have found that the reaction between molecular hydrogen and two membered siloxane rings is exothermic and is expected to form the sites depicted to the right in Figure 5.14, although a substantial activation energy exists for that process [24]. Generating atomic hydrogen (deuterium) may lower the activation energy significantly, allowing the reaction to proceed readily. The SiD species would then be capable of reacting with 3VP, as depicted in Figure 5.3. The observation that the amount ofP3A chemisorbed onto the surface does not change with atomic deuterium exposure is explained by noting that the ≡SiD site is likely capable of also reacting with the amine functional group, forming a ≡Si-NH-R structure, which is identical to the structure formed during the reaction between P3A and the strained siloxane site. Therefore, no difference would be expected in the emission intensity from samples with or without atomic deuterium exposure.

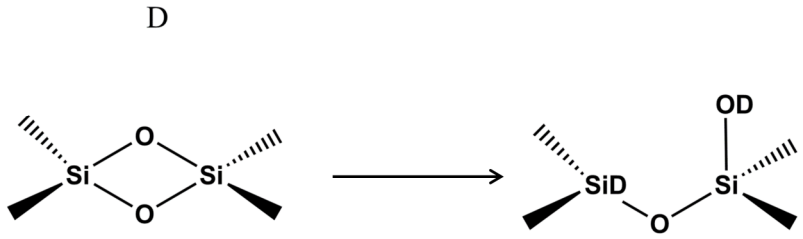

Figure 5.14: Proposed reaction between atomic deuterium and strained siloxane sites.

The interaction of SiH_x fragments with strained siloxane sites is more complex. For low Si exposures (0.1 ML), the emission from the P3A titrated samples decreases substantially with respect to no Si exposure while the emission from 3VP titrated samples

increases substantially with respect to no Si exposure. With higher Si exposures, some excimer-like emission is observed and the intensity decreases. The presence of excimer-like emission means that sites are generated where two perylene moiteies are in close proximity to each other. At 1.0 ML Si exposure, very little P3A chemisorption is observed, and the emission from 3VP titrated samples is lower than for lower Si exposures. Additionally, under these conditions enhanced nucleation of Ge particles was observed on SiO_2 [17]. This suggests that the sites generated by the Si exposure process is capable of trapping adatoms, leading to the formation of stable clusters. Based on this information, a proposed mechanism for the interaction of SiH_x fragments with strained siloxane sites is shown in Figure 5.15. The SiH_x fragments are assumed to open up the strained siloxane site, forming a structure with adjacent ≡Si· or ≡SiH sites. The presence of adjacent ≡SiH sites could explain the observed excimer-like emission for higher Si exposures, as shown in Figure 5.3. Additional capture of SiH_x fragments at higher exposures could then lead to the formation of stable clusters, explaining the induction period observed in the plot of Si^0 2p peak area versus exposure in Figure 5.13. Computational studies on such a process may be necessary to elucidate the detailed structure of such sites.

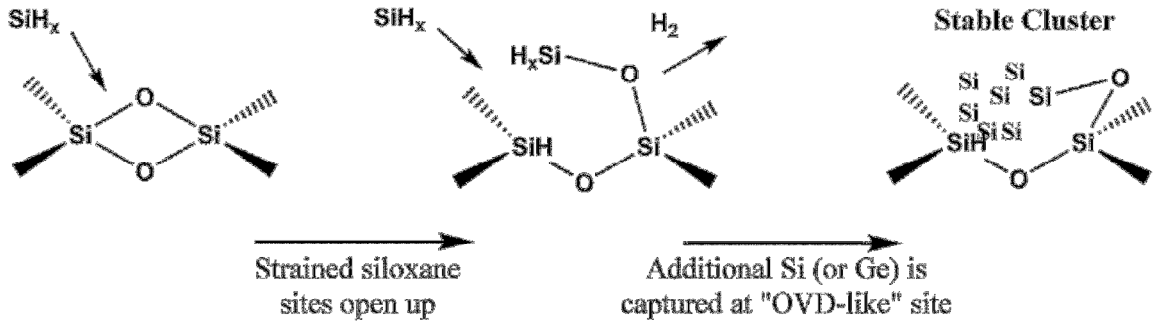

Figure 5.15: Proposed mechanism for the interaction of SiH_x fragments with strained siloxane sites, leading to the formation of OVD-like sites capable of trapping adatoms.

5.4 CONCLUSIONS

A perylene derivative containing a vinyl functional group, 3-vinyl perylene, was used to titrate low density sites that are presumed to be oxygen vacancy defect sites. The density of the intrinsic OVD sites was found to be approximately 10^{11} cm^{-2}, based on the emission intensity from the sample. These sites are therefore much lower in density than either strained siloxane or hydroxyl sites, explaining why they have not previously been identified on even high surface area silica.

The ability to titrate free hydroxyl, strained siloxane, and oxygen vacancy sites was used to understand the chemical nature of sites leading to enhanced nucleation using a Si exposure process. Neither atomic deuterium nor Si exposure was found to affect the density of free hydroxyl sites, suggesting these sites are not involved in nucleation of Ge particles on SiO_2. The Si exposure process was shown to decrease the density of strained siloxane sites, while subsequently increasing the number of sites capable of chemisorbing 3VP. Atomic deuterium exposure does not appear to change the amount of chemisorbed P3A, but does increase the density of sites capable of binding 3VP by approximately a factor of ten.

The titration results are explained by the interaction of SiH_x fragments with strained siloxane sites, creating new sites which are chemically similar to oxygen vacancy sites and are capable of chemisorbing 3VP. Additionally, atomic deuterium is believed to cleave a Si-O-Si bond on the strained siloxane site, forming a ≡Si-D and ≡Si-OD pair. Both P3A and 3VP are believed to be capable of reacting with the deuteride species.

The OVD-like sites generated by the Si exposure process are proposed to be the sites responsible for trapping adatoms and causing enhanced nucleation. This hypothesis is supported by comparing the estimated densities of sites with the nucleation densities of Ge particles on SiO_2 as a function of Si exposure. Further work is necessary to determine the detailed structure of such sites and to study whether additional materials are capable of reacting similarly to Si in forming adatom trap sites from strained siloxane sites.

5.5 REFERENCES

[1] G. Pacchioni, Oxygen Vacancy: The Invisible Agent on Oxide Surfaces, ChemPhysChem. 4 (2003) 1041–1047.

[2] J. McCrate, J. Ekerdt, Titration of Free Hydroxyl and Strained Siloxane Sites on Silicon Dioxide with Fluorescent Probes, Langmuir. 29 (2013) 11868–11875.

[3] J. McCrate, J. Ekerdt, Coverage Dependent Luminescence from Two-Dimensional Systems of Covalently Attached Perylene Fluorophores on Silica, Submitted. (2013).

[4] D.L. Griscom, The Natures of Point Defects in Amorphous Silicon Dioxide, in: G. Pacchioni, L. Skuja, D.L. Griscom (Eds.), Defects SiO_2 Relat. Dielectr. Sci. Technol., Dordrecht, The Netherlands, 2000: pp. 117–159.

[5] G.F. Cerofolini, L. Meda, CO_2 and C_2H_4 grafting to the native defects of ion-bombarded porous silica, 39 (1999) 29–39.

[6] A.A. Bobyshev, V.A. Radtsig, Silanone groups on the surface of mechanically activated silicon dioxide, Kinet. Catal.(Engl. Transl.). 29 (1988) 551–559.

[7] C. Morterra, M. Low, Reactive silica. II. Nature of the surface silicon hydrides produced by the chemisorption of hydrogen, J. Phys. Chem. 73 (1969) 327–333.

[8] L. Vaccaro, A. Morana, V. Radzig, M. Cannas, D. Fisica, Bright Visible Luminescence in Silica Nanoparticles, (2011) 19476–19481.

[9] L. Vaccaro, M. Cannas, V. Radzig, R. Boscaino, Luminescence of the surface nonbridging oxygen hole center in silica: Spectral and decay properties, Phys. Rev. B. 78 (2008) 075421.

[10] V. Radtsig, I. Senchenya, Hydrogenation of the silanone groups $(\equiv Si\text{-}O)_2Si{=}O$. Experimental and quantum-chemical studies, Russ. Chem. Bull. 45 (1996) 1849–1856.

[11] V. Radzig, Point defects in disordered solids: Differences in structure and reactivity of the (≡ Si–O) 2 Si: groups on silica surface, J. Non. Cryst. Solids. 239 (1998) 49–56.

[12] V.A. Radzig, Defects on Activated Silica Surface, in: G. Pacchioni, L. Skuja, D.L. Griscom (Eds.), Defects SiO_2 Relat. Dielectr. Sci. Technol., Klumer Academic, Dordrecht, The Netherlands, 2000: pp. 339–370.

[13] C. Kuo, G. Hwang, Structure and interconversion of oxygen-vacancy-related defects on amorphous silica, Phys. Rev. Lett. 97 (2006) 066101.

[14] C.L. Kuo, S. Lee, G. Hwang, Strain-Induced Formation of Surface Defects in Amorphous Silica: A Theoretical Prediction, Phys. Rev. Lett. 100 (2008) 076104.

[15] K.E. Kweon, G.S. Hwang, Defect-Assisted Covalent Binding of Graphene to an Amorphous Silica Surface: A Theoretical Prediction, ChemPhysChem. 12 (2011) 2155–2159.

[16] B. Morrow, I. Cody, Infrared studies of reactions on oxide surfaces. 6. Active sites on dehydroxylated silica for the chemisorption of ammonia and water, J. Phys. Chem. 80 (1976) 1998–2004.

[17] J.M. McCrate, N. Salivati, J.G. Ekerdt, Hot-wire CVD of Ge nanoparticles on Si-etched silicon dioxide, J. Cryst. Growth. 321 (2011) 131–135.

[18] S. Coffee, D. Shahrjerdi, S. Banerjee, J. Ekerdt, Selective silicon nanoparticle growth on high-density arrays of silicon nitride, J. Cryst. Growth. 308 (2007) 269–277.

[19] Y.V. Razskazovskii, M.V. Roginskaya, M.Y. Mel'nikov, The reactions of silylenes on the chemically activated silica surface, J. Organomet. Chem. 486 (1995) 249–253.

[20] M. Vitiello, N. Lopez, F. Illas, G. Pacchioni, H_2 cracking at SiO_2 defect centers, J. Phys. Chem. A. 104 (2000) 4674–4684.

[21] B. Finlayson-Pitts, Interactlon of Gas-Phase Deuterium Atoms with Silica Surfaces, J. Phys. Chem. 86 (1982) 3499–3501.

[22] B. Bunker, D. Haaland, T. Michalske, W. Smith, Kinetics of dissociative chemisorption on strained edge-shared surface defects on dehydroxylated silica, Surf. Sci. 222 (1989) 95–118.

[23] W.A. Winkenwerder, J.G. Ekerdt, Germanium interactions with Si-etched silicon dioxide, Surf. Sci. 602 (2008) 2796–2800.

[24] N. Lopez, M. Vitiello, F. Illas, G. Pacchioni, Interaction of H_2 with strained rings at the silica surface from ab initio calculations, 271 (2000) 56–63.

Chapter 6: Research Summary

6.1 CONCLUSIONS

The objective of this work was to understand how defect sites on oxide surfaces influence nucleation and to determine the nature of these sites. Defect sites were shown to play a critical role in nucleation of germanium nanoparticles on SiO_2 surfaces. The ability to increase the nucleation density in this system by an order of magnitude demonstrates that controlling defect density may indeed be a viable method for tuning particle and film deposition on oxides.

Undoubtedly, the most significant contribution of this work was the development of the fluorescent probe technique for characterizing low density surface sites in a vacuum environment. The development of this experimental tool required extensive studies to both validate the method and to accurately interpret the results. However, with the groundwork laid, this technique is remarkably straightforward to use and provides an unprecedented ability to characterize low density sites on oxide surfaces.

Perylene derivatives with alcohol, amine, or vinyl functional groups were used to determine the densities of free hydroxyl, strained siloxane, and oxygen-vacancy defect sites, respectively. The densities of these sites on fused silica surfaces span three orders of magnitude, from approximately 10^{11} cm^{-2} for OVD sites to approximately 10^{14} cm^{-2} for free hydroxyl sites. Such low density sites cannot be observed using traditional surface science tools, such as XPS, making this technique valuable for the study of low density sites on many oxide surfaces.

The luminescence from bound perylene moieties depends strongly on the density of fluorophores attached to the surface. In general, monomer emission is observed at low

densities, when fluorophores are too far separated to strongly interact with each other. When fluorophores are in close proximity with each other, excimer-like emission is observed. Such emission is typically observed for high densities of bound perylene-3-methanol molecules; however, excimer-like emission was also observed for much lower densities of bound 3-vinyl perylene molecules on surfaces after the Si exposure process.

The Si exposure process used to enhance germanium nucleation density was shown to create OVD-like sites at the expense of strained siloxane sites. The former sites, along with intrinsic OVD sites, appear to be the sites responsible for adatom capture and subsequent particle growth. Additionally, atomic deuterium exposure was shown to generate sites capable of chemisorbing 3-vinyl perylene from strained siloxane sites.

6.2 Recommendations for Future Work

This work demonstrates that, even for a well-studied system like SiO_2, much remains to be learned regarding the role low density sites play in fundamental surface processes, such as nucleation and catalysis. The present work should be extended to examine whether other semiconductors or metals interact with surface defects on SiO_2 in the same manner as germanium.

Additionally, the same strategy could be applied to other oxide systems, including as Al2O3, HfO2, or SrTiO3. The only constraint for the oxide system is that the highest occupied molecular orbital (HOMO) and lowest unoccupied molecular orbital (LUMO) lie within the band gap of the oxide [1]. For systems in which single crystals or bulk substrates are not available, thin films of the oxide of choice could be studied with this approach. However, emission from fluorophores bound to the surface of a thin film would be modulated both by the presence of an interface with a metal or semiconductor

in close proximity to the fluorophore and by interference effects due to the path length of the optical cavity created by the thin film [2].

In addition to particle and film growth, the techniques developed in this work may also prove relevant for studies of catalysis on either oxides or supported oxide systems. In particular, the ability to detect ultra-low surface defect sites may shed light on the process of hydrogen spillover from metal particles onto silica and other non-reducible supports. Many researchers have attempted to determine exactly how hydrogen migrates from the metal particle and onto the silica surface, as the overall process appears to be energetically unfavorable [3]. Additionally, even though hydrogen atoms appear to migrate across the surface, no evidence is found for atomic hydrogen. One possibility is that hydrogen atoms interact with surface defect sites, making the process thermodynamically favorable and explaining the lack detectable atomic hydrogen species on the surface. In fact, atomic deuterium was shown to interact with strained siloxane sites, presumably forming SiD sites. Such sites may play an important role in the spillover process.

6.3 REFERENCES

[1] J.M. Szarko, A. Neubauer, A. Bartelt, L. Socaciu-siebert, F. Birkner, K. Schwarzburg, T. Hannappel, R. Eichberger, The Ultrafast Temporal and Spectral Characterization of Electron Injection from Perylene Derivatives into ZnO and TiO_2 Colloidal Films, J. Phys. Chem. C. 112 (2008) 10542–10552.

[2] A. Lambacher, P. Fromherz, Fluorescence interference-contrast microscopy on oxidized silicon using a monomolecular dye layer, Appl. Phys. A. 63 (1996) 207–216.

[3] R. Prins, Hydrogen spillover. Facts and fiction., Chem. Rev. 112 (2012) 2714–2738.

Appendix A: Supporting Information for Chapter 3

A.1 Synthesis of Compounds

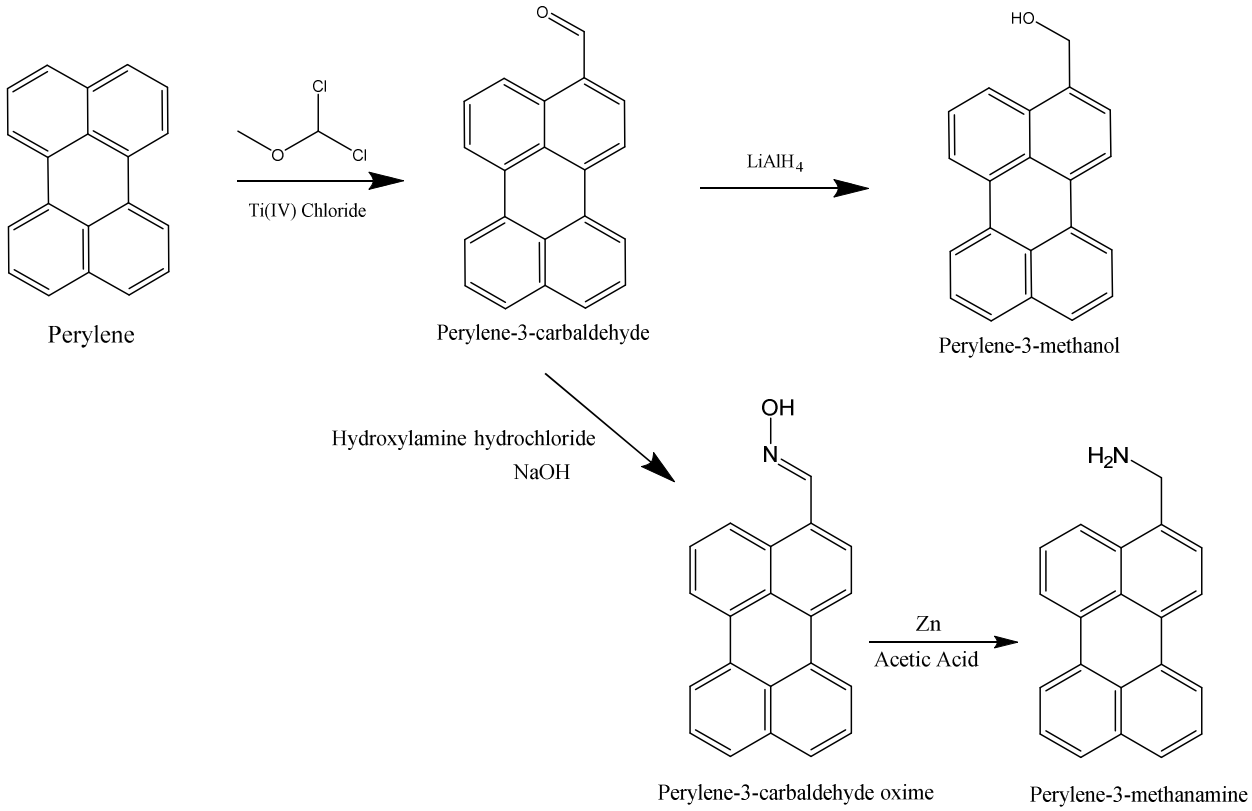

Figure A.1: Schematic of synthetic route taken to create compounds used in this work.

A.1.1 Synthesis of Perylene-3-Carbaldehyde

The synthesis of this compound has been reported elsewhere [1]. A stirred flask containing perylene (5.0 g, 19.8 mmol) dissolved in 300 ml 1,2-dichlorobenzene was flushed with Ar and placed on an ice bath. To this solution was added 1,1-dichloromethyl methyl ether (2.5 ml) and $TiCl_4$ (3.5 ml) (Caution: hazardous vapors), which caused an immediate change of color in the solution. After stirring for 2.5 h, the

dark green solution was removed from the ice bath, then poured into a beaker containing 300 g ice and 25 ml concentrated HCl solution. After adding chloroform (200 ml), the mixture was washed with 2 M HCl (100 ml), then water (3× 300 ml). The organic layer was then dried over Na_2SO_4 and solvent removed by evaporation. The crude residue was purified by recrystallization from toluene, yielding an orange solid (3.8 g, 68% yield). R_f ($CHCl_3$) = 0.38. CI MS: *m/z* = 281 $[MH]^+$. ^1H NMR (500 MHz, $CDCl_3$): δ 10.27 (s, 1H); 9.10 (d, 1H); 8.25-8.14 (m, 4H); 7.87 (d, 1H); 7.78 (d, 1H); 7.71 (d, 1H); 7.65 (t, 1H); 7.52 (t, 2H).

A.1.2 Synthesis of Perylene-3-Methanol (P3M)

To a dried flask on ice was added 15 ml of 1.0 M $LiAlH_4$ in THF. A solution of perylene-3-carbaldehyde (1.1 g, 3.9 mmol) in 200 ml anhydrous tetrahydrofuran (THF) was added dropwise over 5 min to the $LiAlH_4$ solution while stirring. The dark green solution was stirred for 30 min on ice, and then allowed to warm to room temperature. To the mixture was added 100 ml 10 vol% aq. H_2SO_4 solution, resulting in a red-orange solution. After adding chloroform (150 ml), the mixture was washed with water (3× 150 ml). The organic layer was dried over Na_2SO_4 and solvent removed by evaporation, affording a brownish yellow solid. The crude residue was purified by column chromatography on silica gel using $CHCl_3$, then 10:1 $CHCl_3$:EtOH, yielding an orange solid (0.81 g, 73% yield). R_f ($CHCl_3$) = 0.25. CI MS: *m/z* = 283 $[MH]^+$. ^1H NMR (500 MHz, $CDCl_3$): δ 8.27 – 8.13 (m, 4H); 7.96 (d, 1H); 7.70 (d, 2H); 7.57-7.47 (m, 4H); 5.10 (s, 2H).

A.1.3 Synthesis of Perylene-3-Carbaldehyde Oxime

Procedures for the conversion of the aldehyde derivative of perylene to an oxime and subsequent reduction to an amine were adapted from work using the same derivatives of pyrene [2]. To a stirred flask containing perylene-3-carbaldehyde (0.300 g, 1.1 mmol) and hydroxylamine·HCl (0.200 g, 2.9 mmol) in 200 ml ethanol and 40 ml water was added NaOH (0.370 g, 9.2 mmol). The mixture was brought to reflux for 5 min. After 2 h of additional stirring at room temperature, the red mixture was added to 100 ml 0.5 M HCl solution, causing the precipitation of brown residue. The precipitate was collected by filtration and rinsed with DI water, dried, then purified via column chromatography on silica gel using $CHCl_3$, yielding the desired compound as brown solid (0.08 g, 25 % yield). R_f ($CHCl_3$) = 0.13. CI MS: *m/z* = 296 $[MH]^+$. ^1H NMR (600 MHz, $CDCl_3$): δ 8.73 (s, 1H); 8.37 (d, 1H); 8.27-8.19 (m, 4H); 7.76 (d, 1H); 7.71 (d, 2H); 7.58 (t, 1H); 7.50 (t, 2H).

A.1.4 Synthesis of Perylene-3-methanamine (P3A)

To a stirred flask containing peryelene-3-carbaldehyde oxime (0.040 g, 0.14 mmol) in 200 ml acetic acid was added zinc powder (3.5 g). After stirring for 12 h at room temperature, the mixture was filtered and the filtrate neutralized by addition of NaOH. The solid residue was collected by filtration rinsed with water, dried, and then subsequently dissolved in hot ethyl acetate / THF solution. The mixture was filtered hot and the filtrate was evaporated. The resulting residue was purified via silica gel column chromatography, with $CHCl_3$ then 10:1 $CHCl_3$: n-propylamine, yielding the desired compound as a yellow solid (0.014 g, 37% yield). R_f ($CHCl_3$) ≈ 0. CI MS: *m/z* = 282 $[MH]^+$. ^1H NMR (600 MHz, $CDCl_3$): δ 8.23-8.15 (m, 4H); 7.90 (d, 1H); 7.68 – 7.66 (m, 2H); 7.54 (t, 1H); 7.50 – 7.45 (m, 3H); 4.27 (s, 2H).

A.2 EXPERIMENTAL

A.2.1 Preparation of Wafers

Fused silica wafers (Sydor Optics) were diced into 1.6 × 1.6 cm^2 sections. The wafers were then rinsed in acetone, ethanol, and 18.2 MΩ deionized (DI) water before being placed in a 6:2:1 sulfuric acid : hydrogen peroxide : water solution for approximately 30 min. The wafers were then rinsed in DI water and then placed in a 2% hydrofluoric acid solution for 10 s to slightly etch the silica surface to remove any remaining impurities. The wafers were rinsed again in DI water and stored in DI water prior to loading into the UHV system.

A.2.2 Preparation of Standards

Aqueous P3M solutions were prepared by first diluting 1 ml of 1×10^{-5} M P3M in ethanol by addition of deionized (DI) water to create 100 ml of 1×10^{-7} M aqueous P3M solution. Such a step was required due to the low solubility of P3M in water. This solution was then diluted with DI water to create a 1×10^{-8} M aqueous P3M solution. A standard solution of 1×10^{-8} M P3M was prepared by adding 1 ml of 1×10^{-7} M P3M solution to 10 ml volumetric flasks along with 1 ml 0.1 M n-propylamine solution. DI water was added to bring the volume to 10 ml. The remaining standards were prepared by adding the appropriate quantity of 1×10^{-8} M solution to a volumetric flask along with 1 ml 0.1 M n-propylamine solution and then bringing the total volume to 10 ml using DI water.

A.2.3 Solution Fluorescence Measurements

Solutions were placed in optical glass cuvettes and fluorescence emission spectra from the standards and solutions prepared from samples were collected on a FluoroLog-3

fluorimeter (Horiba Jobin Yvon) using a 405 nm excitation wavelength with 5 nm spectral slit width and 420 – 600 nm emission wavelength with 5 nm spectral slit width and 1 nm increment. The signal from a photomultiplier tube was collected and divided by the signal from a reference detector to account for fluctuations in the Xenon lamp intensity. The intensity of the 443 nm peak from the uncorrected P3M fluorescence emission spectrum was used to construct a standard curve.

A.3 RESULTS

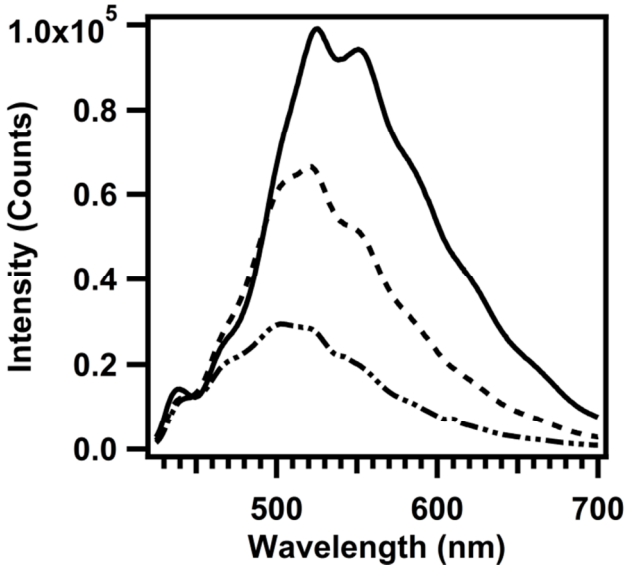

Figure A.2: *In situ* photoluminescence (PL) spectra collected after anneal step from 700 °C fused silica samples exposed to P3M using P3A (———), n-propylamine (– – – –), or nothing (— · · –) to catalyze the reaction between P3M and the silanol sites. n-Propylamine was introduced into the exposure chamber through a leak valve such that the uncorrected ion gauge pressure was maintained at 2×10^{-6} torr for the duration of the P3M exposure step.

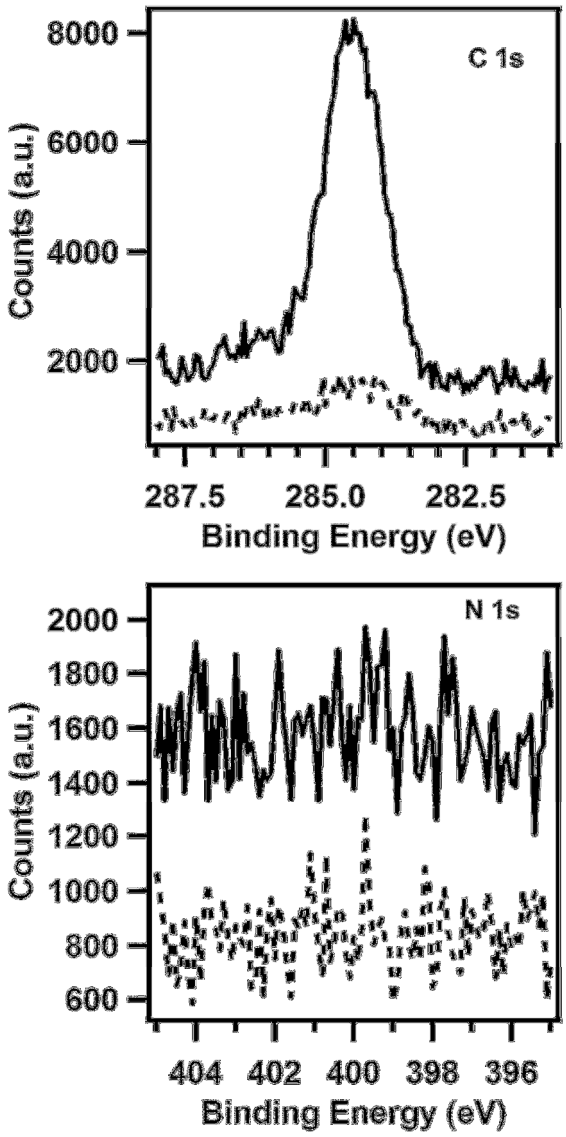

Figure A.3: *Ex situ* high resolution X-ray photoelectron (XP) spectra of the carbon 1s (left) and nitrogen 1s (right) regions from a 700 °C pretreated sample titrated with P3M (——) and a 300 °C pretreated sample exposed to 500 mTorr n-propylamine vapor for 5 min (– – – -). The spectra were collected with a takeoff angle of 60 ° to enhance surface sensitivity. A readily detectable peak is present in the C 1s spectrum for the P3M titrated sample, while only a weak peak attributed to adventitious carbon is present on the n-propylamine exposed sample. No features are observed in the energy range where N 1s peaks occur for either sample.

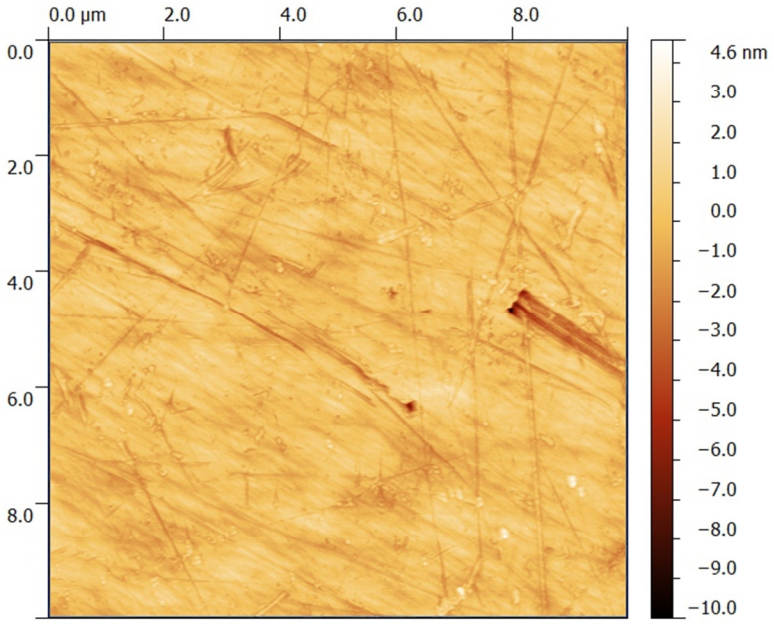

Figure A.4: Atomic force microscopy (AFM) image of 400 °C preteated sample after P3M titration, demonstrating no particles are present on the surface after the titration process.

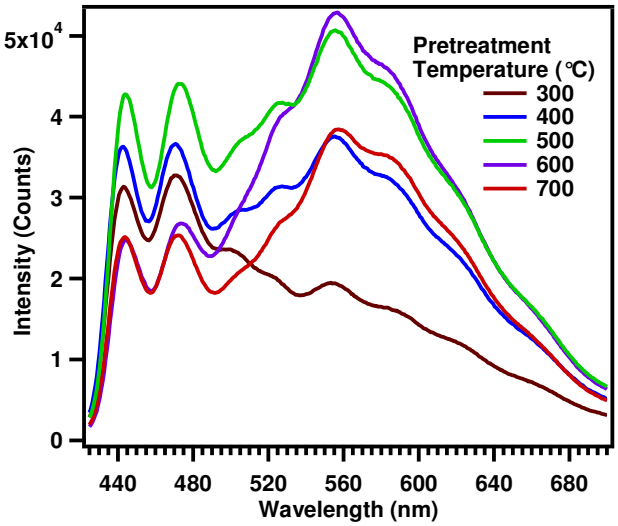

Figure A.5: *In situ* PL spectra from fused silica samples preheated to various temperatures after P3M exposure.

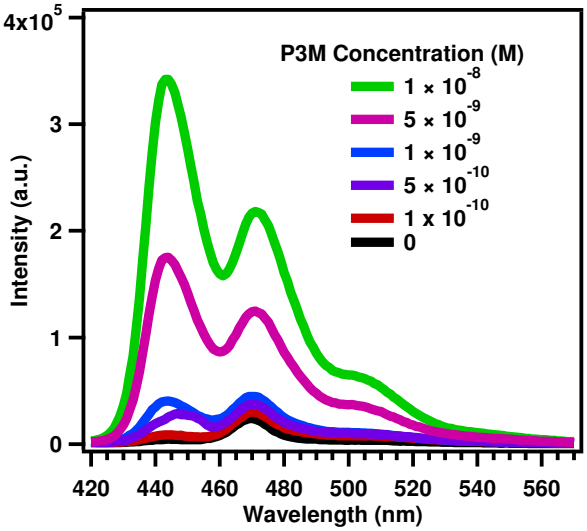

Figure A.6: Fluorescence emission measurements of 0.01 M n-propylamine solutions containing various concentrations of P3M, using an excitation wavelength of 405 nm.

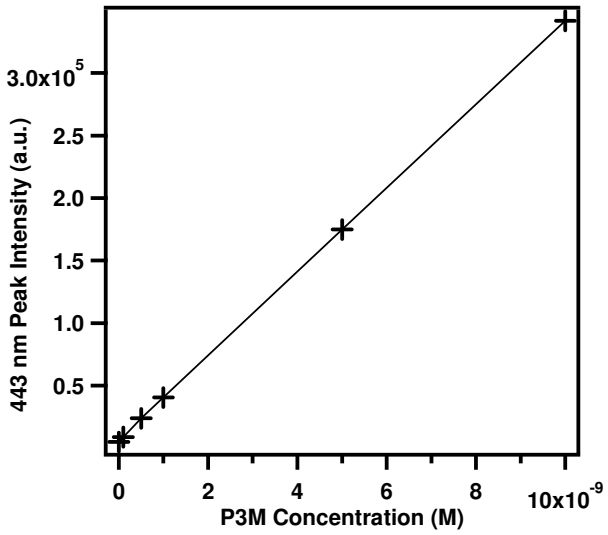

Figure A.7: Fluorescence standard curve prepared using the 443 nm emission peak from the standards in the previous figure. This peak was used to avoid overlap with the water Raman peak at ~470 nm. A linear relationship was observed between emission intensity and concentration over the range of concentrations used in this work.

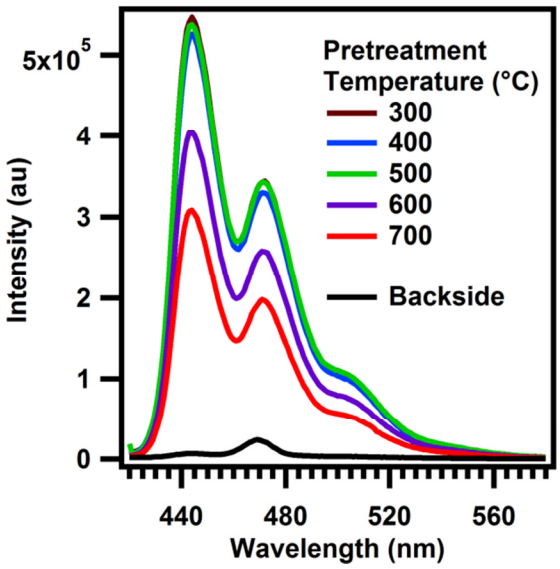

Figure A.8: Fluorescence emission measurements from solutions created by cleaving bound P3M into solution. The spectrum labeled "Backside" corresponds to a solution prepared by removing bound P3M from the backside of a 700 °C pretreated sample titrated with P3M.

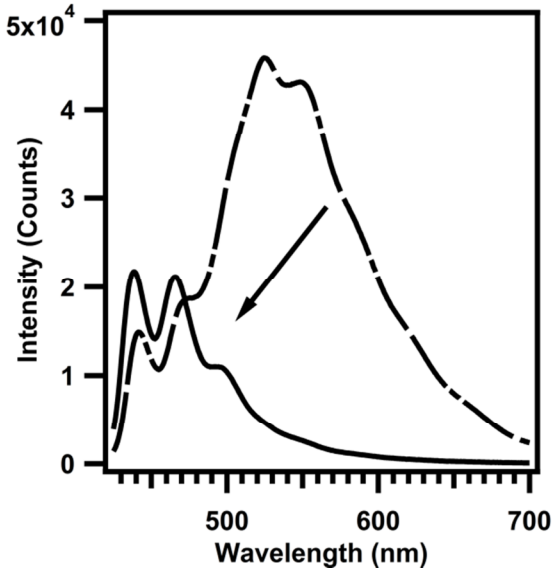

Figure A.9: *In situ* PL spectra after P3A exposure (— · —) and after subsequent annealing at 300 °C (———) from fused silica samples pretreated at 700 °C

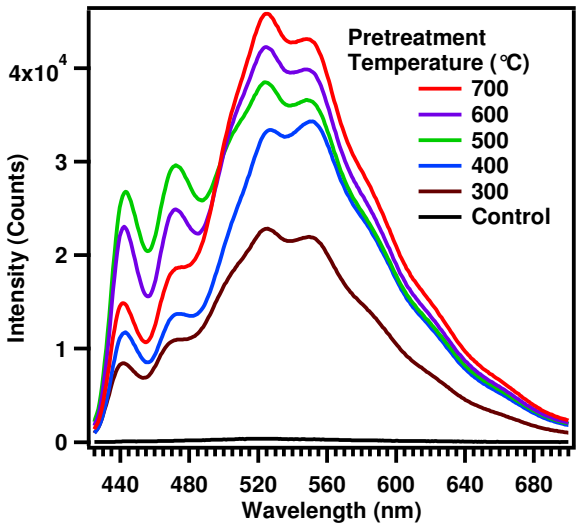

Figure A. 10: *In situ* PL spectra from fused silica samples preheated to various temperatures after P3A exposure.

A.4 REFERENCES

[1] M. V. Skorobogatyi, A. a. Pchelintseva, A.L. Petrunina, I. a. Stepanova, V.L. Andronova, G. a. Galegov, et al., 5-Alkynyl-2′-deoxyuridines, containing bulky aryl groups: evaluation of structure–anti-HSV-1 activity relationship, Tetrahedron. 62 (2006) 1279–1287.

[2] H. Lee, E. Luna, M. Hinz, J.J. Stezowski, A.S. Kiselyov, R.G. Harvey, Synthesis of oligonucleotide adducts of the bay region diol epoxide metabolites of carcinogenic polycyclic aromatic hydrocarbons, J. Org. Chem. 60 (1995) 5604–5613.

Appendix B: Supporting Information for Chapter 4

B.1 Results

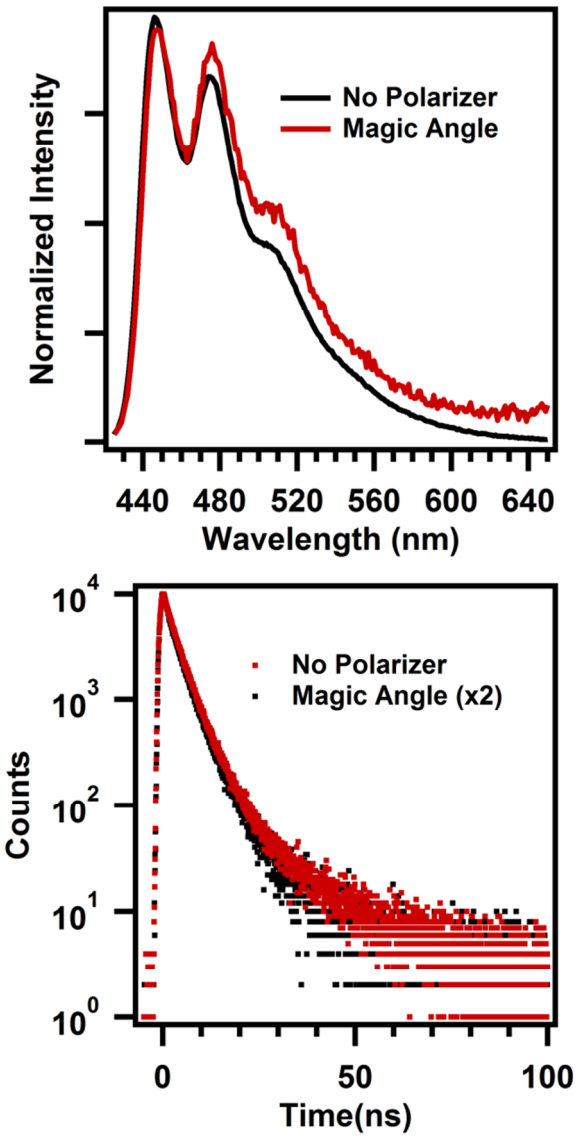

Figure B.1: *Ex situ* emission spectra (Left) and fluorescence decay curves (Right) from 0.08 P3M / nm^2 sample collected using either no polarization (Unpolarized) or with a polarizer set at 0° between excitation monochromator and sample and a polarizer set at 55° between sample and detector monochromator (Magic Angle). Both the steady-state and time-resolved measurements appear nearly identical between the two settings. The decay curve collected using magic angle polarizer settings was scaled by a factor of two, due to the very low hit rate obtained with polarizers in place.

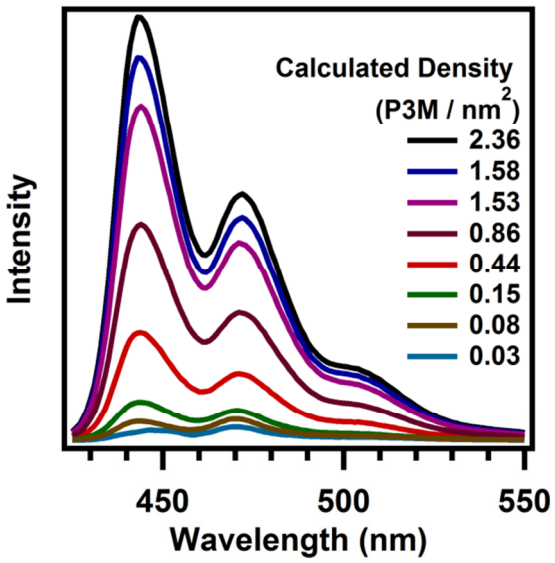

Figure B.2: Fluorescence spectra from solutions prepared by removing P3M molecules from sample surfaces that had been cleaved from the center of the sample, to ensure molecules adsorbed on the edges did not contribute. The cleaved wafers were generally approximately 0.9 cm × 0.9 cm; however, the final dimensions of each sample were measured and used in the calculations.

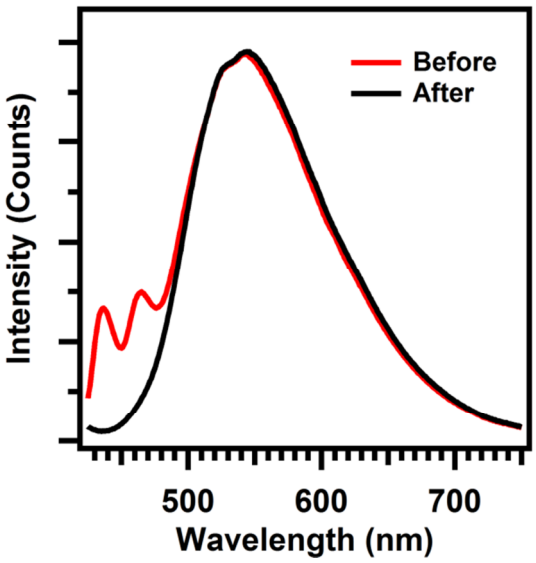

Figure B.3: *In situ* emission spectra collected before and after the backside of the sample was exposed to atomic deuterium generated on a hot tungsten filament. The low wavelength features are attributed to low densities of fluorophores (monomer emission) on the back of the sample, which are eliminated by the atomic deuterium exposure.

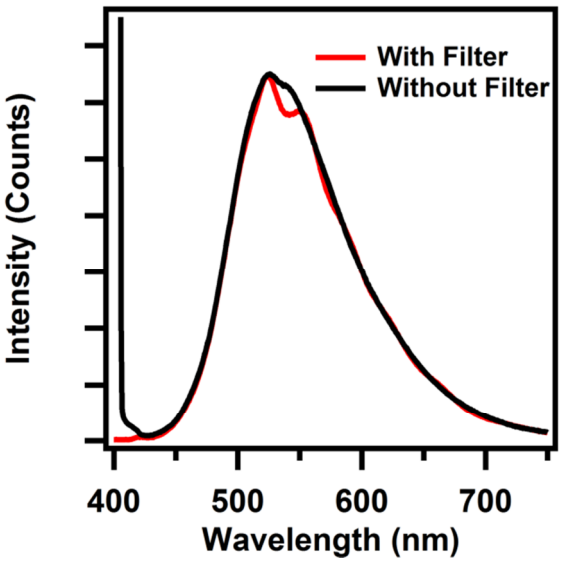

Figure B.4: *In situ* emission spectra collected with our without 425 nm long-pass filter in place, showing the artifact around 550 nm due to the filter.

`

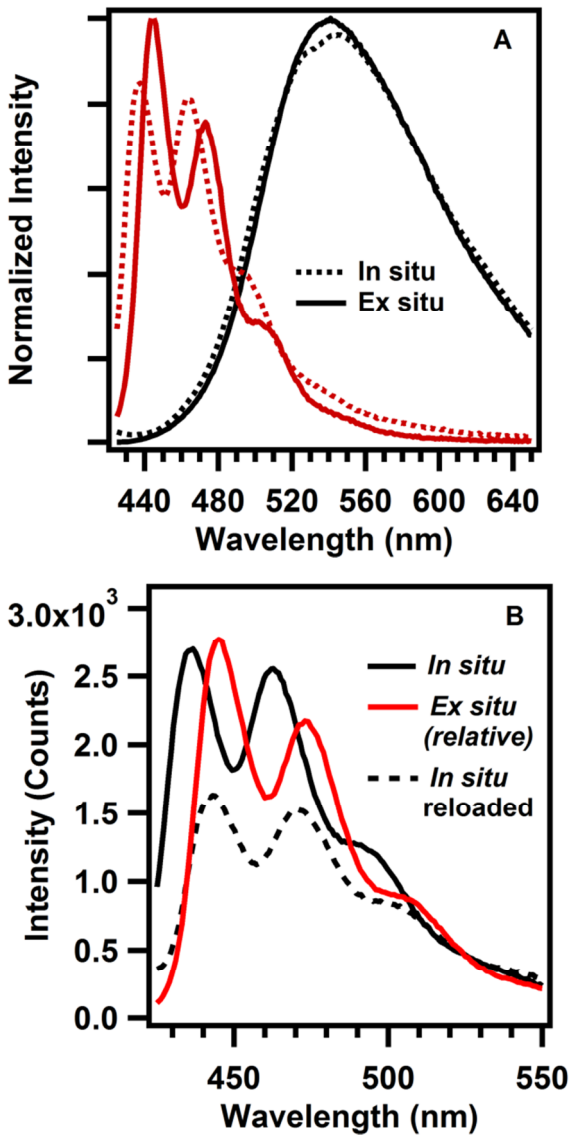

Figure B.5: **(A)** Normalized *in situ* and *ex situ* emission spectra from low density (red line) and high density (black line) samples. **(B)** *In situ* emission spectra from sample collected after P3M exposure process (*In situ*) and after reloading sample back into vacuum system after *ex situ* measurements (*In situ* reloaded). The relative *ex situ* emission spectrum is shown for comparison.

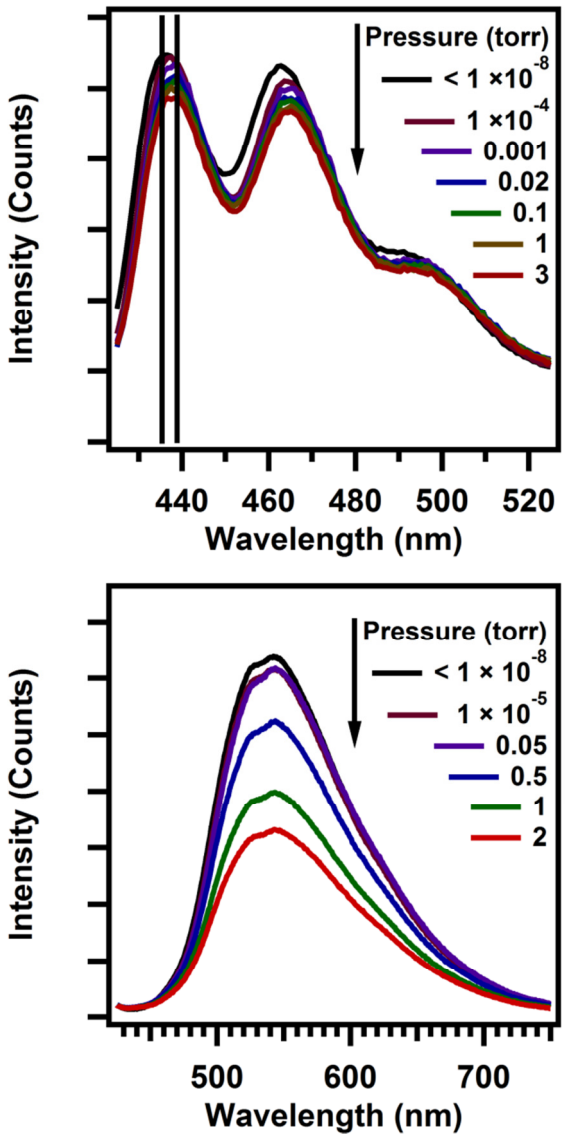

Figure B.6: *In situ* emission spectra from samples displaying monomer (left) and excimer-like (right) emission collected at various chamber pressures. Pressures were increased by isolating pumps and leaking in air. Monomer emission displays a slight shift in the position of the vibronic peaks when the pressure is increased to 10^{-4} torr, and the intensity decreases only slightly with pressure up to 3 torr. The position of the excimer-like peak does not change with pressure, but the intensity decreases by approximately half between the $< 10^{-8}$ torr and 2 torr measurements. However, *ex situ* measurements were performed with pressures below 15 mtorr, so that little fluorescence quenching is expected for either sample at this pressure.

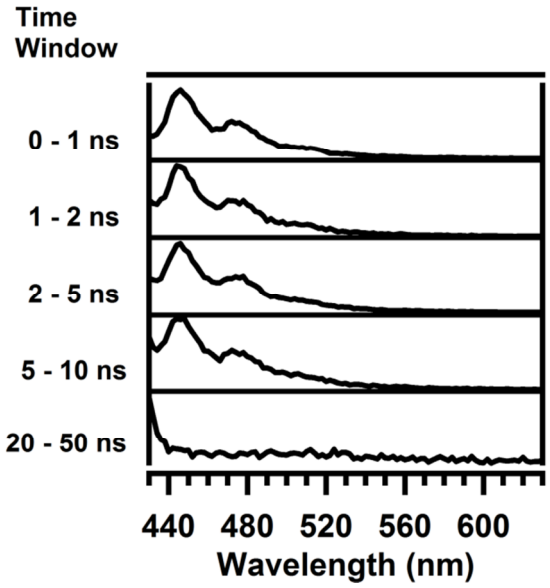

Figure B.7: Time-resolved emission spectra from the sample with 0.03 P3A / nm^2 showing only monomer emission in all time windows. Essentially no signal is observed in the latest time window.

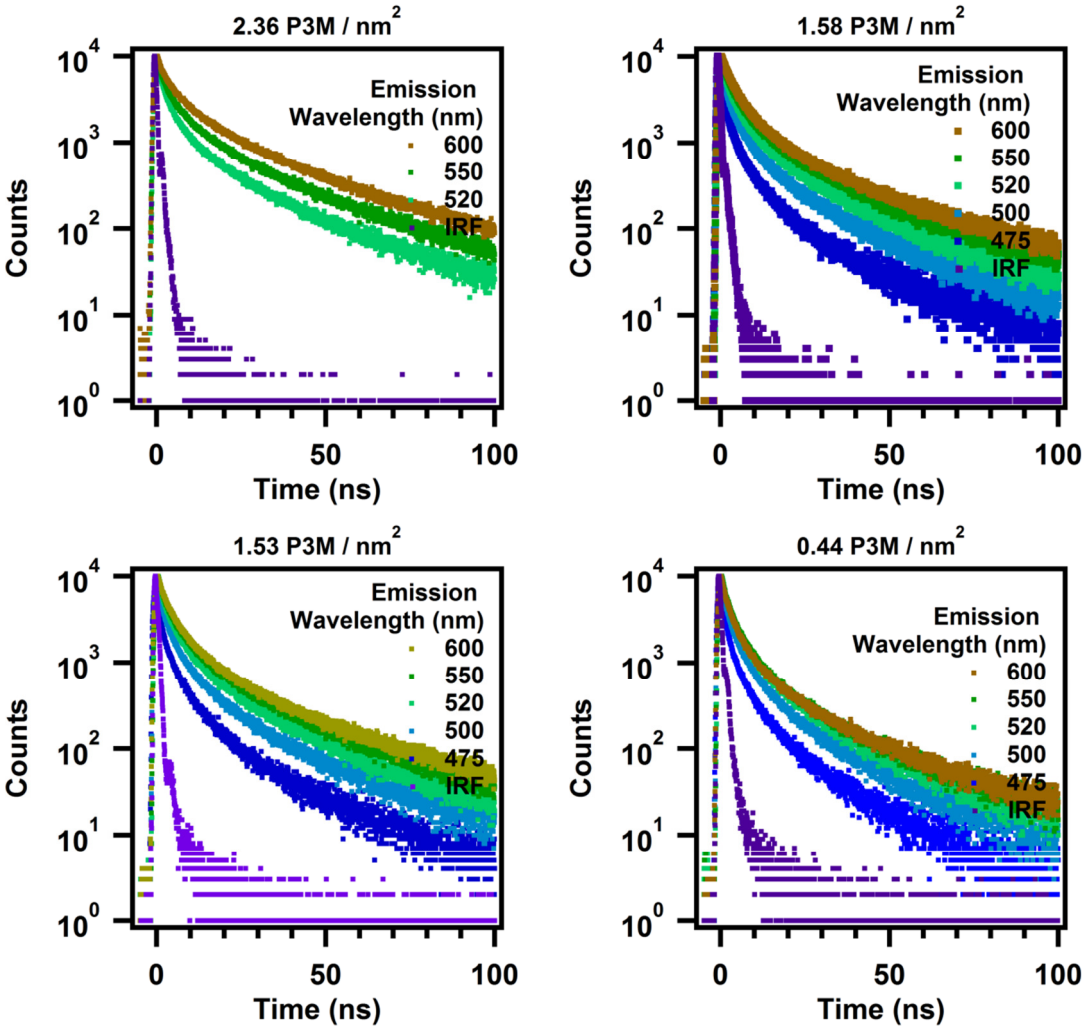

Figure B.8: Fluorescence decay profiles from samples with various fluorophore densities.

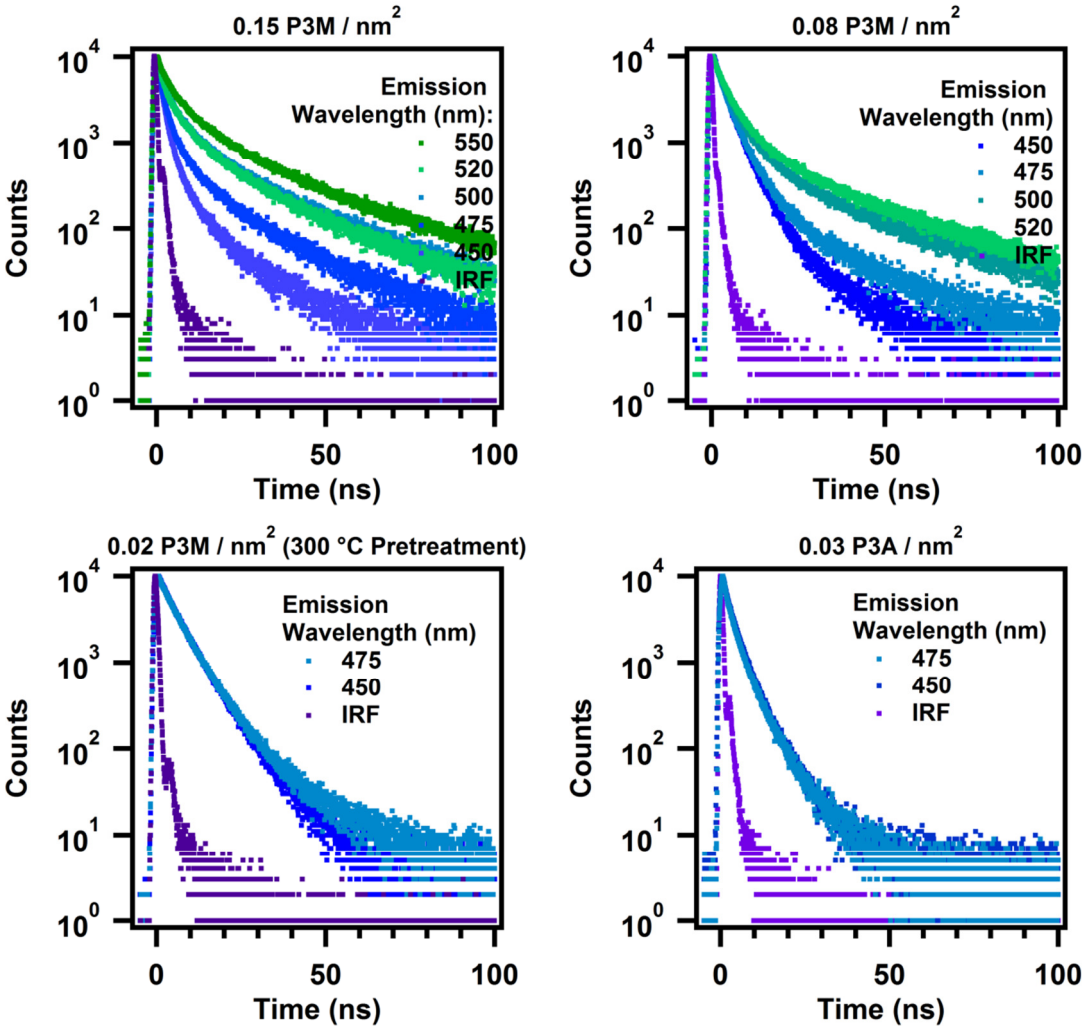

Figure B.9: Fluorescence decay profiles from samples with various fluorophore densities.

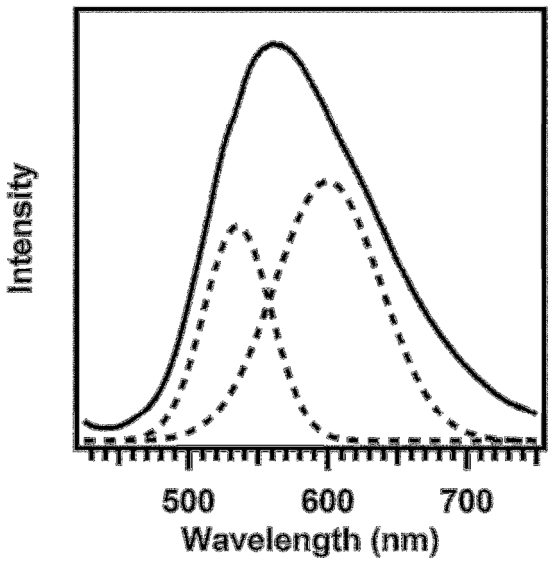

Figure B.10: Deconvoluted emission spectrum from a sample with physisorbed material (2.36 P3M / nm^2) showing large contribution from a fully relaxed (600 nm centered) emission feature. The integrated intensity is approximately two-thirds attributed to fully relaxed emission and one-third attributed to emission from a partially relaxed species. The contribution from fully relaxed species is significantly larger than from samples with chemically bound P3M (maximum density of 1.56 nm^{-2}).

Appendix C: Supporting Information for Chapter 5

C.1 Results

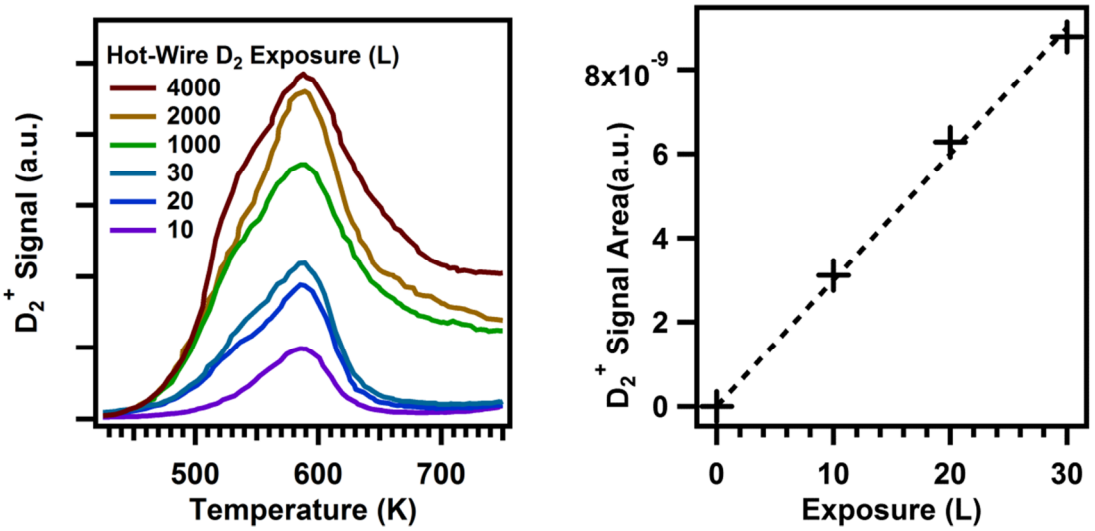

Figure C.1: (Left) TPD spectra showing D_2^+ (m/z 4) signal from Ge(100) samples given various exposures of atomic deuterium. (Right) Plot of D_2^+ signal versus exposure for low exposures.

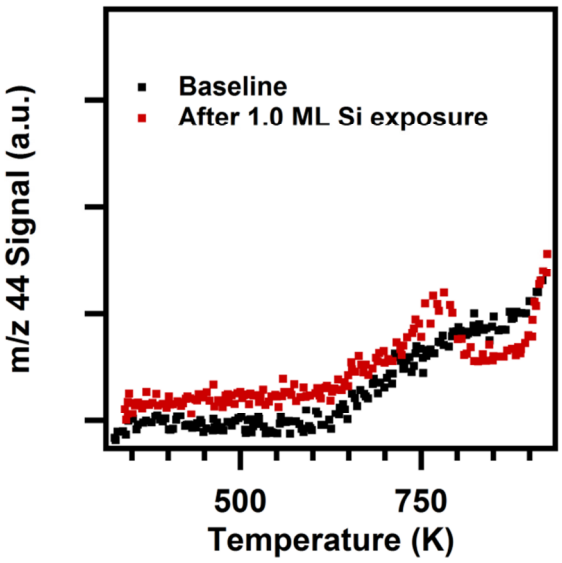

Figure C.2: TPD spectra of m/z 44 (SiO^+) from thermal oxide on Si(100) before and after exposure to 1.0 ML Si.

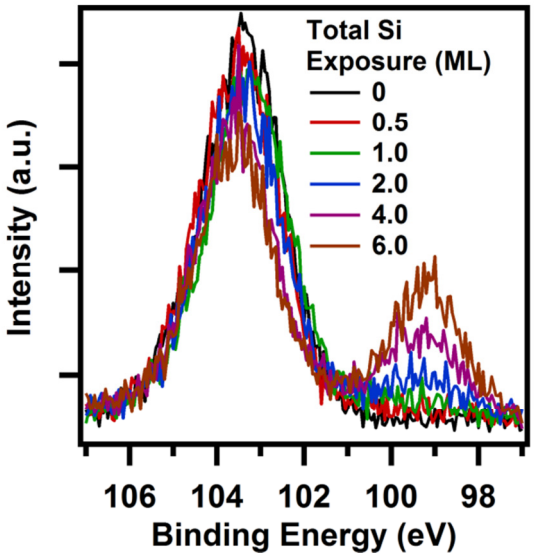

Figure C.3: Si $2p_{3/2}$ XP spectra from fused silica samples given various Si exposures. Spectra have been shifted so that the Si^{4+} peak is centered at 103.5 eV to account for charging.

References

P. Anfinrud, R.L. Crackel, W.S. Struve, Excitation transport and trapping in a two-dimensional disordered system: cresyl violet on quartz, J. Phys. Chem. 88 (1984) 5873–5882.

S. Akimoto, A. Ohmori, I. Yamazaki, Dimer Formation and Excitation Relaxation of Perylene in Langmuir-Blodgett Films, J. Phys. Chem. B. 101 (1997) 3753–3758.

J.G. Amar, F. Family, Critical Cluster Size: Island Morphology and Size Distribution in Submonolayer Epitaxial Growth, Phys. Rev. Lett., 74 (1995) 2066-2069.

R. Azrak, C. Angell, Study of alcohol-silica surface reactions via infrared spectroscopy, J. Phys. Chem. 77 (1973) 3048–3052.

C. Ballard, E. Broge, R. Iler, D.S. St. John, J.R. McWhorter, Esterification of the surface of amorphous silica, J. Phys. Chem. 65 (1961) 20–25.

P. Ballet, M. Van der Auweraer, F. De Schryver, H. Lemmetyinen, E. Vuorimaa, Global analysis of the fluorescence decays of N, N'-Dioctadecyl rhodamine b in Langmuir-blodgett films of diacylphosphatidic acids, J. Phys. Chem. 100 (1996) 13701–13715.

T. Baron, B. Pelissier, L. Perniola, F. Mazen, J.M. Hartmann, G. Rolland, Chemical vapor deposition of Ge nanocrystals on SiO_2, Appl. Phys. Lett., 83 (2003) 1444-1446.

I. Berbezier, A. Karmous, A. Ronda, A. Sgarlata, A. Balzarotti, P. Castrucci, M. Scarselli, M. De Crescenzi, Growth of ultrahigh-density quantum-confined germanium dots on SiO_2 thin films, Appl. Phys. Lett., 89 (2006) 063122.

V.M. Bermudez, A Proton Nuclear Magnetic Resonance Technique for Determining the Surface Hydroxyl Content of Hydrated Silica Gel, J. Phys. Chem. 74 (1970) 4160–4161.

V. Bermudez, V. Ritz, Investigation of the silica surface via electron-energy-loss spectroscopy, Phys. Rev. B. 20 (1979) 3446–3455.

I. Berlman, Handbook of Fluorescence Spectra of Aromatic Molecules, 2nd ed., Academic Press, New York, 1971.

I. Berlman, Energy Transfer Parameters of Aromatic Compounds, Academic Press, New York, 1973.

J.B. Birks, Photophysics of Aromatic Molecules, Wiley-Interscience, New York, 1970.

G. Blomfield, L. Little, Chemisorption of ammonia on silica, Can. J. Chem. 51 (1973) 1771–1781.

A.A. Bobyshev, V.A. Radtsig, Silanone groups on the surface of mechanically activated silicon dioxide, Kinet. Catal.(Engl. Transl.). 29 (1988) 551–559.

A. Bogicevic, D. Jennison, Effect of oxide vacancies on metal island nucleation, Surf. Sci. 515 (2002) L481–L486.

C. Bronnimann, R. Zeigler, G. Maciel, Proton NMR study of dehydration of the silica gel surface, J. Am. Chem. Soc. 110 (1988) 2023–2026.

B. Bunker, D. Haaland, T. Michalske, W. Smith, Kinetics of dissociative chemisorption on strained edge-shared surface defects on dehydroxylated silica, Surf. Sci. 222 (1989) 95–118.

G.W. Burr, B.N. Kurdi, J.C. Scott, C.H. Lam, K. Gopalakrishnan, R.S. Shenoy, Overview of candidate device technologies for storage-class memory, IBM J. Res. Dev. 52 (2008) 449–464.

G. Buscarino, S. Agnello, F. Gelardi, Characterization of E′δ and triplet point defects in oxygen-deficient amorphous silicon dioxide, Phys. Rev. B. 73 (2006) 1–8.

G.F. Cerofolini, L. Meda, CO_2 and C_2H_4 grafting to the native defects of ion-bombarded porous silica, 39 (1999) 29–39.

D. Chambliss, K. Johnson, Nucleation with a critical cluster size of zero: Submonolayer Fe inclusions in Cu (100), Phys. Rev. B. 50 (1994) 5012–5015.

C. Chiang, B. Zegarski, L. Dubois, First observation of strained siloxane bonds on silicon oxide thin films, J. Phys. Chem. 97 (1993) 6948–6950.

I. Chuang, G.E. Maciel, Probing Hydrogen Bonding and the Local Environment of Silanols on Silica Surfaces via Nuclear Spin Cross Polarization Dynamics, J. Am. Chem. Soc. 118 (1996) 401–406.

F. Cinquini, C. Di, E. Finazzi, L. Giordano, Theory of oxides surfaces , interfaces and supported nano-clusters, (2007) 827–845.

S. Coffee, J. Ekerdt, Investigation of Volmer-Weber growth mode kinetics for germanium nanoparticles on hafnia, J. Appl. Phys. 102 (2007) 1149129.

S.S. Coffee, D. Shahrjerdi, S.K. Banerjee, J.G. Ekerdt, Selective silicon nanoparticle growth on high-density arrays of silicon nitride, J. Cryst. Growth, 308 (2007) 269-277.

L. Crowe, L. Tolbert, Silica Passivation Efficiency Monitored By a Surface-Bound Fluorescent Dye, Langmuir. 24 (2008) 8541–8546.

R. Devine, The structure of SiO_2, its defects and radiation hardness, Nucl. Sci. IEEE Trans. 41 (1994) 452–459.

V. Dugas, Y. Chevalier, Surface hydroxylation and silane grafting on fumed and thermal silica, J. Colloid Interface Sci. 264 (2003) 354–361.

T. Dürkop, E. Bugiel, I. Costina, A. Ott, R. Peibst, K.R. Hofmann, PE-CVD fabrication of germanium nanoclusters for memory applications, Mater. Sci.Eng. B, 147 (2008) 213-217.

K. Eisenbeiser, Device Principles of High-K Dielectrics, in: A. Demkov, A. Navrotsky (Eds.), Mater. Fundam. Gate Dielectr., Springer, Dordrecht, The Netherlands, 2005: pp. 37–56.

Y. Eyal, R. Evron, Y. Cohen, Defect Structure of Ion-Irradiated Amorphous SiO_2, J. Appl. Crystallogr. 30 (1997) 618–622.

J. Ferguson, Absorption and Emission Spectra of the Perylene Dimer, J. Chem. Phys. 44 (1966) 2677.

B. Finlayson-Pitts, Interactlon of Gas-Phase Deuterium Atoms with Silica Surfaces, J. Phys. Chem. 86 (1982) 3499–3501.

S. Flink, F.C van Veggel, D.N. Reinhoudt, Functionalization of self-assembled monolayers on glass and oxidized silicon wafers by surface reactions, J. Phys. Org. Chem. 14 (2001) 407–415.

S. Foss, T.G. Finstad, A. Dana, A. Aydinli, Growth of Ge nanoparticles on SiO_2/Si interfaces during annealing of plasma enhanced chemical vapor deposited thin films, Thin Solid Films, 515 (2007) 6381-6384.

J. Gallas, J. Goupil, A. Vimont, J. Lavalley, Quantification of Water and Silanol Species on Various Silicas by Coupling IR Spectroscopy and in-Situ Thermogravimetry, Langmuir. 57 (2009) 5825–5834.

L. Gao, Y. Fang, X. Wen, Y. Li, D. Hu, Monomolecular layers of pyrene as a sensor to dicarboxylic acids, J. Phys. Chem. B. 108 (2004) 1207–1213.

R. Giulian, P. Kluth, L.L. Araujo, D.J. Llewellyn, M.C. Ridgway, Pt nanocrystals formed by ion implantation: A defect-mediated nucleation process, Appl. Phys. Lett., 91 (2007) 093115-093113.

B. Granqvist, T. Sandberg, M. Hotokka, Adsorption of organic probes on silica through Lewis interactions: A comparison of experimental results and quantum chemical calculations, J. Colloid Interface Sci. 310 (2007) 369–376.

D.L. Griscom, The Natures of Point Defects in Amorphous Silicon Dioxide, in: G. Pacchioni, L. Skuja, D.L. Griscom (Eds.), Defects SiO_2 Relat. Dielectr. Sci. Technol., Dordrecht, The Netherlands, 2000: pp. 117–159.

S. Guha, V. Narayanan, High-k/Metal Gate Science and Technology, Annu. Rev. Mater. Res. 39 (2009) 181–202.

A. Grabbe, T. Michalske, W. Smith, Strained siloxane rings on the surface on silica: their reaction with organosiloxanes, organosilanes, and water, J. Phys. Chem. 99 (1995) 4648–4654.

G. Haas, A. Menck, H. Brune, J. Barth, J.A. Venables, K. Kern, Nucleation and growth of supported clusters at defect sites: Pd/MgO (001), Phys. Rev. B. 61 (2000) 105–108.

M. Halbwax, C. Renard, D. Cammilleri, V. Yam, F. Fossard, D. Bouchier, Y. Zheng, E. Rzepka, Epitaxial growth of Ge on a thin SiO_2 layer by ultrahigh vacuum chemical vapor deposition, J. Cryst. Growth, 308 (2007) 26-29.

F. Iacona, R. Kelly, G. Marletta, Regular Articles-X-ray photoelectron spectroscopy study of bombardment-induced compositional changes in ZrO2, SiO2, and ZrSiO4, J. Vac. Sci. Technol. A Vacuum, Surfaces, Film. 17 (1999) 2771–2778.

R.K. Iler, The Chemistry of Silica : Solubility, Polymerization, Colloid and Surface Properties, and Biochemistry, 1979.

M. Kanoun, C. Busseret, A. Poncet, A. Souifi, T. Baron, E. Gautier, Electronic properties of Ge nanocrystals for non volatile memory applications, Solid State Electron., 50 (2006) 1310-1314.

K. Kemnitz, N. Tamai, I. Yamazaki, N. Nakashima, K. Yoshihara, Fluorescence decays and spectral properties of rhodamine B in submono-, mono-, and multilayer systems, J. Phys. Chem. 90 (1986) 5094–5101.

J. Klafter, A. Blumen, Fractal behavior in trapping and reaction, J. Chem. Phys. 80 (1984) 875–877

C. Kuo, G. Hwang, Structure and interconversion of oxygen-vacancy-related defects on amorphous silica, Phys. Rev. Lett. 97 (2006) 066101.

C. L. Kuo, S. Lee, G. Hwang, Strain-Induced Formation of Surface Defects in Amorphous Silica: A Theoretical Prediction, Phys. Rev. Lett. 100 (2008) 076104.

K.E. Kweon, G.S. Hwang, Defect-Assisted Covalent Binding of Graphene to an Amorphous Silica Surface: A Theoretical Prediction, ChemPhysChem. 12 (2011) 2155–2159.

J. Lakowicz, Princples of Fluorescence Spectroscopy, 2nd ed., Kluwer Academic / Plenum Publishers, New York, 1999.

A. Lambacher, P. Fromherz, Fluorescence interference-contrast microscopy on oxidized silicon using a monomolecular dye layer, Appl. Phys. A. 63 (1996) 207–216.

W.T. Leach, J.H. Zhu, J.G. Ekerdt, Cracking assisted nucleation in chemical vapor deposition of silicon nanoparticles on silicon dioxide, J. Cryst. Growth, 240 (2002) 415-422.

W.T. Leach, J.H. Zhu, J.G. Ekerdt, Thermal desorption effects in chemical vapor deposition of silicon nanoparticles, J. Cryst. Growth, 243 (2002) 30-40.

D. Leonhardt, S.M. Han, Energetics of Ge nucleation on SiO_2 and implications for selective epitaxial growth, Surf. Sci., 603 (2009) 2624-2629.

Q. Li, S.M. Han, S.R.J. Brueck, S. Hersee, Y.B. Jiang, H. Xu, Selective growth of Ge on Si(100) through vias of SiO_2 nanotemplate using solid source molecular beam epitaxy, Appl. Phys. Lett., 83 (2003) 5032-5034.

Q.M. Li, J.L. Krauss, S. Hersee, S.M. Han, Probing interactions of Ge with chemical and thermal SiO_2 to understand selective growth of Ge on Si during molecular beam epitaxy, J. Phys. Chem. C, 111 (2007) 779-786.

C. Liu, G. Maciel, The fumed silica surface: a study by NMR, J. Am. Chem. Soc. 118 (1996) 5103–5119.

H. Liu, W. Winkenwerder, Y.R. Liu, D. Ferrer, D. Shahrjerdi, S.K. Stanley, J.G. Ekerdt, S.K. Banerjee, Core-Shell Germanium-Silicon Nanocrystal Floating Gate for Nonvolatile Memory Applications, IEEE T. Electron. Dev., 55 (2008) 3610-3614.

C. Lochmuller, A. Colborn, M. Hunnicutt, Organization and distribution of molecules chemically bound to silica, Anal. Chem. 55 (1983) 1344–1348.

C.H. Lochmuller, A.S. Colborn, M.L. Hunnicutt, J.. Harris, Bound Pyrene Excimer Photophysics and the Organization and Distribution of Reaction Sites on Silica, J. Am. Chem. Soc. 106 (1984) 4077–4082.

C.H. Lochmuller, M.T. Kersey, Effect of thermal pretreatment on the surface reactivity of amorphous silica, Langmuir. 4 (1988) 572–578.

N. Lopez, M. Vitiello, F. Illas, G. Pacchioni, Interaction of H_2 with strained rings at the silica surface from ab initio calculations, 271 (2000) 56–63.

G. Lucovsky, Electronic Structure and Chemical Bonding in High-K Transition Metal and Lanthanide Series Rare Earth Alternative Gate Dielectrics, in: A.A. Demkov,

A. Navrotsky (Eds.), Mater. Fundam. Gate Dielectr., Springer, Dordrecht, The Netherlands, 2005: pp. 109–178.

W.K. Lowen, E.C. Broge, Effects of dehydration and chemisorbed materials on the surface properties of amorphous silica, J. Phys. Chem. 65 (1961) 16–19.

Y. Maeda, Visible photoluminescence from nanocrystallite Ge embedded in a glassy SiO_2 matrix: Evidence in support of the quantum-confinement mechanism, Phys. Rev. B, 51 (1995) 1658 -1670.

J. Mahrt, F. Willig, W. Storck, D. Weiss, R. Kietzmann, K. Schwarzburg, B. Tufts, B. Trösken, Luminescence and configurations of perylene dimers in a Langmuir-Blodgett film, J. Phys. Chem. 98 (1994) 1888–1894.

L. Masarotto, K. Yckache, A. Fanton, F. Aussenac, F. Fillot, Embedding of reduced pressure-chemical vapor deposition grown Ge nanocrystals in a high quality SiO_2 matrix for non-volatile memory applications, Thin Solid Films, 518 (2010) 5382-5386.

F. Mazen, T. Baron, G. Bremond, N. Buffet, N. Rochat, P. Mur, et al., Influence of the chemical properties of the substrate on silicon quantum dot nucleation, J. Electrochem. Soc. 150 (2003) G203–G208.

M. Mazur, G. Blanchard, Probing intermolecular communication with surface-attached pyrene, J. Phys. Chem. B. 109 (2005) 4076–4083.

E.A. McArthur, T. Ye, J.P. Cross, S. Petoud, E. Borguet, Fluorescence detection of surface-bound intermediates produced from UV photoreactivity of alkylsiloxane SAMs., J. Am. Chem. Soc. 126 (2004) 2260–2261.

J.M. McCrate, N. Salivati, J.G. Ekerdt, Hot-wire CVD of Ge nanoparticles on Si-etched silicon dioxide, J. Cryst. Growth. 321 (2011) 131–135.

J.M. McCrate, J.G. Ekerdt, Titration of Free Hydroxyl and Strained Siloxane Sites on Silicon Dioxide with Fluorescent Probes, Langmuir. 29 (2013) 11868–11875.

J.M. McCrate, J. Ekerdt, Coverage Dependent Luminescence from Two-Dimensional Systems of Covalently Attached Perylene Fluorophores on Silica, Submitted. (2013).

R. Métivier, I. Leray, M. Roy-Auberger, N. Zanier-Szydlowski, B. Valeur, Characterization of alumina surfaces by fluorescence spectroscopy. Part 1. Grafting a pyrene derivative on γ- and δ-alumina supports, New J. Chem. 26 (2002) 411–415.

B. Min, W. Wallace, A. Santra, D.W. Goodman, Role of defects in the nucleation and growth of Au nanoclusters on SiO_2 thin films, J. Phys. Chem. B. 108 (2004) 16339–13343.

B.A. Morrow, I.A. Cody, An Infrared Study of Some Reactions with Reactive Sites on Dehydroxylated Silica, J. Phys. Chem. 79 (1975) 761–762.

B. Morrow, I. Cody, Infrared studies of reactions on oxide surfaces. 5. Lewis acid sites on dehydroxylated silica, J. Phys. Chem. 80 (1976) 1995–1998.

B. Morrow, I. Cody, Infrared studies of reactions on oxide surfaces. 6. Active sites on dehydroxylated silica for the chemisorption of ammonia and water, J. Phys. Chem. 80 (1976) 1998–2004.

B.A. Morrow, I.D. Gay, Infrared and NMR Characterization of the Silica Surface, in: E. Papirer (Ed.), Adsorpt. Silica Surfaces, Marcel Dekker, Inc., New York, 2000: pp. 9–34.

B. Morrow, A. McFarlan, Infrared and gravimetric study of an aerosil and a precipitated silica using chemical and hydrogen/deuterium exchange probes, Langmuir. (1991) 1695–1701.

C. Morterra, M. Low, Reactive silica. II. Nature of the surface silicon hydrides produced by the chemisorption of hydrogen, J. Phys. Chem. 73 (1969) 327–333.

R. Mueller, H. Kammler, K. Wegner, OH Surface Density of SiO_2 and TiO_2 by Thermogravimetric Analysis, Langmuir. 19 (2003) 160–165.

C. Mukherjee, H. Seitz, B. Schroder, Growth of epitaxial germanium films on silicon using hot-wire chemical vapor deposition, Appl. Phys. Lett., 78 (2001) 3457-3459.

L.H. Nguyen, V. Le Thanh, D. Débarre, V. Yam, D. Bouchier, Selective growth of Ge quantum dots on chemically prepared SiO_2/Si(001) surfaces, Mater. Sci. Eng. B, 101 (2003) 199-203.

G.C. Ossenkamp, T. Kemmitt, J.H. Johnston, New Approaches to Surface-Alkoxylatd Silica with Increased Hydrolytic Stability, Chem. Mater. 13 (2001) 3975–3980.

J. Peri, A.L. Hensley, The surface structure of silica gel, J. Phys. Chem. 2 (1968) 242–247.

G. Pacchioni, Oxygen Vacancy: The Invisible Agent on Oxide Surfaces, ChemPhysChem. 4 (2003) 1041–1047.

R. Prins, Hydrogen spillover. Facts and fiction., Chem. Rev. 112 (2012) 2714–2738.

C. Ratsch, J. Venables, Nucleation theory and the early stages of thin film growth, J. Vac. Sci. Technol. A Vacuum, Surfaces, Film. 21 (2003) S96–S109.

V. Radtsig, I. Senchenya, Hydrogenation of the silanone groups $(\equiv Si\text{-}O)_2Si{=}O$. Experimental and quantum-chemical studies, Russ. Chem. Bull. 45 (1996) 1849–1856.

V. Radzig, Point defects in disordered solids: Differences in structure and reactivity of the (≡ Si–O)$_2$Si: groups on silica surface, J. Non. Cryst. Solids. 239 (1998) 49–56.

V.A. Radzig, Defects on Activated Silica Surface, in: G. Pacchioni, L. Skuja, D.L. Griscom (Eds.), Defects SiO_2 Relat. Dielectr. Sci. Technol., Klumer Academic, Dordrecht, The Netherlands, 2000: pp. 339–370.

Y.V. Razskazovskii, M.V. Roginskaya, M.Y. Mel'nikov, The reactions of silylenes on the chemically activated silica surface, J. Organomet. Chem. 486 (1995) 249–253.

C. Renard, M. Halbwax, D. Cammilleri, F. Fossard, V. Yam, D. Bouchier, Y. Zheng, Ge growth over thin SiO_2 by UHV-CVD for MOSFET applications, Thin Solid Films, 517 (2008) 401-403.

S. Ruetten, J. Thomas, Fluorescence and triplet quantum yields of arenes on surfaces, J. Phys. Chem. B. 102 (1998) 598–606.

J. Robertson, P. Peacock, Atomic Structure, Interfaces, and Defects of High Dielectric Constant Gate Oxides, in: A.A. Demkov, A. Navrotsky (Eds.), Mater. Fundam. Gate Dielectr., Springer, Dordrecht, The Netherlands, 2005: pp. 179–214.

N. Salivati, Y.Q. An, M.C. Downer, J.G. Ekerdt, Hot-wire chemical vapor deposition of silicon nanoparticles on fused silica, Thin Solid Films, 517 (2009) 3481-3483.

N. Salivati, J.G. Ekerdt, Temperature programmed desorption studies of deuterium passivated silicon nanocrystals, Surf. Sci. 603 (2009) 1121–1125.

R. Schaub, E. Wahlström, A. Rønnau, E. Lagsgaard, I. Stensgaard, F. Besenbacher, Oxygen-mediated diffusion of oxygen vacancies on the TiO_2(110) surface., Science. 299 (2003) 377–379.

A.A. Shklyaev, M. Ichikawa, Visible photoluminescence of Ge dots embedded in Si/SiO_2 matrices, Appl. Phys. Lett., 80 (2002) 1432-1434.

M. Sluch, A. Vitukhnovsky, L. Ande, Fluorescence of perylene-4-octadecanon in Langmuir-Blodgett films, Thin Solid Films. 248 (1994) 230–233.

M. Sluch, A. Vitukhnovsky, M. Petty, Pyrene excimer formation in Langmuir-Blodgett films, Thin Solid Films. 285 (1996) 622–626.

O. Sneh, S. George, Thermal stability of hydroxyl groups on a well-defined silica surface, J. Phys. Chem. 99 (1995) 4639–4647.

A. D'Souza, C. Pantano, K. Kallury, Determination of the surface silanol concentration of amorphous silica surfaces using static secondary ion mass spectroscopy, J. Vac. Sci. Technol. A Vacuum, Surfaces, Film. 15 (1997) 526–531.

S.K. Stanley, S.V. Joshi, S.K. Banerjee, J.G. Ekerdt, Surface reactions and kinetically-driven patterning scheme for selective deposition of Si and Ge nanoparticle arrays on HfO_2, Surf. Sci., 600 (2006) L54-L57.

S.K. Stanley, S.V. Joshi, S.K. Banerjee, J.G. Ekerdt, Ge interactions on HfO_2 surfaces and kinetically driven patterning of Ge nanocrystals on HfO_2, J. Vac. Sci. Technol. A, 24 (2006) 78-83.

D.C. Streit, F.G. Allen, Thermal and Si-Beam Assisted Desorption of SiO_2 from Silicon in Ultrahigh-Vacuum, J. Appl. Phys., 61 (1987) 2894-2897.

J.M. Szarko, A. Neubauer, A. Bartelt, L. Socaciu-siebert, F. Birkner, K. Schwarzburg, T. Hannappel, R. Eichberger, The Ultrafast Temporal and Spectral Characterization of Electron Injection from Perylene Derivatives into ZnO and TiO_2 Colloidal Films, J. Phys. Chem. C. 112 (2008) 10542–10552.

N. Tamai, T. Yamazaki, I. Yamazaki, Two-dimensional excitation energy transfer between chromophoric carbazole and anthracene in Langmuir-Blodgett monolayer films, J. Phys. Chem. 91 (1987) 841–845.

N. Tamai, T. Yamazaki, I. Yamazaki, Excitation energy relaxation of rhodamine B in Langmuir-Blodgett monolayer films: Picosecond time-resolved fluorescence studies, Chem. Phys. Lett. 147 (1988) 25–29.

J. Tanaka, The electronic spectra of aromatic molecular crystals. II. The crystal structure and spectra of perylene, Bull. Chem. Soc. Jpn. 36 (1963) 1237–1249.

H. Tachikawa, L. Faulkner, Anomalous luminescence from perylene in thin polymer films, Chem. Phys. Lett. 39 (1976) 436–441.

S. Tiwari, F. Rana, H. Hanafi, A. Hartstein, E.F. Crabbe, K. Chan, A silicon nanocrystals based memory, Appl. Phys. Lett., 68 (1996) 1377-1379.

L. Vaccaro, A. Morana, V. Radzig, M. Cannas, D. Fisica, Bright Visible Luminescence in Silica Nanoparticles, (2011) 19476–19481.

L. Vaccaro, M. Cannas, V. Radzig, R. Boscaino, Luminescence of the surface nonbridging oxygen hole center in silica: Spectral and decay properties, Phys. Rev. B. 78 (2008) 075421.

B. Valeur, Molecular Fluorescence, Wiley-VCH Verlag, Weinheim, 2002.

E.F. Vansant, P. Van Der Voort, K.C. Vrancken, Characterization and Chemical Modification of the Silica Surface, Elsevier B.V., Amsterdam, 1995.

J. Venables, Nucleation and growth on defect sites: experiment–theory comparison for Pd/MgO (001), J. Physics-Condensed Matter. 18 (2006) S411–S427.

K. Vikulov, G. Martra, S. Coluccia, D. Miceli, F. Arena, A. Parmaliana, et al., FTIR spectroscopic investigation of the active sites on different types of silica catalysts for methane partial oxidation to formaldehyde, Catal. Letters. 37 (1996) 235–239.

M. Vitiello, N. Lopez, F. Illas, G. Pacchioni, H_2 cracking at SiO_2 defect centers, J. Phys. Chem. A. 104 (2000) 4674–4684.

A. Vitukhnovsky, M. Sluch, J. Warren, M. Petty, The Fluorescence of Perylene-Doped Langmuir—Blodgett Films, Chem. Phys. Lett. 173 (1990) 425–429.

E. Wahlström, N. Lopez, R. Schaub, P. Thostrup, a. Rønnau, C. Africh, E. Lægsgaarad, J.K. Nørskov, F. Besenbacher, Bonding of Gold Nanoclusters to Oxygen Vacancies on Rutile TiO_2(110), Phys. Rev. Lett. 90 (2003) 1–4.

B. Walker, H. Port, H. Wolf, The two-step excimer formation in perylene crystals, Chem. Phys. 92 (1985) 177–185.

C. Wang, N. Kuzuu, Y. Tamai, Effects of charge transfer on a-SiO_2 surface structure: A molecular dynamics study, J. Appl. Phys. 92 (2002) 4408.

H. Wang, J. Harris, Origins of bound-probe fluorescence decay heterogeneity in the distribution of binding sites on silica surfaces, J. Phys. Chem. 99 (1995) 16999–17009.

J.B. Wedding, G.C. Wang, T.M. Lu, Vacancy-enhanced submonolayer nucleation of Si on Si(111), Surf. Sci., 504 (2002) 28-36.

D. Weiss, R. Kietzmann, J. Mahrt, B. Tufts, W. Storck, F. Willig, E-excimer and Y-type luminescence of perylene dimers in a Langmuir-Blodgett film at 1.5 K, J. Phys. Chem. 96 (1992) 5320–5325.

W.A. Winkenwerder, J.G. Ekerdt, Interaction of germanium with silicon dioxide, Surf. Sci., 602 (2008) 2796-2800.

W.A. Winkenwerder, J.G. Ekerdt, Germanium interactions with Si-etched silicon dioxide, Surf. Sci. 602 (2008) 2796–2800.

E.A. Wovchko, J.C. Camp, J.A. Glass, J.T. Yates, Active Sites on SiO_2: Role in CH_3OH Decomposition, Langmuir. 11 (1995) 2592–2599.

Y. Xing, E. Borguet, Specificity and sensitivity of fluorescence labeling of surface species, Langmuir. 23 (2007) 684–688.

Y. Xu, B.P. Nelson, L.M. Gedvilas, R.C. Reedy, Improving narrow bandgap a-SiGe:H alloys grown by hot-wire chemical vapor deposition, Thin Solid Films, 430 (2003) 197-201.

I. Yamazaki, N. Tamai, T. Yamazaki, Picosecond Fluorescence Spectroscopy on Excimer Formation and Excitation Energy Transfer of Pyrene in Langmuir-Blodgett Monolayer Films, J. Phys. Chem. 91 (1987) 3572–3577.

I. Yamazaki, N. Tamai, T. Yamazaki, Electronic excitation transfer in organized molecular assemblies, J. Phys. Chem. 94 (1990) 516–525.

M. Yang, T.P. Chen, J.I. Wong, C.Y. Ng, Y. Liu, L. Ding, S. Fung, A.D. Trigg, C.H. Tung, C.M. Li, Charge trapping and retention behaviors of Ge nanocrystals distributed in the gate oxide near the gate synthesized by low-energy ion implantation, J. Appl. Phys., 101 (2007) 124313.

L. Zanzig, W. Beyer, H. Wagner, High quality hydrogenated amorphous germanium prepared by the hot wire technique, Appl. Phys. Lett., 67 (1995) 1567-1569.

S. Zhang, F. Lü, L. Gao, L. Ding, Y. Fang, Fluorescent sensors for nitroaromatic compounds based on monolayer assembly of polycyclic aromatics, Langmuir. (2007) 1584–1590.

L. Zhang, H. Ye, Y.R. Huangfu, C. Zhang, X. Liu, Densely packed Ge quantum dots grown on SiO_2/Si substrate, Appl. Surf. Sci., 256 (2009) 768-772.

J. Zhou, D. a. Chen, Controlling size distributions of copper islands grown on TiO_2-(1×2), Surf. Sci. 527 (2003) 183–197.

L.T. Zhuravlev, Concentration of hydroxyl groups on the surface of amorphous silicas, Langmuir. 3 (1987) 316–318.

L. Zhuravlev, The surface chemistry of amorphous silica. Zhuravlev model, Colloids Surfaces A. 173 (2000) 1–38.

G. Zumofen, A. Blumen, Energy trapping in mixed molecular crystals, Chem. Phys. Lett. 98 (1983) 393–397.

Vita

Joseph Michael McCrate attended the University of Missouri-Columbia where he received a B.S. in Chemical Engineering, in Chemistry, and in Mathematics in May 2008. During his time in Columbia, he conducted undergraduate research in both the development of radiopharmaceuticals and in nanomaterial synthesis.

After a summer internship at the Naval Research Laboratory in Washington, D.C., Joseph joined Dr. John Ekerdt's research group at The University of Texas at Austin in the fall of 2008. Here he studied defect mediated nucleation on oxide surfaces. At the time of the writing of this dissertation, Joseph has published two first author publications with another publication in review and was a co-author on eleven other publications. He has also presented results of his research at the AVS 60th International Symposium in November 2013.

E-mail: jmccrate@gmail.com

This dissertation was typed by the author.